Study of the risk of impact between a spacecraft and space debris.

Project report

Tomas Arrufat Jackson

09/09/2013

Supervisors: Diego Escobar Antón (GMV) & Fatiha Nejjari (ETSEIAT).

This page is intentionally left in blank.

ACKNOWLEDGMENTS

I would like to thank GMV to give me this great opportunity to develop my final thesis project in a serious, strict and professional environment and specifically to Diego Escobar which has leaded me along all the development of the project and has awakened my passion for the orbital mechanics science.

I would also like to thank my entire family that has provided since the first moment all the support to face this five tricky years that involve studding an engineering.

Finally, I want to thank my friends that have contributed to make this last five years much more bearable.

ABSTRACT

This work lies in the field of Space Situational Awareness (SSA). Nowadays there is a clear interest within Europe to know in detail the real time distribution of space debris objects orbiting around the Earth. One of the main problems from that population is the collision risk between operational satellites and the space debris. For this reason, it is necessary to characterize the probability of collision between the objects in near Earth altitudes whose orbits are known with certain level of uncertainty.

First of all, as part of this work, a review of the existing methods to compute the probability will be done. Some of them are based on the hypothesis of statistical distribution of the object trajectory uncertainties, while others are based on Monte Carlo methods. It is necessary to compare those methods and select one for its operational implementation.

Moreover, nowadays the most accurate available information for space operators to compute the conjunction probability is the Conjunction Summary Message (CSM) provided by the US Strategic Command to all commercial operators. These messages characterize geometrically the conjunction but do not provide information related to the collision probability.

The central objective of the project will be to develop a tool able to handle the information contained in the CSM and calculate the probability related to the specific conjunction described in the CSM. In addition, in order to better understand the conjunction and produce some graphical representations, additional information will be also extracted from the CSM.

Open Source Java libraries will be used for the code implementation. Those libraries implement the necessary algorithms to propagate orbits or transform coordinate systems particularly between inertial and Earth fixed frames. However, those libraries do not contain any algorithm to compute the collision risk.

For the tool validation, some published examples in the literature will be analyzed and compared with the tool developed in the project. Furthermore, a Monte Carlo method will be also used as an independent validation.

A methodology similar to that proposed by the ECSS standards from the European Space Agency will be used for the development of the tool. This implies defining the following clear phases for the project: requirements engineering, design, implementation, validation and acceptance.

Key words: **conjunction risk, space debris, close approach, Monte Carlo algorithm, and numerical propagation.**

AIM

The aim of this project is to create or select a set of algorithms to evaluate the conjunction risk between near orbiting objects and implement them to build a Java library. It will be also in the bounds of this project to assess the new algorithms and the feasibility of using the Java programming language in the field of Astro-dynamics.

JUSTIFICATION

Nowadays, there is a growing need within the European space institutions to have access to the situational information of the near Earth space objects and more specifically to predict the conjunction risk between them. The most accurate available information for space institutions to compute the conjunction probability is the Conjunction Summary Message (CSM) provided by the US Strategic Command to all commercial operators. These messages characterize geometrically the conjunction but do not provide information related to the collision probability.

This is the reason why in this project a JAVA conjunction risk assessment library will be developed with the aim to integrate it to a commercial product.

SCOPE

The report is structured in six chapters.

Chapter one is an introduction to the topic of the report. It presents the space debris problematic and the ESA SSA program explaining its purposes and principal segments that will compose it. Afterwards, the SST section from the SSA program is explained in more detail to introduce the reader to the space debris observation and detection needs in the current European market. Finally, a brief description of the European Space sensors is provided.

Chapter two is a summary of the most remarkable subjects analyzed during the literature review. The chapter is divided in four parts: the risk reduction operations, the collision problem, the collision probability algorithms and the space reference frames.

Chapter three is a deeper description of the algorithms that will be used in the collision risk computation software. It contains a description of Akella and Alfriend's linear method for short time encounters, there is also a description of Alfano's maximum probability method, to evaluate encounters with poor quality data and finally, three approaches of Monte Carlo algorithms are described which are used to produce accurate results for all types of encounters.

Chapter four presents the collision probability software specifications in a table format and in a more reader friendly format of standard description.

Chapter five is devoted to the software design where the software architecture is detailed. The description contains UML2 static class and sequence diagrams to provide a visual explanation of the distribution of classes and packages. The chapter is divided in several sections, each section describes a package from the conjunction risk evaluation Java library.

Chapter six presents the validations of all the algorithms implemented in the conjunction assessment library. Akella and Alfriend's and the Monte Carlo algorithms have been validated comparing their results against reference values found in the literature reviewed. However, the Maximum Probability algorithms are validated comparing their results between them since no reference data was found in the literature. Finally there is also a part with some tests of the OREKIT library to ensure high accuracy levels of the conjunction assessment library.

The report also contains a project planning, environmental report, the budget and the final conclusions of the study.

TABLE OF CONTENTS

LIST OF FIGURES

LIST OF TABLES

NOMENCLATURE

Miss distance = $\vec{\rho}$

Position = $\vec{r}$

Relative Position = $\overrightarrow{r_r}$

Velocity = $\vec{v}$

Relative Velocity = $\overrightarrow{v_r}$

Dot product of the relative position and relative velocity = $f(t)$

Object radius = R

Combined Object Radius = COR

Aspect Ratio = AR

Standard Deviation = σ

Time of Closest Approach = t_{tca}

Number of Monte Carlo Trials = N

CHAPTER ONE: INTRODUCTION

Because the field of this project is rather specific, this first chapter provides a brief introduction to the space collision topic. The introduction contains the most relevant concepts regarding the collision risk problem within the Space debris field, the European Space Situational Awareness program and its more relevant segment in terms of the project, the Space Surveillance and Tracking Segment. Finally, a short overview of the actual European Space Tracking is also provided.

The explanation is simple and carefully detailed to provide an appropriate frame for the non-experienced reader. The sections are organized starting from the most general to the most specific topics.

1.1 A FEW IDEAS ABOUT SPACE DEBRIS

Space Debris can also be referred as space waste, space junk or orbital debris. It is defined in [1] as: "all man-made objects including fragments thereof, in Earth orbit or re-entering the atmosphere, that are non-functional". This definition comprehends not only decommissioned satellites but also final stages of launchers, items released during space missions and fragments of intentioned and accidental space explosions. By 2005, about 14000 space objects of diameter larger than 5 to 10 cm were tracked, being only a 5% operational space crafts.

1.1.1 SPACE DEBRIS SOURCES

The first detected on-orbit break up occurred on June 29, 1961. The US Transit-4A satellite was launched from Kennedy Space Center on a Thor-Ablestar rocket; it was the 116th space object launched after Sputnik-1 on October 4, 1957. After 77 minutes of the injection and separation of Transit-4A and two additional payloads, the Ablestar upper stage exploded, distributing 625 Kg in 298 trackable fragments of which almost 200 still remain nowadays. This event was the first detected on-orbit break up, but at the moment of the explosion a 46.5% of space objects were already space debris.

During the following thirty years, the launch and deployment activities were frenetic, partially caused by the technological war between the US and the USSR. During that period hundreds of GEO satellites were placed in orbit and in 1978 the first explosion occurred in GEO. Just only one year after, in 1979 Luboš Perek presented a paper "Outer Space Activities versus Outer Space" which was the first

space debris mitigation measure, to re-orbit GEO satellites into a disposal orbit at the end of their lives.

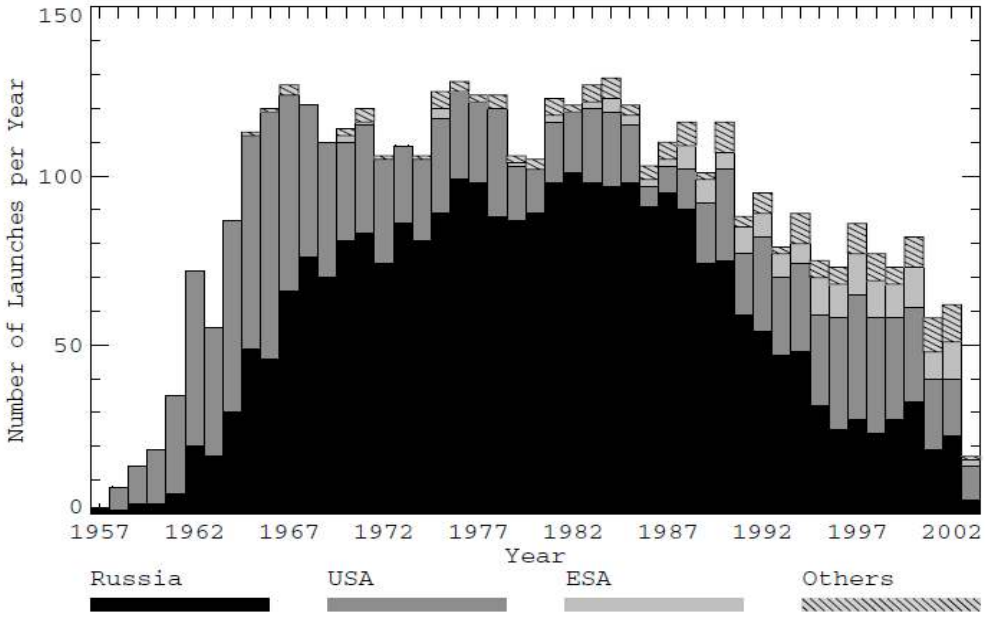

Figure 1: Evolution of annual launches rates and their shares between the major operator's nations. Source: [1]

In that period many explosions took place like the anti-satellite missile tested on Cosmos-249 in 1968, the nine Delta second stages explosions between 1975 and 1981 or the first collision between two satellites in 1996.

In 1990 Donald Kessler[1] proved that the space debris concentration in some space regions could exceed a self-sustainable limit. That means that after a given debris concentration, the main source of debris is the fragmentation process, and once reached this phase the process can hardly be stopped.

A remarkable fact is that approximately 66% of all objects released into space have decayed and in most of the cases have burned out due to the great temperatures reached during re-entry. However, in some particular cases it can suppose a great risk if the satellite contains dangerous materials or if the mass is large enough to survive the re-entry. The most famous event of uncontrolled re-entry was in January 1972 when the Cosmos-954 spread its nuclear reactor with 30Kg of radioactive uranium over Canada.

[1] Donald Kessler published: "Collision Cascading: The Limits of Population Growth in Low-Earth Orbits". The fragmentation mechanism that he describes in his paper is now known as the "Kessler Syndrome".

Apart from object fragmentation or satellite decommissioning, another important source of space debris is the solid rocked slag and dust released during the burning process of the fuel. The slug particles of Al_2O_3 can reach sizes of 5cm. The energy resultant of a 5cm diameter object is equivalent to a hand grenade explosion. This means that special protective shells have to be placed on the satellites superficies.

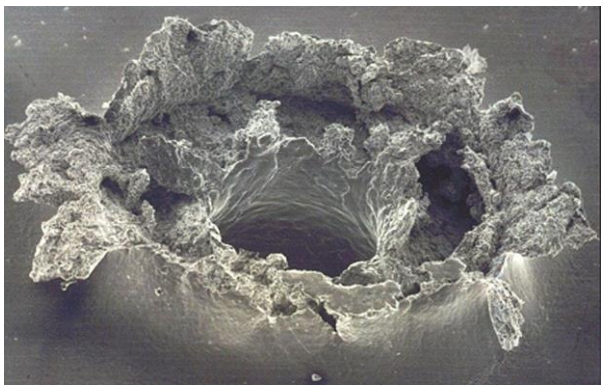

Figure 2: Example of Small Space Debris Impact Source: [2]

The accepted consequences of debris impacts can be summarized in the following table:

Debris size	*Damage*
Less than 0.01cm	Erosion of surfaces
0.01 to 1 cm	Significant damage
	Small perforations as Figure 2
	On-board equipment failures
	Very significant damage
Larger than 10 cm	Catastrophic consequences

Table 1: Possible Effects of Space Debris over Satellites. Source: [2]

1.1.2 General Mitigation Activities

The main future source of space debris proliferation is found in the LEO altitudes with a high density of objects beyond 100Kg. During the course of history different solutions to mitigate the space debris proliferation have been proposed. The best measures from the technical, economic and operational point of view are:

- Reduction of the number of objects dedicated for each mission.
- Prevention of on-orbit explosions.
- Prevention of non-explosive release events.

- Disposal of the decommissioned satellites in less used orbits.
- Removal of passive on-orbit objects.
- Collision avoidance between tracked objects.

This study is related to the last described mitigation activity: the collision avoidance between tracked objects. More particularly it will be centered in the collision risk assessment, which, as it will be described in Section 2, is the first activity in the collision avoidance procedure of the most remarkable European space agencies.

1.2 ESA SPACE SITUATIONAL AWARENESS

1.2.1 ACTUAL FRAME

The actual socio-economic framework in the European region produces a present and future market demand for a large range of services such as communication, navigation or security among many others. Those services are highly dependent on satellite space systems, and at the same time are of critical importance for our current society. That is why the lost or malfunction of any operational satellite would result catastrophic in economic and social terms. The reality as seen in "Space Debris Sources" is that the near Earth space is a really hostile environment and it will become worse if no control and strict protocols are established.

Besides this reality, the European countries are highly dependent on external information about the location and threads of the satellites to ensure the proper work of space systems. Specifically, the major provider of space situational information is the United States of America through agencies such as NORAD[2] or JSpOC [3] in the case of collision risk warnings.

1.2.2 SSA GENERAL CONCEPT

Space Situational Awareness (SSA) is a new initiative conceived in 2007 within Europe with the purpose of providing an independent European SSA. It is defined as a comprehensive knowledge, understanding and maintained awareness of the population of space objects, of the space environment, and of the existing threads

[2] NORAD: The abbreviation of the North American Aerospace Defense Command, it is a United States and Canada bi-national organization charged with the missions of aerospace warning and control for North America.

[3] JSpOC: The abbreviation of Joint Space Operations Center is a command and control weapon system focused on planning and executing the US Strategic Command's Joint Functional Component Command for Space.

[3]. The system's aim is to provide timely and accurate information, data and services regarding the space environment, the threads and the sustainable exploitation of the near Earth outer space.

1.2.3 SSA INSIDE STRUCTURE

The future SSA functions have been divided in three main segments following the criteria of the threat origin.

1.2.3.1 Space Surveillance and Tracking (SST)

Concerning the SST, the principal requisite for this segment is to maintain a catalogue of manmade Objects in near Earth orbits. Furthermore, it is also important to detect, track and correlate all the objects above a given size threshold for a given orbit. The information will be provided for all relevant orbit regions LEO, MEO and GEO. Another important task will be the detection and prediction of collision and re-entry events as well as fragmentation events.

1.2.3.2 Space Weather (SWE)

The Space Weather Segment will be in charge of detecting and forecasting Space Weather and its potential effects over space systems. This purpose will be achieved by monitoring the Sun, Solar Wind, Radiation Belts, Magnetosphere, Ionosphere and Ground based effects. Support services, such as Dynamic perturbations, Induced currents, Radiation and Spacecraft Charging hazards, will be provided.

1.2.3.3 Near Earth Objects (NEOs)

The Near Earth Objects[4] segment will identify and rank the collision risk with the Earth of the natural near Earth orbiting objects. They include a few thousand of Asteroids, Comets and large meteoroids. Also tracking and monitoring activities will be performed with their correspondent orbit determination.

[4] NEOs are Asteroids and Comets whose orbits bring them to within 0.983 and 1.3 AU of the Sun.

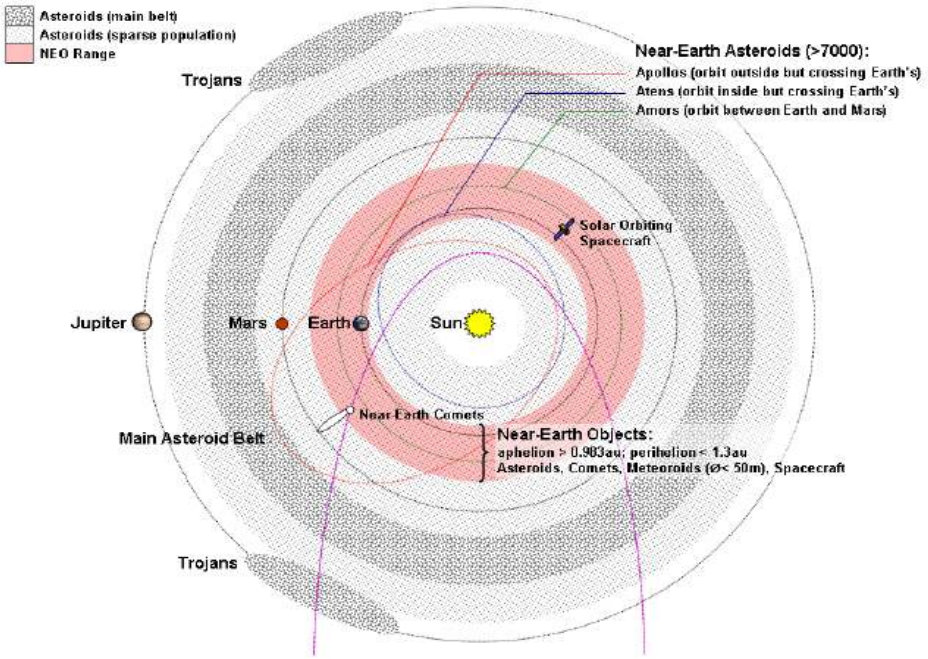

Figure 3: Visual scheme of natural Near-Earth Objects.

1.3 SPACE SURVEILLANCE AND TRACKING SEGMENT

1.3.1 GENERAL DESCRIPTION

It is the core segment of the SSA system; its aim is to maintain awareness of the population of man-made space objects. Providing a response to ESA and other National space agencies in Europe that for several applications, largely depend on limited data shared by other organizations [4].

1.3.2 SERVICES

To respond to all the existing needs of the space operators, the SST will provide the following functionalities.

1.3.2.1 Catalogue of Man-made Objects (CAT)

This service will consist on the creation and maintenance of the catalogue making sure that the accuracy constrains are preserved all the time. The previous objective must be accomplished by performing the surveillance and detection of objects with a minimum number of infrastructures. Also the catalogue has to be capable to start from zero without any initial external information.

1.3.2.2 Collision Warning (COL)

The Collision Warning service will be in charge of carrying out the conjunction analysis using the Catalogue of Man-made Objects. Such analysis will be done in two phases; first a rough risk computation of all the objects in the catalogue, and then a more detailed analysis of all the possible encounters accounted in the first phase. Finally, the system will inform the users about the risky encounters.

1.3.2.3 Detection and Characterization of In-Orbit Fragmentations (FRG)

Due to the high density of objects in the near space, sometimes is inevitable to elude the collision between objects mostly when those are out of service. This is why the FRG is of great importance. Its main function will consist on a constant space screening and notification of new detected objects and if it is possible, the determination of its progenitor. Once, the progenitor is detected the collision event will be characterized.

1.3.2.4 Re-entry Predictions for Risk Objects (RER)

To protect people and property from space threats it is important to have information of the risk of space objects that are close to a natural uncontrolled re-entry. Besides the risk, it will also be necessary to predict the re-entry time and location in order to take preventive measures. Since the re-entry problem is quite complex, refined analysis will be required in order to achieve satisfactory accuracy levels.

1.3.2.5 Object and Maneuver/Mission Characterization (OMC)

The OMC service will monitor and identify the active spacecraft; also it will offer the required data to execute orbit changes. Finally, after the active objects maneuvers it will characterize its new orbit.

1.3.2.6 Special Mission Support (SMS)

When special mission support is required, the SMS service will make an in-time tracking of the orbit with high precision. The most common situations when mission support is needed are in release or maneuvers operations.

1.3.2.7 Characterization of sub-catalogue[5] debris (DEB)

When the sensors are not in use, it is possible to use them to track some specific regions of the space to characterize the sub-catalogue debris environment. The detailed specific information will be used to develop a database with the derived statistical information and validate models of the sub-catalogue population.

1.4 Overview of the current European Space Sensors

It has been mentioned that Europe through the SSA is after an autonomous system in order to eliminate its external dependence. It is forecasted to be fully operational around 2019, so in the meantime, the European Space Agencies will still depend on the information provided by NORAD and JSpOC. In this section, an overall review of the actual available SST sensors will be done in order to see the actual limitations, but also to understand the great accuracy of these sensors.

1.4.1 TIRA Radar

Figure 4: FGAN Tracking and Imaging Radar (TIRA). Source: [1]

[5] Sub-catalogue: it will contain objects out of the lower threshold of the catalogue but larger tan 1/10 of what is specified to be catalogued.

TIRA is the abbreviation of Tracking and Imaging Radar; it is located in Wachtberg, Germany and it belongs to FGAN[6] (Forschungsgesellschaft fur angewandte Naturwissenchaften) and can track non cooperative targets in L-band (1.33 GHz) with a minimum diameter of 2 cm at a distance of 1000 Km. However, its normal operational resolution is in the magnitude order of meters with a pulse period of 30 Hz and an angular resolution of 0.0002 deg.

Its data is transmitted in ASCII[7] format and contains information about azimuth (deg), elevation (deg), range (Km), range rate (Kms^{-1}) and echo amplitude (dB).

1.4.2 ARMOR RADAR

On the other hand, the only European installation with similar specifications than the FGAN's TIRA radar is the French Navy "Monge" ship. It is a missile range instrumentation ship to support operations of the French ballistic missile program. When the ship is not used for military operations it is anchored in its home base Brest, Brittany. It is in such periods that it provides space tracking services with its two ARMOR radars. They perform non-cooperative tracking in C-band (5.5 GHz) with an angular resolution of 0.0005 deg. The main disadvantage of the ARMOR radar is its location because it is mobile. That means that all the measurements taken on the ship have dependence on GPS positions of the radar.

1.4.3 ESA ZEISS TELESCOPE

The Zeiss telescope is located in Tenerife; it has a liquid nitrogen cooled CCD array that accumulates photons during exposure times from 1 to 4 seconds. This technology allows the detection of objects with a minimum diameter of 15 cm at GEO altitudes ([1] page 42). It has an aperture of 1m and a field of view of 0.7º, another special feature of the telescope is that the detected object position is defined relative to reference stars. This technique makes the pointing errors of the telescope irrelevant.

1.4.4 GRAVES ELECTRONIC FENCE

[6] FGAN: Research Institute for High Frequency Physics and Radar Techniques (FHR) is located on the southern boundary of North Rhine-Westphalia, on the slopes of the Wachtberg near Bonn. Its conspicuous characteristic is the "Kugel" (ball), the world´s largest radome with a diameter of 49 meters, which houses the space observation radar TIRA (tracking and imaging radar).

[7] ASCII (American Standard Code for Information Interchange): is a character-encoding scheme originally based on the English alphabet for computers and communication equipment.

The GRAVES system (Grande Réseau Adapté à la Ville Spatial) is a set of VHF antennas array located near Dijon, France. It is owned by the French Department of Defense and it can track objects up to altitudes of 1000 Km. In this case the emitter and receiver, which is an array of Yagi antennas, are located in different locations. The GRAVES system produces a self-starting catalog that autonomously builds up and maintains the data. The great advantage of the antenna array is that it has an orbit coverage that reaches inclinations of 28º and at the same time it can handle multiple targets simultaneously. However, the detection size threshold at 1000 Km is of 1m.

CHAPTER TWO: LITERATURE REVIEW

This chapter provides a general overview of the most relevant content found in the literature reviewed. This chapter is divided in four sections that provide essential knowledge for the development of the project. The first section describes the collision risk reduction operations that are done by the most relevant European Space Operators and the main difficulties that they find. In the second and third part the collision detection and collision risk problems are developed because they compound the basic theory for the project. Finally, the fourth section provides a general view of all the reference frames and international conventions that are going to be used in the project.

2.1 SATELLITE COLLISION RISK REDUCTION OPERATIONS

After some concepts about space debris, an overview of the future European SSA system and the current sensors in Europe, in this section the general Collision Risk Reduction procedures will be exposed, based on those followed by the most detachable European space operators as ESA, the French Space Agency CNES[8], the German Space Agency DLR/GSOC[9], EUMETSAT [10]and ASTRIUM[11].

2.1.1 INTRODUCTION

After the collision between Iridium 33 and Cosmos 2251 debris in January 2009, it became obvious that the European satellites operators had very limited capacity to handle risky satellite encounters.

Before the Iridium accident the only way for the European space operators and space agencies to have access to information about space debris was through the TLE.

[8] Centre National d'Etudes Spatiales (CNES): founded in 1961 it is the government agency responsible for shaping and implementing France's space policy in Europe.

[9] GSOC: is the abbreviation of German Space Operations Center.

[10] EUMETSAT: is the European Organization for the Exploitation of Meteorological Satellites.

[11] Astrium: is a European Aeronautic Defense and Space Company that belongs to the EADS group.

TLE (Two-line Elements message) is a data format that informs about the positions of the objects collected by NORAD database. The North American Aerospace Defense Command (NORAD) database contains the real time position of about 16K near Earth orbiting objects with a size larger than 10 cm. The database is freely available in the internet for all users. However, after the Iridium collision it was proved that the accuracy of TLEs was not enough to satisfactorily predict the collision risk of space objects.

The main disadvantage of the TLE data is that no covariance information is provided; this is why no risk assessment can be done. The only safety procedure that can be performed is to define a volumetric safety envelope that cannot be trespassed by any object. But, the low accuracy of the data and the high density of near Earth orbiting objects, especially in LEO, would force to perform too many avoiding maneuvers.

After the Iridium incident, the Joint Space Operations Center (JSpOC) started to provide to the space operators emails containing conjunction alerts when one of their satellites was going to have a close approach with an overall miss distance lower than 1 Km for LEO and 5 Km for upper trajectories. Nowadays, these alerts still inform the satellite operators that one of its satellites is under a collision risk. The operators have the possibility to subscribe to the Conjunction Summary Messages (CSM) to have access to more accurate data. For LEO satellites, the CSM is currently provided when the minimum distance is less than 1 Km or the radial distance is less than 200 m and the time of closest approach is less than 72h. The CSM contains data of the position of the objects with a relative higher accuracy than the TLE and it also provides the covariance information.

Currently, when a space operator receives an alert from JSpOC the operator starts a standard procedure to give a fast response to the threat. Generally, the process can be divided in the following steps.

- Warning reception.
- Risk computation.
- Maneuver calculation.
- Confirmation.
- Maneuver.

In the following sections the previous steps will be detailed explained.

2.1.2 Coarse Assessment

The Coarse Assessment is the most open phase of all, in some cases the assessment is indirectly done by JSpOC when sending the conjunction alert or the

CSM. In [5] it is explained how GSOC uses the TLE information to make an initial conjunction detection for the next upcoming 7 days, the collision envelope used is 10 km distance for in-track and cross-track and 3km in radial direction.

The coarse assessment depends on the collision criteria of the operator and also depends on the access to a refined assessment. Reference [6] describes an example of conjunction risk alerts management. In that specific case the most accurate information that they have is the CSM. So they decide if the maneuver has to be done based on that information. On the other hand GSOC and CNES have access to space sensors, so when they receive a CSM the first step is to program a radar tracking campaign.

2.1.3 Refined Assessment

When the operator has access to the tracking systems previously described in section 1.4, new and more precise orbit information is obtained. After that, a new conjunction risk analysis is carried out. The maneuver decision is not taken until the last moment because all operators agree that in most cases the risk of collision decreases as the time of closest approach is closer and the computation becomes more accurate. However, in the negative case that the risk remains high, a notification to the flight dynamics department is done to announce that a maneuver has to be done.

2.1.4 Maneuver Computation

The flight dynamics department computes several maneuvers. From those, only three are selected following the criteria of lower probability risk and also lower fuel consumption. The most common practice is to send back to JSpOC the new three ephemerides[12] of the maneuver result.

2.1.5 JSpOC Confirmation

Typically, within a few hours JSpOC provides an answer to the sent ephemeris, they do not provide any recommendation or probability value, because they cannot assume any commitment concerning the management of an operator owned satellite. The only information that they offer is if the new orbit is still under risk of collision or not.

2.1.6 Final Maneuver

[12] Ephemeris: it is a table of values that provides the position of an astronomical object during a given time interval. JSpOC only accepts ephemeris in the Mean Equator Mean Equinox frame in Cartesian coordinates using km as a length unit and with the date format: 77dddhhmmss.sss as described in [6]

If the new maneuver is confirmed by JSpOC to be safe, it will be done. There are many different types of avoiding maneuvers and its discussion is out of the bounds of this project. However, as it can be appreciated in Figure 5 a very simple strategy would be to perform a tangential speed increment in the semi period before the conjunction and a tangential speed decrement of the same module than the previous in the semi period after the conjunction in order to recover the original orbit.

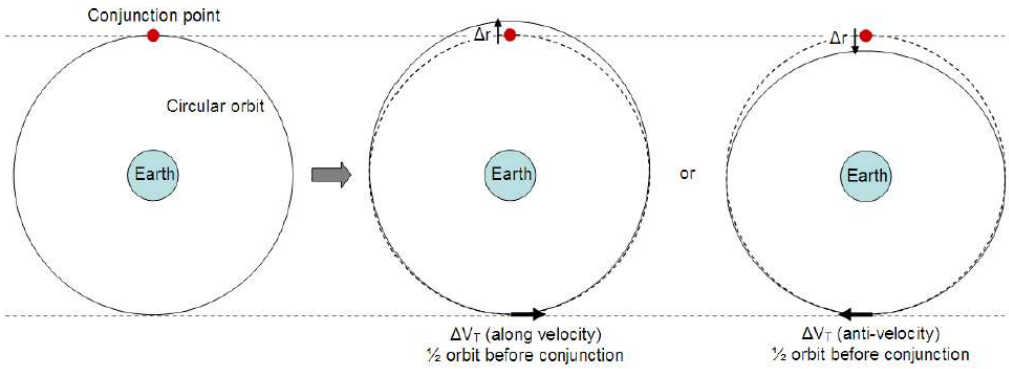

Figure 5: Radial separation performed through a tangential maneuver. Source: [6]

2.2 Conjunction Detection

The conjunction detection problem for a large spacecraft catalog is not a simple task as it has been proved in [7] and [8]. However, for the study of conjunction risk assessment, the conjunction detection is only required to be done for two objects, that's why no complex filtering systems are required.

In this section the bisection, Regula-Falsi, Newton-Raphson, Alfano and Brent methods are going to be exposed. Nevertheless, it is important to underline a couple of concepts before exposing the previously noted methods.

The point of closest approach is defined as one point along the path of two objects where their relative velocity ($\overrightarrow{v_r}$) is normal to their relative position ($\overrightarrow{r_r}$), so when ($f(t) = 0$). Where:

$$f(t) = \overrightarrow{v_r} \cdot \overrightarrow{r_r} \qquad \textbf{Eq. 1}$$

To simplify the notation of the whole report, $f(t)$ will keep the same meaning in all the following sections. Note that this condition is equivalent to a zero pole in the relative velocity, which can lead to a maximum or minimum distance point. In order to disambiguate this, it is necessary to impose an additional condition for the relative acceleration, which should be positive (condition for minimum).

2.2.1 BISECTION METHOD

The starting point of the bisection method is a time interval $[a\,,b]$ where $a = t_0 - T/2$ and $b = t_0 + T/2$ being (T) the time span and (t_0) the center of the time span. Such interval fulfills $sign(f(a)) \neq sign\big(f(b)\big)$ which basically means that there is a close approach of two objects within the interval.

The bisection method divides the space between the two points each step, and evaluates in which of the two resultant intervals the close approach takes place. So a third point is computed $c = (a + b)/2$ and then if $sign(f(a)) \neq sign\big(f(c)\big)$ the point to be is assigned a new value $b' = c$, on the other hand if $sign(f(c)) \neq sign\big(f(b)\big)$ then $a' =$ c. This process is repeated as many times until the resultant interval is below a user established minimum time difference precision value.

2.2.2 REGULA-FALSI ROOT FINDER

The Regula-Falsi method is very similar to the bisection method, with the difference that instead of dividing the time interval by half each step, it takes into account the module of the $f(t)$ function at each extreme. The advantage of this method with respect to the previous one is that it has a faster convergence. So in this method the middle point (c) is computed the following way:

$$c = \frac{(a \cdot f(b) - b \cdot f(a))}{f(b) - f(a)} \qquad \textbf{Eq. 2}$$

This method has problems when the real time of closest approach is very close to one of the bounds of the range.

2.2.3 NEWTON-RAPHSON METHOD

The Newton-Raphson method is a well know iterative method to find the roots of a real-valued function. Given $f(t)$, its derivative $f'(t) = df(t)/dt$ and a first time of closest approach estimation (t_0), the function is approximated by its tangent line at the first guess time.

$$t_{n+1} = t_n - \frac{f(t_n)}{f'(t_n)} \qquad \textbf{Eq. 3}$$

The iterative process is done until $abs(t_{n+1} - t_n) \leq minimum\ error$ where the minimum error is established by the user. The most important drawback of this method is the need to compute $f'(t)$ but on the other hand it has a better convergence.

2.2.4 ALFANO AND NEGRON METHOD

Alfano exposes in [9] a method to compute the time of closest approach by approximating the relative velocity equation to a cubic polynomial equation and then once found the time of the closest approach the miss distance is computed by a fifth order polynomial approximation. This method also requires knowing the relative accelerations between the two objects.

The relative position and its derivatives are calculated using the following formulas.

$$g(t) = \vec{r_r} \cdot \vec{r_r} \quad \text{Eq. 4}$$

$$\dot{g}(t) = 2 \cdot \vec{r_r} \cdot \dot{\vec{r_r}} \quad \text{Eq. 5}$$

$$\ddot{g}(t) = 2 \cdot \left(2 \cdot \vec{r_r} \cdot \ddot{\vec{r_r}} + 2 \cdot \dot{\vec{r_r}} \cdot \dot{\vec{r_r}}\right) \quad \text{Eq. 6}$$

Then the TCA is computed by finding the root of the cubic polynomial equation of $\dot{g}(t)$ considering that $\dot{g}(tca) = 0$ and $\ddot{g}(tca) > 0$.

$$C(\tau) = \gamma_3\tau^3 + \gamma_2\tau^2 + \gamma_1\tau^1 + \gamma_0 \quad \text{Eq. 7}$$

The fifth polynomial order approximation is done component by component, so in other words three equations must be computed in order to get the miss distance value by calculating the module of the three components.

$$Q_i(\tau) = \sigma_5\tau^5 + \sigma_4\tau^4 + \sigma_3\tau^3 + \sigma_2\tau^2 + \sigma_1\tau^1 + \sigma_0 \quad \text{Eq. 8}$$

2.2.5 BRENT'S METHOD

Brent's method as exposed in [10] is a combination of the secant method and the inverse quadratic interpolation in order to increase the convergence with respect to the bisection method.

It follows the same basic principles as the bisection method with the main difference that it uses two methods to compute the (c) value and it switches between them in order to improve the global convergence.

The algorithm ensures all the time that $|f(b)| < |f(a)|$ so if this expression is not fulfilled the values of (a) and (b) are switched, this ensures that the b value is always closer to the root.

The inverse quadratic interpolation is applied when the two interval extremes are different from the previous (b) extreme ($\{f(b_n)\ \&\ f(a_n)\} \neq f(b_{n-1})$).

$$c_n = \frac{a_n f(b_n) f(b_{n-1})}{(f(a_n) - f(b_n))(f(a_n) - f(b_{n-1}))} + \frac{b_n f(a_n) f(b_{n-1})}{(f(b_n) - f(a_n))(f(b_n) - f(b_{n-1}))} + \frac{b_{n-1} f(a_n) f(b_n)}{(f(b_{n-1}) - f(a_n))(f(b_{n-1}) - f(b_n))} \quad \text{Eq. 9}$$

In the normal case when $(\{f(b_n)\ or\ f(a_n)\} = f(b_{n-1}))$ the secant method is applied.

$$c_n = b_n - f(b_n)\frac{b_n - a_n}{f(b_n) - f(a_n)} \quad \text{Eq. 10}$$

2.2.6 Conjunction Detection Conclusions

From the previous exposed conjunction detection methods the Newton-Raphson and Alfano are not suitable for the purpose of this project since they require information about the acceleration and only advanced propagators provide the acceleration in the ephemeris. Brent's Method does not require knowledge about the object acceleration but since it switches between two different expressions in some situations it has an unusual behavior that leads to convergence problems.

On the other hand, the bisection method is an extremely simple method but it has a very low convergence rate. This is the reason why the Regula-Falsi rood finder seems to be the most appropriate solution for this project, since it has a greater convergence rate than the bisection method but it preserves its simplicity.

2.3 Collision Probability Problem

In section 2.1, different European space agency's collision avoidance procedures have been described. As it has been clearly exposed one of the first response measures for a potential collision between two spacecraft is the collision probability computation. In this section, an overall description of the Collision Probability problem will be exposed, showing the most popular solving approximations and approaches. First of all, the general problem will be presented, then it will be simplified through a set of assumptions. After that, three general methodologies: linear, non-linear, Monte Carlo and their particular solutions will be exposed.

2.3.1 Problem definition

Given two orbiting objects, being operational satellites or space debris, the collision risk of the two objects is the probability that one object could intercept the other,

resulting a catastrophic or lethal encounter. In the standard terminology the object of interest is referred as the target and the threating object is the chaser.

The current orbit acquisition systems provide information about the objects trajectories and velocities with a certain level of uncertainty. That is why theoretically, the position of an orbiting object is defined as the addition of a mean position vector ($\vec{\bar{r}}$) with some uncertainty($\vec{e}$); this uncertainty is supposed to follow a normal Gaussian distribution and is provided through the position covariance matrices.

$$\vec{\bar{r}_t} = \vec{\bar{r}_t} + \vec{e_t} \quad and \quad \vec{\bar{r}_c} = \vec{\bar{r}_c} + \vec{e_c} \qquad \textbf{Eq. 11}$$

Figure 6 provides a visual idea of the general problem. Two objects: target and chaser are presented with their respective position vectors ($\vec{\bar{r}_t}$, $\vec{\bar{r}_c}$), the two ellipses represent the position uncertainty cloud. Each object has a different velocity ($\vec{v_t}, \vec{v_c}$) with some amount of uncertainty. However, in the next pages it will be proved that the velocity uncertainty is not as relevant as the positional. The relative position between the two objects is ($\vec{\bar{\rho}}$), which at the time of closest approach (TCA) is named: miss distance. As seen in [11] the miss distance as well as the collision probability are decisive factors when evaluating the risk of collision.

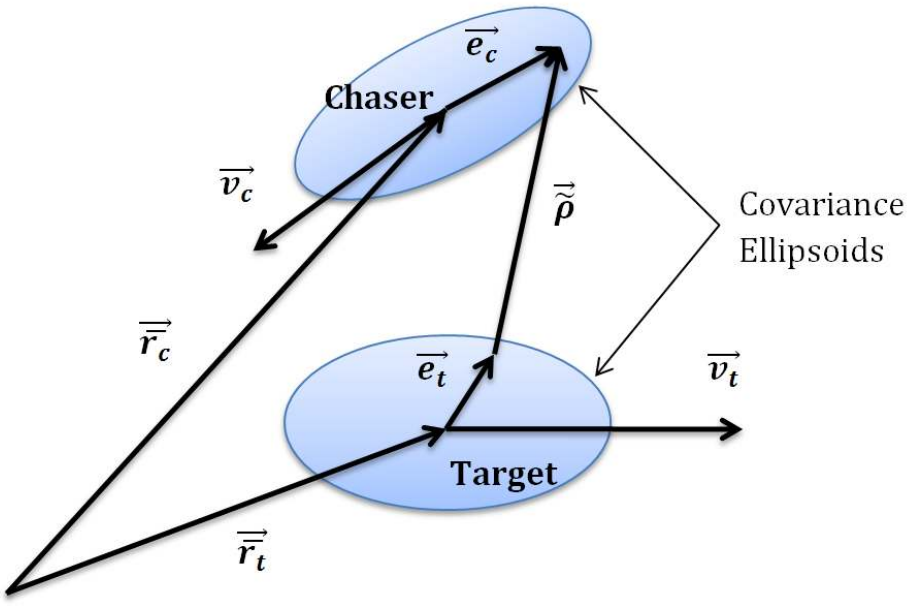

Figure 6: Encounter variable definition, Inspiration source: [18].

To continue with the problem approach, the combined position covariance matrix of the two objects must be computed and the resultant ellipsoid is centered in the

target. An interesting concept is the encounter region which is obtained by multiplying the combined covariance matrix by a scaling factor (n) to define the encounter region. Generally, the scaling factor goes from 3 to 8.5 to accommodate conjunction probabilities ranging from 97.070911% to 99.999999%. As is can be appreciated in Figure 7 the chaser trespasses the encounter region creating a swept tube named collision tube. Hence, the total probability of collision is the integration of the probability density function contained inside the collision tube and the covariance ellipsoid.

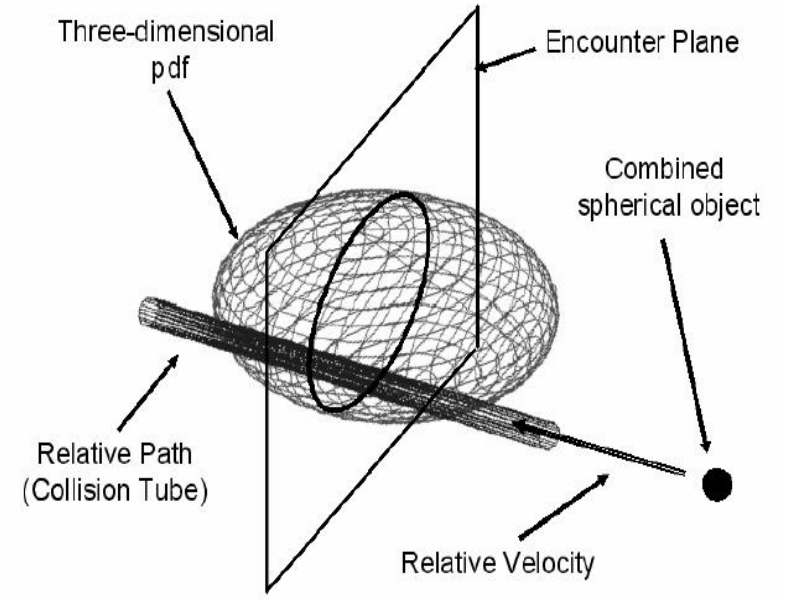

Figure 7: Conjunction Encounter Visualization [12].

The mathematical expression of P is the following volumetric integral of the portion of the combined Gaussian probability density distribution of the two objects that is swept out by the combined bodies of the two objects.

$$P = \frac{1}{(2\pi)^{1.5} \cdot \sqrt{\det(p)}} \int_V \exp(-S)\, dV \qquad \textbf{Eq. 12}$$

Where S is:

$$S = (\tilde{\rho} - \bar{\rho})^T p^{-1} (\tilde{\rho} - \bar{\rho})/2 \qquad \textbf{Eq. 13}$$

The bracket section of the formula is the diagonal frame of the position covariance matrix. Probably, the most difficult aspect is the evaluation of the integration volume.

The analytical computation of such integral is not feasible because only very few cases have an analytical solution and the direct numerical computation as seen in [13] has very high computational costs that make its operational application not

feasible. This is why the best is to make some assumptions to considerably simplify the problem.

2.3.2 SIMPLIFICATIONS OF THE PROBLEM

2.3.2.1 Body spheres

In a first approach the objects will be treated as perfect spheres in order to simplify the problem and avoid the complication of considering the object's attitude. However, in some papers [14], [12] it is suggested or directly explained that this assumption is not done and random shapes are considered, which means that it is possible to consider the shape of the objects but it makes the solving routines more complex. In addition, considering the bodies as spheres is a conservative hypothesis that provides a safer result. The collision is accounted when the relative position of the target and chaser is less than the sum of the two bodies' radii.

2.3.2.2 Uncorrelated covariance matrices

The estimation of the object trajectories are done sometimes by common sensors or systems, with common biases or estimation algorithms. So it is difficult to declare that all the measurements taken are uncorrelated. This fact implies an obstacle when computing the combined covariance matrix for the computation of the collision probability risk.

$$P_{\Delta\Delta} = P_{tt} + P_{cc} - (P_{ct} + P^{T}{}_{ct}) \qquad \textbf{Eq. 14}$$

As seen in the previous equation; to obtain the combined covariance matrix it is required to know the correlation between the two existing covariance. This data is not known because the correlations in such a complex system as the orbit determining systems depend on so many variables that are impossible to know. However, assuming that $P_{ct} = 0$, as seen in [15], only introduces a small amount of error, about 7% in the worst cases; also it is known that the correlation dissipates fast over a short period of time.

This is why it is necessary to make the assumption of uncorrelated covariance. The result of this assumption is that the correlated matrix is obtained with a simple addition.

$$P_{\Delta\Delta} = P_{tt} + P_{cc} \qquad \textbf{Eq. 15}$$

2.3.2.3 Linear path

It is fully known that near Earth orbiting objects follow curvilinear trajectories due to the influence of the gravitational field of the Earth. Nevertheless, it is also known that typical orbiting speeds of those objects are for an order of magnitude of 7 Kms[1]

as exposed in [16] which means that relative velocities can even be higher. Consequently, in most of the cases the encounter time is extremely short, and the trajectory can be easily considered linear during the encounter.

To prove that the consideration of linear path does not introduce much error, a comparison between rectilinear and curvilinear encounter is going to be done. Figure 8 describes the relative configuration of two circular trajectories with radius R and their straight line approximations. The separation between the two objects is a distance S and their velocities each make an angle α with a straight line joining them. Let C denote the arc length and L denote the linear approximation of the arc.

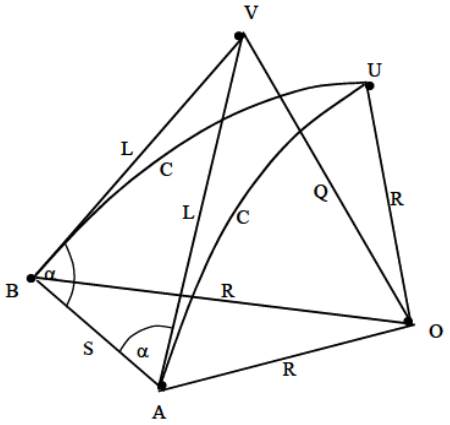

Figure 8: Linear Approximation of Motion in Encounter Region. Source: [17].

U is the intersection point of the two curvilinear trajectories and V it is analogous of the linear paths. Thus, the following expressions can be easily extracted.

$$L = \frac{S}{2 \cdot \cos\alpha} \quad ; \quad C = R \cdot \tan^{-1}\left(\frac{L}{R}\right) \qquad \textbf{Eq. 16}$$

Let ε and δ be the accuracy level of the approximation of C by L and the approximation of R by Q.

$$\varepsilon = \frac{L}{C} - 1 \quad ; \quad \delta = \frac{Q}{R} - 1 = \sqrt{\left[1 + \left(\frac{L}{R}\right)^2\right]} - 1 \qquad \textbf{Eq. 17}$$

As seen in Table 2 and in [17] the accuracy parameter is exceptionally good, so it can be concluded that the linear approximation for most of the cases is perfectly acceptable, as a consequence the mathematical complexity of the problem is reduced and also the computational load is minimized.

Angle α	45°	80°	89°
Line L (km)	1.41421356	5.758770	57.298
Arc C (km)	1.41421354	5.758769	57.297
Accuracy ε	10^{-8} : 1	10^{-7} : 1	10^{-5} : 1
Accuracy δ	10^{-8} : 1	10^{-7} : 1	10^{-5} : 1

Table 2: Approximation errors for some example cases with a separation S= 2Km and R= 7151Km as parameters. Source [17].

2.3.2.4 Velocity uncertainty

As explained in the previous section the speeds of the orbiting objects are quite high and the normal values of speed uncertainties are of some meters, this means that the magnitude of the error is of 10^{-4}. That is why in most of the collision probability approaches the velocity covariance is neglected.

Furthermore, it is also rational to consider that the speed remains constant during the encounter because of the short encounter time and the linearity of the path.

2.3.2.5 Simplification of the integral

In the problem definition, the perturbed trajectories of the space objects are defined as $(\vec{\tilde{r}}_t, \vec{\tilde{r}}_c)$.

$$\vec{\tilde{r}}_t = \vec{r}_t + \vec{e}_t \quad \text{and} \quad \vec{\tilde{r}}_c = \vec{r}_c + \vec{e}_c \qquad \textbf{Eq. 18}$$

Thus, regarding a rectilinear trajectory and neglecting the uncertainty in the speed, the trajectory of the objects during the encounter is modeled as:

$$\vec{\tilde{r}}_t(t) = \vec{\tilde{r}}_t + \vec{V}_t \cdot t \quad \text{and} \quad \vec{\tilde{r}}_c(t) = \vec{\tilde{r}}_c + \vec{V}_c \cdot t \qquad \textbf{Eq. 19}$$

Then, the miss distance vector between the chaser and the target is defined as:

$$\begin{aligned} \vec{\tilde{\rho}}(t) &= \vec{\tilde{r}}_c(t) - \vec{\tilde{r}}_t(t) \\ &= \vec{r}_c - \vec{r}_t + (\vec{V}_c - \vec{V}_t) \cdot t + \vec{e}_c - \vec{e}_t \\ &= \vec{\rho} + \vec{V}_r \cdot t + \vec{e}_c - \vec{e}_t \\ &= \vec{\tilde{\rho}} + \vec{V}_r \cdot t \end{aligned} \qquad \textbf{Eq. 20}$$

Both last terms are the nominal miss distance and the relative velocity, viewed from the target's point of view. From geometry, the time of closest approach must satisfy $\delta/\delta t \cdot (\tilde{\rho} \cdot \tilde{\rho}) = 0$ leading to the following condition:

$$\begin{aligned} \frac{d}{dt}\left(\vec{\tilde{\rho}}(t) \cdot \vec{\tilde{\rho}}(t)\right) &= \frac{d}{dt}\left[(\vec{\tilde{\rho}} + \vec{V}_r \cdot t) \cdot (\vec{\tilde{\rho}} + \vec{V}_r \cdot t)\right] \\ &= \frac{d}{dt}\left[\vec{\tilde{\rho}} \cdot \vec{\tilde{\rho}} + 2 \cdot (\vec{\tilde{\rho}} \cdot \vec{V}_r)t + (\vec{V}_r \cdot \vec{V}_r)t^2\right] \\ &= 2\vec{\tilde{\rho}} \cdot \vec{V}_r + 2(\vec{V}_r \cdot \vec{V}_r)t = 0 \end{aligned} \qquad \textbf{Eq. 21}$$

Solving the previous equation, the result is the time of closest approach (TCA).

$$t_{ca} = -\frac{\vec{\tilde{\rho}} \cdot \overrightarrow{V_r}}{\overrightarrow{V_r} \cdot \overrightarrow{V_r}} \qquad \text{Eq. 22}$$

Once the time of closest approach has been obtained, the projection of the error of the miss distance onto the relative speed vector will be investigated.

$$\begin{aligned} \left[\vec{\tilde{\rho}}(t_{ca}) - \bar{\rho}\right] \cdot \overrightarrow{V_r} &= \left[\vec{\tilde{\rho}} + \overrightarrow{V_r} \cdot t_{ca} - \bar{\rho}\right] \cdot \overrightarrow{V_r} \\ &= \left(\vec{\tilde{\rho}} \cdot \overrightarrow{V_r}\right) + \left(\overrightarrow{V_r} \cdot \overrightarrow{V_r}\right) \cdot t_{ca} - \bar{\rho} \cdot \overrightarrow{V_r} \\ &= -\bar{\rho} \cdot \overrightarrow{V_r} = 0 \end{aligned} \qquad \text{Eq. 23}$$

That last result is highly relevant for the simplification of the integral computation because for instance, if the error is defined as $e_a = 0,\ e_b = 0$ then $\tilde{\rho} = \bar{\rho}$ and $t_{ca} = 0$. The tca equation becomes:

$$\bar{\rho} \cdot \overrightarrow{V_r} = 0 \qquad \text{Eq. 24}$$

So, there is not uncertainty in the miss distance in the direction of relative velocity in the time of closest approach and also the result is true for all possible collision cases. To take advantage of the previous found property a new set of orthogonal coordinate system is defined as seen in [18]. With one axis pointing through the relative velocity and another normal to the collision plane, one axis of this system is left without uncertainty and the integral becomes two-dimensional. Consequently the total probability can be computed integrating the probability distribution in the encounter plane contained in the combined radii circle centered in the chaser relative position.

2.3.2.6 Two-dimensional equation

Regarding all previous simplifications, the three-dimensional integral exposed at the beginning of this section, gets significantly simplified and becomes the following two-dimensional equation.

$$\begin{aligned} P &= \frac{1}{2\pi|p^*|^{1/2}} \int_{-R}^{R} \int_{-\sqrt{R^2-x^2}}^{\sqrt{R^2-x^2}} \exp(-S^*)\, dxdy \\ S^* &= \frac{1}{2}(\tilde{\rho} - \bar{\rho})^T p^{*-1} (\tilde{\rho} - \bar{\rho}) \end{aligned} \qquad \text{Eq. 25}$$

Where the radii combination of the target and chaser is $COR = R_t + R_c$, P^* is the covariance matrix projected into the encounter plane, $\tilde{\rho}$ is the uncertain miss distance and $\bar{\rho}$ is the mean miss distance with a fixed value.

In the following section, once the linear problem has been fully developed, different linear solutions proposed by Foster, Chan, Patera and Alfano will be exposed.

2.3.3 LINEAR METHODS

Taking advantage of the previous simplifications there are several approaches proposed by different authors to compute the linear conjunction risk.

2.3.3.1 Akella and Alfriend's Method

Akella and Alfriend's method simply consists on performing a bi-dimensional numerical integration of the equation obtained in the previous section. It is the simplest method although it is the one with the highest computational load. However, with the current processors accurate results can be obtained in times shorter than one second.

2.3.3.2 Foster's Method

It is similar to the previous methodology; the idea also is to compute directly the two-dimensional integral dividing the projected area in small sections and adding each probability section value to the final probability result. In this approach the coordinate system is switched to polar coordinates in the encounter plane. Where Ro and ϕ define the combined object center location. COR is the combined object radius, σ_u and σ_w are the principal axes standard deviations and r and θ are the polar variables. With the coordinate system change, the probability expression exposed in the previous section becomes:

$$P = \frac{1}{2\pi\sigma_u\sigma_w}\int_0^{COR}\left[\int_0^{2\pi}\exp\left[\frac{-1}{2}\left[\left(\frac{R_o\cdot\sin\phi - r\cdot\sin\theta}{\sigma_u}\right)^2 + \left(\frac{R_o\cdot\cos\phi - r\cdot\cos\theta}{\sigma_w}\right)^2\right]\right]rd\theta\right]dr \qquad \text{Eq. 26}$$

In [12] the angle θ step of 0,5º and radius r step of COR/12 are recommended. This model is the current one used by NASA to assess the collision risk of the ISS. However, this method presents some problems in special cases when the object radius is smaller than the miss distance, but larger than the standard deviation. Anyway, this small problem is solved decreasing the step size.

2.3.3.3 Chan's Method

Chan developed an analytical solution for the collision probability in the form of an infinite series which is convergent for most of the common values. For a combined

object radius between 1-100m, a miss distance of 10m-100Km and a covariance between 1-10Km. Using the concept of equivalent areas, the two-dimensional probability distribution function is transformed into a one-dimensional Rician function:

$$P = \exp\left(\frac{-v}{2}\right) \cdot \sum_{m=0}^{\infty} \left[\frac{v^m}{2^m \cdot m} \cdot \left(1 - \exp\left(\frac{-u}{2}\right) \cdot \sum_{k=0}^{m} \frac{u^k}{2^k \cdot k!} \right) \right] \quad \text{Eq. 27}$$

Where:

$$u = \frac{COR^2}{\sigma_x \cdot \sigma_y} \quad ; \quad v = \frac{{x_m}^2}{{\sigma_x}^2} + \frac{{x_m}^2}{{\sigma_x}^2} \quad \text{Eq. 28}$$

The combined object radius is centered in the encounter plane (x_m, y_m) and the σ_x, σ_y are the principal axes standard deviations. Despite having a limited application, this formula simplifies the probability evaluation and makes it very fast. Obviously, the more terms of the series are used the slower is the evaluation. Nevertheless, in [12] it is recommended not to exceed m=10.

2.3.3.4 Patera's Method

Patera uses a mathematical equivalence to transform the base integral to a one-dimensional path integral. In order to make it possible, a scaling factor has to be applied to one of the main axis of the covariance in the encounter plane. With the scaling, the probability distribution becomes symmetrical and then the equation can easily be transformed into polar coordinates.

If the origin is excluded from the two-body ellipse the probability is:

$$P = \frac{-1}{2\pi} \oint_{ellipse} \exp(-\alpha r^2)\, d\theta \quad \text{Eq. 29}$$

When the origin is included in the hard-body ellipse:

$$P = 1 - \frac{1}{2\pi} \oint_{ellipse} \exp(-\alpha r^2)\, d\theta \quad \text{Eq. 30}$$

One of the main advantages of this method is that it can handle random shapes of objects altering the way of solving the linear integral. However, the hypothesis of spherical objects, as previously stated, is more conservative and accurate enough for this study.

2.3.3.5 Alfano's Method

Alfano in [19] makes use of a series of combined error functions and exponential terms to approximate the two-dimensional equation. Given the center of the combined object (x_m, y_m) and the standard deviations (σ_x, σ_y) of the encounter plane.

$$P = \frac{2COR}{n\sigma_x\sqrt{8\pi}} \sum_{i=0}^{n} \left[\operatorname{erf}\left[\frac{y_m + \frac{2COR}{n}\sqrt{(n-i)i}}{\sigma_y\sqrt{2}} \right] + \operatorname{erf}\left[\frac{-y_m + \frac{2COR}{n}\sqrt{(n-i)i}}{\sigma_y\sqrt{2}} \right] \exp\left[\frac{-\left(\frac{COR(2i-n)}{n} + x_m\right)^2}{2{\sigma_x}^2} \right] \right] \quad \text{Eq. 31}$$

The numerical integration method used to evaluate the expression is the Simpson's one-third rule and the series is broken into m-even and m-odd components.

$$m = \operatorname{int}\left(\frac{5COR}{\min\left(\sigma_x, \sigma_y, \sqrt{{x_m}^2 + {y_m}^2}\right)} \right) \quad \text{Eq. 32}$$

The previous expression provides the minimum number of terms with a lower bound of 10 and upper limit of 50.

2.3.3.6 Maximum Probability Assessment

All the five methods previously exposed have been designed considering that the covariance matrix is well defined. Nevertheless, in frequent situations the positional data of the objects is very poor and the resultant probability obtained with the previous methods is below its real value. In [20] Alfano develops a complex method to compute the maximum probability for rectangular objects. However, from that study an extremely simple expression is obtained to find a higher bound for the probability risk assessment when no quality data is available.

$$P_{max} = 0.48394 \cdot r \quad \text{when } r < 0.8 \quad \text{Eq. 33}$$

$$P_{max} = 0.21329 \cdot \exp(1.01511 \cdot r) - 0.09025 \quad \text{when } 0.8 \leq r < 1 \quad \text{Eq. 34}$$

$$P_{max} = 0.5 \quad \text{when } r = 1 \quad \text{Eq. 35}$$

Where:

$$r = \frac{COR}{MissDistance} \qquad \text{Eq. 36}$$

r: the combined object radius scaled with the Miss Distance. The previous expression is the result of the approximation to three significant figures of a non-linear equation that expresses the probability of collision in the worst possible configuration. Such configuration regards that the principal axis of the covariance projected ellipse is larger than the minor axis and that the relative position of the object is aligned with the major axis of the combined covariance ellipse. Consequently, the resultant probability risk will be over inflated. However it is still the best way to evaluate the conjunction risk when poor data is provided because it generates a conservative result.

2.3.4 NON-LINEAR METHODS

In some rare cases the assumption of linear relative motion may not be valid, as it will be explained in this section. Some authors proposed different criteria to determine if the hypothesis of linearity is applicable. Generally non-linearity is associated with long-term encounters where the relative path cannot be considered a straight line and the covariance can no longer be assumed static. Then, a different approach to the problem must be taken.

There is a huge offer of solutions for the non-linear problem. Nevertheless, in this paper only the most relevant and original methods will be summarized. There are also different criteria to establish if the conjunction can be assumed linear, Dolado provides an interesting solution because of its simplicity.

2.3.4.1 Dolado's methodology

This method is extremely simple; Dolado establishes in [21] through a geometric and probabilistic analysis relative velocity intervals to determine the encounter type.

If the relative velocity is between 1 to 5ms^{-1}, the conjunction cannot be considered linear, and both the position and velocity errors must be taken into account to compute the conjunction probability.

When the relative velocity is in the range between 5 to 10ms^{-1}, the conjunction can be considered linear but the position and velocity errors have to be considered.

Finally, if the relative velocity is higher than 10ms^{-1} at TCA the conjunction is considered linear and the velocity errors can be dismissed.

2.3.4.2 Adjacent cylinders

The method of adjoining tubes consists on dividing the encounter time in short time steps that fulfill the user linear tolerance. Each time step is small enough that the covariance and velocity can be assumed constant and the linear simplifications can be applied. Each section is transformed into the Mahalanobis[13] space. The two-dimensional section probability is computed as described in the linear methods by projecting the combined object shape onto the plane perpendicular to the relative velocity. Also, a one-dimensional probability is computed along the relative velocity vector by determining the component position from the mean at each end

[13] Mahalanobis space concept: it was first introduced by P. C. Mahalanobis in 1936. The axes of a coordinate system are scaled following the standard deviations of a given covariance matrix.

of the tube and then dividing it by the standard deviation for that axis, thus producing each endpoint's Mahalanobis distance. The cylinder endpoints (M_i, M_f) are used to compute the long-axis probability P_{1d} from:

$$P_{1d} = \left| \frac{1}{2} \cdot \left(\operatorname{erf}\left(\frac{M_f}{\sqrt{2}}\right) - \operatorname{erf}\left(\frac{M_i}{\sqrt{2}}\right) \right) \right| \qquad \text{Eq. 37}$$

The product between the previous probabilities leads to the sectional probability. Finally, all the sectional probabilities are added to obtain the global collision probability.

Figure 9 shows the main disadvantage of this method; when the path is curvilinear, between the tubes appear gaps and overlaps that disturb the final results of the global probability. In the overlaps the probability distribution is computed twice, and in the gaps, the probability distribution is neglected. To reduce the gaps and overlaps influence in the global error, the step size can be reduced. However, the computational cost increases significantly.

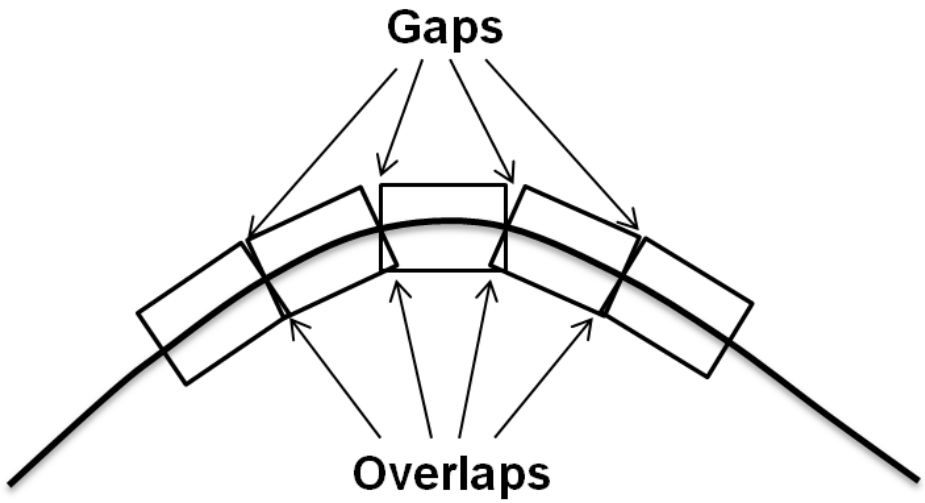

Figure 9: Tube Sections for Nonlinear Relative Motion Track. Source: [22].

The method of adjoining tubes is quite flexible and has several approaches regarding the way to compute the sectional probability. In [23] an alternative approach is exposed with precise results that differ 2% from Monte Carlo [14] simulations.

[14] Monte Carlo: direct numeric approach that provides the most precise results of Collision Probability, extended description in section 2.3.4.6.

2.3.4.3 McKinley's method

To solve the problem of laps and overlaps, McKinley in [24] proposes an algorithm that computes the angle between two consecutive tubes. Then, the tubes are cut in the proper angle to fit consecutive cylinders. This method only accounts for nonlinearities in-plane motion, so if the out-of-plane motion is significant, additional measures are required.

The integration is done in new local frame *(V, N, B)* for each time step, where V points through the axial direction of the cylinder, N is normal to the plane that contains the path and the B completes the right-handed system.

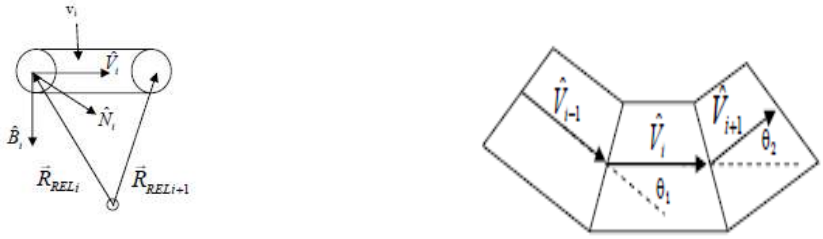

Figure 10: At left the visual definition of the integration frame and at right the overlap correction that the algorithm offers. Source: [24].

2.3.4.4 Method of parallelepipeds

Another method thought to solve the problem of the gaps or overlaps between the cylinders is the method of parallelepipeds. The cylinders are replaced by sets of abutting parallelepipeds. Each parallelepiped end is adjusted to form a compound miter where neighboring tubes meet, thereby eliminating gap or overlap. As in the cylinder method, each section is small enough so that, over the interval, the relative motion can be assumed linear with a constant covariance. Then, the probability of each parallelepiped is computed and summed to obtain the overall probability of the tube section. All sections are summed to produce the overall probability.

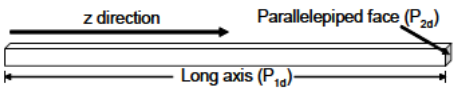

Figure 11: Parallelepiped description. Source: [25].

The general approach applies for all relative motions and is coupled with a modified error function to allow any object shape.

2.3.4.5 Method of voxels

This method is the most precise but also the one that has the highest computational load. As all the methods exposed in this section the method starts with position, velocity data of each object, their covariance matrices and the time of closest approach. The propagation is done forward and backward in time until the user linear limit is reached. At every time step the object and their positional covariance are transformed into the Mahalanobis space. Then it is determined which voxels are contained within the combined, transformed hard body. The voxels that have been accounted in previous iterations are not taken into account in the next iterations. The probabilities of the remaining voxels are computed and added to the total probability computation.

The incremental limits of the time steps have to be carefully selected in order to avoid the combined hard body to skip any voxels. Also the size of the voxels has to be properly chosen in order to match the shape of the object through its path.

2.3.4.6 The Monte Carlo Method

The Monte Carlo methodology is a statistical procedure where random numbers are used to solve numeric problems by running simulations many times over to calculate the probability heuristically. The Monte Carlo Method is used when there is not any alternative left, normally in complex problems with many coupled degrees of freedom involved, or to solve integrals with complicated boundary conditions. The collision probability problem qualifies both previous characteristics, because without any simplification the probability is a 12-dimensional integral with quite complex boundary limits. Coppola in [26] declares that the collision probability without any assumption is the following integral.

$$P = \int_{V_{12}} PDF_0(X_0; t_0) dX_0 \qquad \textbf{Eq. 38}$$

Where X_0 is the initial state matrix that contains the position and velocity of both target and chaser, t_0 is the initial time and (PDF_0) is the probability distribution function. Thus, roughly in can be proved that despite from the beginning of the text the problem has been presented partially simplified the real problem is very complex and the only direct numerical solution is the Monte Carlo method.

The idea is to use the six-by-six position and velocity covariance matrix of each object to generate random perturbations over the initial state vectors. The covariance matrix is diagonalized, and then the standard deviations are used to produce six random perturbations, that are rotated back to the initial frame and added to the state vectors. Once, the perturbed state vectors are obtained, they

are propagated and if the minimum relative distance between the two trajectories is less than the combined object radius, a collision is accounted. To obtain reliable probability estimation, a minimum number of cases are needed. Although this method can be extremely accurate, and can be applied for all cases including linear and nonlinear, the number of trials that have to be tested is dramatically high, resulting in very large computational times, which is why this method can only be used for research or verification purposes.

In [13] the Chernoff-Hoeffding bound is used to determine the minimum number of Monte Carlo simulations (n) needed to achieve a user defined accuracy (ε) with a confidence level of (1-δ) and expected probability (PT).

If the following expression is satisfied:

$$\varepsilon < (1 - P_T) \cdot P_T \qquad \textbf{Eq. 39}$$

Then the upper bound is represented by:

$$n > \frac{4 \cdot (e - 2) \cdot [(1 - P_T) \cdot P_T]}{\varepsilon^2} \cdot \ln\left(\frac{2}{\delta}\right) \qquad \textbf{Eq. 40}$$

A statistics technique called importance sampling [21] can be used to reduce the needed amount of trials. The basic idea of this technique is to concentrate the distribution of the sample points in the parts of the interval that are of most importance instead of spreading them out evenly.

2.3.5 CONJUNCTION PROBLEM CONCLUSIONS

The short-term methods previously summarized were addressed in [12] and a comparison between the different algorithms and a direct computation using MATCAD was done. It is seen that all methods are accurate enough to satisfactorily compute the conjunction risk. However, despite Chan's method is the fastest, it presents some limitations related to the relative object size. On the other hand, Foster's method is computationally the slowest and it also presents poor performance when the COR is small. Nevertheless, it is possible to improve its efficiency by decreasing its number of integration points without sacrificing notoriously its accuracy. The Patera's and Alfano's methods are between the previous two algorithms in terms of computational load and accuracy.

When selecting a Linear conjunction probability algorithm the computational time is not an issue because all algorithms present a very acceptable performance with the actual speeds of processors. Which is more important is to ensure a good performance in all situations. That is the reason why the Akella and Alfriend's method has been selected.

The long-duration encounter methods were addressed in [13] where they were compared with a high accuracy Monte Carlo analysis. The method of adjacent cylinders can exceed 5% error when the relative speed is lower than 0.05m/s, the method of parallelepipeds exceeds 5% error when the relative speed is lower than 0.005m/s. Finally, the method of Voxels reaches error rates higher than 5% when the relative speed is lower than 0.0005m/s.

The long-duration methods feature very diverse computational performances from the method of Voxels which is the slowest compared to the method of adjoining cylinders. At the same time its implementation is quite complex due to the geometric complexity of the problem. That is the reason why a Monte Carlo approach has been selected with the aim to address non-linear close approaches.

2.4 Reference Frames

When performing space orbits propagations or analytical determinations it is convenient to work with quasi-inertial or Newtonian reference systems. Those systems move through the space fixed to the center of the Earth, but do not follow its rotation. However, most of the human space observations are made from the Earth's surface, consequently, it is more appropriate to use Earth fixed reference systems that follow the rotation of the Earth.

Historically, as explained in [27], the inertial or celestial reference frames were tied to the Earth's rotation and its annual revolution around the Sun. So there were two global coordinate systems: one referred to the ecliptic and the second one referred to the equatorial plane, both with one of their axis pointing to the vernal equinox or First Point of Aries.

Nevertheless, the vernal equinox is not a constant property because the orientation of the Earth's North Pole is far from being a constant property. Due to the action of the gravity of the Sun and the Moon making the Earth oblate, the terrestrial spin axis describe circles of an average of 23º27' around the normal of the ecliptic plane, with an approximate period of 26,000 years. Such phenomenon is known as precession of the Earth's axis.

On the other hand, the plane of the orbit of the Moon has also a precession with a period of 18.6 year, which produces small alterations over the precession movement known as nutation.

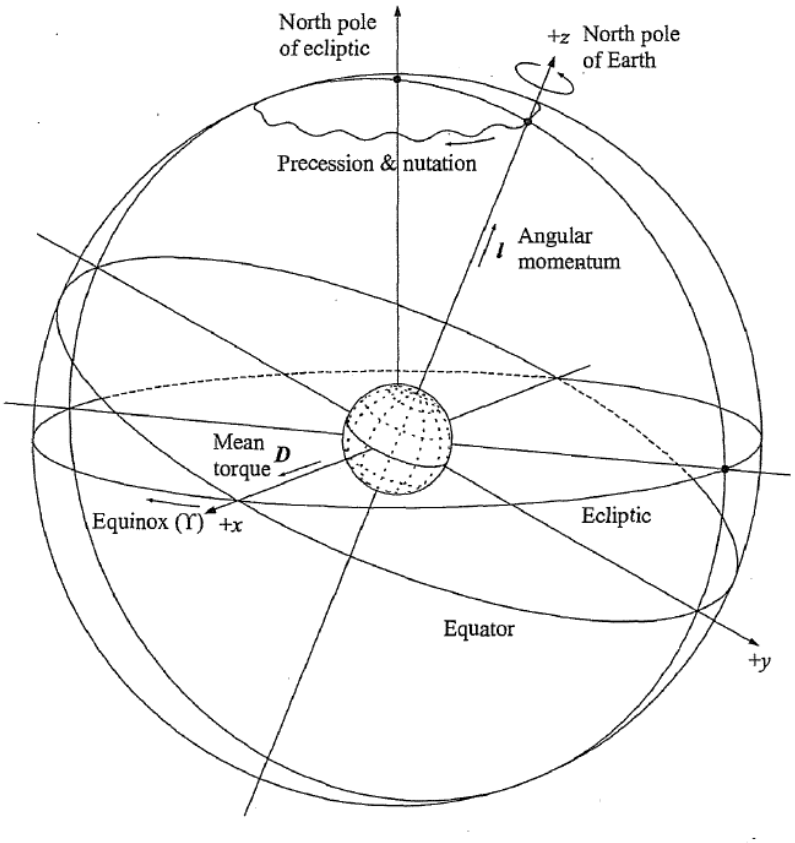

Figure 12: Motion of the Earth's axis under solar and lunar torques.

In addition to precession and nutation, the North Pole describes shorter period variations known as Polar Motion. It is composed by two principal semi periodic components, one with a period of 435 days known as the Candler period and the second one with an annual period. Those are caused by the internal motion of the melted Earth core, tides, redistribution of the water around the Earth and also by Earthquakes. Unlike the previous cases, there is not a strong mathematical model that can predict the Polar Motion variations; this is why there is an institution called International Earth Rotation and Reference Systems Service (IERS) that tracks the actual orientation of the Earth and provides a historical, current and short term future data about the orientation of the Earth. It is also the duty of the IERS to maintain the reference frame and time standards.

Due to all the phenomena previously explained, the relation between a terrestial and a celestial reference frame is a series of rotations well defined by IERS. There exists several IERS convention, however for the purpose of this project the most relevant conventions are IERS 96 and IERS 03.

2.4.1 IERS 1996 CONVENTION

The Geocentric Celestial Reference Frame is the celestial reference frame of the IERS since January 1, 1997; their axes are quite close to the J2000 frame but with a small bias. The relation can be approximated using the following semi orthogonal rotation.

$$r_{GCRF} = \begin{bmatrix} 1 & 2.73E-4 & -9.740996E-8 \\ -2.73E-4 & 1 & -1.324146E-8 \\ 9.740996E-8 & 1.324146E-8 & 1 \end{bmatrix} r_{J2000} \quad \text{Eq. 41}$$

Both frames GCRF and J2000 define a Newtonian inertial space, perfect to perform orbital propagations. The traditional series of rotations that the IERS 96 convention proposes to transform form GCRF to Earth fixed frame named True Earth Fixed (TEF) is the following one:

$$r_{TEF} = [W][\Re][Q][N][P] \cdot r_{GCRF} \quad \text{Eq. 42}$$

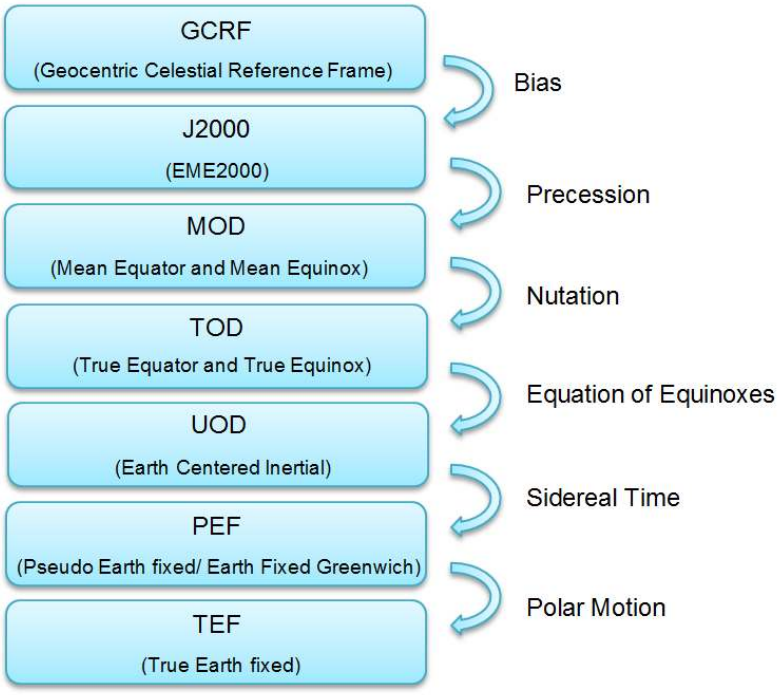

Figure 13: Visual description of the space reference systems and its relations for IERS 1996 convention.

The orientation of the mean equator and equinox with respect to the equator and equinox of J2000 is defined by three angles: ζ, ϑ, z. The three of them depend on the epoch. In other words, to switch from J2000 to MOD three consecutive rotations are required.

$$[P] = R_z(-z)R_x(\vartheta)R_z(-\zeta) \quad \text{Eq. 43}$$

Nutation is mostly caused by the changing orientation of the Moon's orbit with respect to the Earth's equator; it means that the ascending node of the moon creates a periodic shift of the vernal equinox $\Delta\psi$ and a change of the obliquity of the ecliptic $\Delta\varepsilon$. So the relation from MOD to TOD is also the product of three rotations.

$$[N] = R_x(-\varepsilon - \Delta\varepsilon)R_z(-\Delta\psi)R_x(\varepsilon) \quad \text{Eq. 44}$$

As explained before, the temporal equinox is the intersection of the ecliptic plane with the equatorial plane, and due to the constant changing nature of those two planes, the temporal equinox varies through time. In [28] the "uniform equinox" concept is explained as the direction of the temporal equinox minus the "Equation of the Equinoxes" $(Eq_{equinox})$. So, the relation between TOD and NOD is a single rotation.

$$[Q] = R_z(Eq_{equinox}) \quad \text{Eq. 45}$$

The relation between the uniform equinox and the Earth rotation is the Greenwich Mean Sidereal time θ_{GMST}, while the most common used relation between the temporal equinox and Earth rotation is the Greenwich Sidereal angle θ_{GST}.

$$[\Re] = R_z(\theta_{GMST}) \quad \text{Eq. 46}$$

Finally, the relation between PEF and TEF is provided by IERS through the Earth Orientation Parameters (EOP) that define the polar motion matrix.

$$[W] = R_y(-x_p)R_x(-y_p) \quad \text{Eq. 47}$$

2.4.2 IERS 2003 CONVENTION

The main difference between the IERS 03 and IERS 96 is the elimination of the dependency on the ecliptic of date. An alternative transformation more conceptually simple and computationally efficient is done a matrix form. Consequently, the set of rotations gets considerably simplified:

$$r_{ITRF} = [W'][R'][NP] \cdot r_{GCRF} \quad \text{Eq. 48}$$

As seen in Figure 14 the Nutation and Precession rotation matrix $[NP]$ relates the GCRF to a Celestial Intermediate Reference Frame (CIRF) which is slightly different from the previous TOD frame.

$$[NP] = R_z(s) \cdot \begin{bmatrix} 1 - aX^2 & -aXY & -X \\ -aXY & -aY^2 & -Y \\ X & Y & 1 - a(X^2 + Y^2) \end{bmatrix}, \qquad \text{Eq. 49}$$

$$a = \frac{1}{2} + \frac{1}{8}(X^2 + Y^2)$$

Where (X, Y, s) describe the position of the Celestial Intermediate Pole (CIP) and the Celestial Ephemeris Origin (CEO).

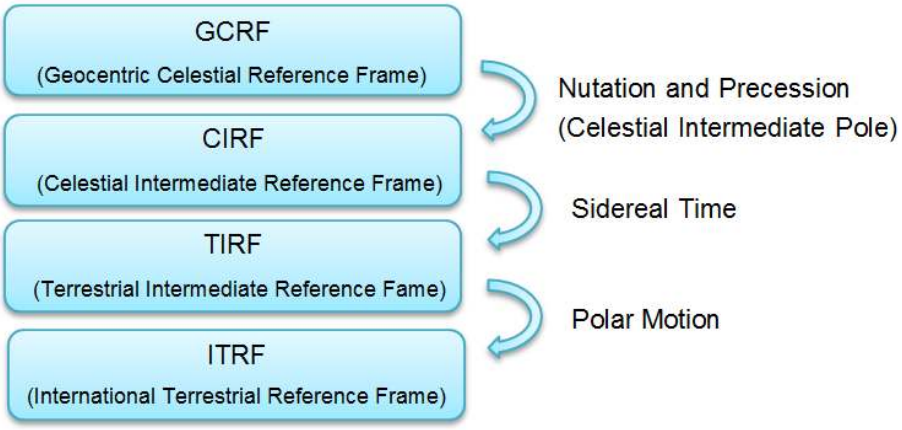

Figure 14: Visual description of the space reference systems and its relations for IERS 2003 convention.

The Sidereal rotation introduces the stellar angle (θ) which is the angle between a reference meridian of the Earth and a fixed celestial point.

Then the rotation between the Celestial Intermediate Reference Plane to the Terrestrial Intermediate Reference Frame is: $[R'] = R_z(\theta)$.

Finally, the polar motion correction is very similar to the IERS 96 convention with the following rotation matrix with the s' term which makes reference to the Terrestrial Ephemerides Origin.

$$[W'] = R_x(y) \cdot R_y(x) \cdot R_z(-s') \qquad \text{Eq. 50}$$

CHAPTER THREE: ALGORITHMS DEFINITION

From the described algorithms in the literature review, three have been selected to be implemented. The Akella and Alfriend's method and two of Alfano's maximum probability routines have been chosen for a daily operational use, since their computational load is very low and large sets of potential collisions can be handled. The maximum probability algorithms will be used as a substitute of the Akella and Alfriend algorithm when there is no covariance available or the user suspects that the quality of the conjunction characterization data is not appropriate.

On the other hand, the Monte Carlo method will be used as a reference concept point to implement three different algorithms. The three algorithms will follow three different levels of simplification. The objective of the Monte-Carlo method is to provide reference results for the previous methods but also to have a method to compute the collision probability with a minimum number of hypothesis behind.

3.1 AKELLA & ALFRIEND METHOD

The Akella and Alfriend's method has been selected among the other reviewed linear methods because it is the most conceptually simple despite it is the one with higher computational cost. Nowadays with the current standard PC's processor speeds, the computing time is not a critical decision factor among the linear methods.

The algorithm starts from the 2D probability expression deduced in [18] and, instead of doing any simplification, it directly performs the numerical bi-dimensional integration.

$$\mathrm{P} = \frac{1}{2\pi|p^*|^{1/2}} \int_{-\mathrm{COR}}^{\mathrm{COR}} \int_{-\sqrt{\mathrm{COR}^2-\mathrm{x}^2}}^{\sqrt{\mathrm{COR}^2-\mathrm{x}^2}} \exp(-S^*)\,\mathrm{dxdy} \qquad \textbf{Eq. 51}$$

Before getting into detail of the fundamental parts that compose the algorithm, it is important to remark its aim. The Akella & Alfriend algorithm will be feed with the position, velocity and positional covariance of the two objects in the GRCF frame. It will also require information about the combined object radius and the time of closest approach. With all that information, the algorithm will compute the collision probability as well as additional information like the mean deviation of the miss distance and TCA and the relative orientation of the bi-dimensional projection of the covariance in the encounter plane by providing the angles of the principal axes with respect to the local encounter plane frame.

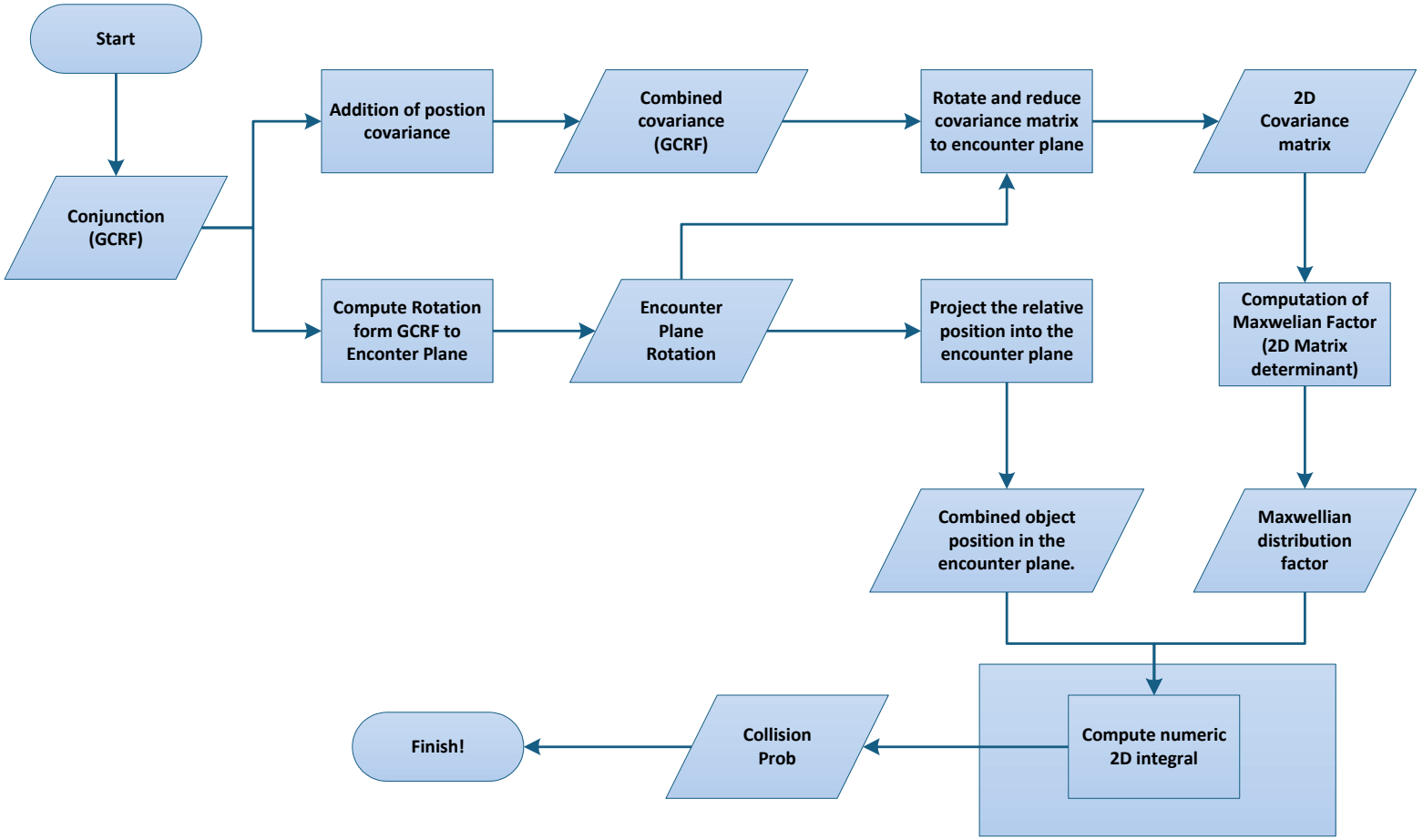

Figure 15: Flow diagram of the Akella & Alfriend Algorithm. (Rectangles represent processes and diamonds data).

Figure 15 provides a general idea about the sequence of processes that will take place during the execution of the algorithm. First of all, the two covariance matrices of the target and chaser have to be added in order to calculate the combined covariance distribution, which corresponds to the covariance of the relative position vector at the TCA. At the same time, taking advantage of the information provided by the velocity and position vectors the conjunction plane will be determined, and with it the rotation matrix to project the combined covariance to the encounter plane frame. Once achieved, the component normal to the encounter plane is ignored to get the bi-dimensional covariance matrix contained in the encounter plane. Then, the determinant of the bi-dimensional covariance is calculated to compute the Maxwellian factor which is the initial term of the left-hand side of the probability equation. After that, the sampling distance for the numerical integral is computed, to finally perform the integral and produce the collision probability value. The post process calculations are not specified in the diagram.

After the reader has understood the general working principle of Akella & Alfriend's algorithm, some specific steps that require a more detailed explanation will be discussed.

3.1.1 Encounter Frame

Considering that the algorithm receives as an input the position of both target and chaser ($\overrightarrow{r_{ta}}, \overrightarrow{r_{ch}}$), and their velocities ($\overrightarrow{v_{ta}}, \overrightarrow{v_{ch}}$), the relative vectors ($\overrightarrow{r_r}, \overrightarrow{v_r}$) will be computed.

$$\overrightarrow{r_r} = \overrightarrow{r_{ch}} - \overrightarrow{r_{ta}} \ , \qquad \overrightarrow{v_r} = \overrightarrow{v_{ch}} - \overrightarrow{v_{ta}} \qquad \textbf{Eq. 52}$$

The encounter plane frame is based on the previous vectors.

$$\vec{\imath} = \frac{\overrightarrow{v_r}}{|\overrightarrow{v_r}|} \ , \qquad \vec{\jmath} = \frac{\vec{\imath} \times \overrightarrow{r_r}}{|\vec{\imath} \times \overrightarrow{r_r}|} \ , \qquad \vec{k} = \vec{\imath} \times \vec{\jmath} \qquad \textbf{Eq. 53}$$

The frame is completely orthonormal and if arranged in the following way;$[R_1] = \left[\vec{\imath}, \vec{\jmath}, \vec{k}\right]$ it perfectly fulfills the tensor rotation property $[R_1] \cdot [R_1]^T = [I]$. Using the rotation matrix, both the combined covariance [C] and the relative position vector $\overrightarrow{r_r}$ are rotated to the encounter plane frame.

$$[C'] = [R_1]^T \cdot [C] \cdot [R_1] \ , \quad \overrightarrow{r_r}' = [R_1]^T \cdot \overrightarrow{r_r} \qquad \textbf{Eq. 54}$$

Because of the specific integration method that will be applied, it is necessary to perform a second rotation to provide the combined covariance [C] and the relative position vector $\overrightarrow{r_r}$ in the main directions of the combined covariance frame. Being $[R_2]$ the eigenvectors matrix of $[C']$ the rotation to the diagonal frame is achieved by:

$$[C''] = [R_2]^T \cdot [C'] \cdot [R_2]\,, \quad \vec{r_r}'' = [R_2]^T \cdot \vec{r_r}' \qquad \textbf{Eq. 55}$$

3.1.2 SAMPLING DISTANCES

Two sampling distances are defined each one for each main directions of the covariance. The sampling distance is chosen as one fiftieth of the minimum between the combined object radius and the standard deviation in the direction of the sampling distance. However, it is just a convention so if the sampling distance is decreased the final probability calculation will be more accurate but computationally slower.

3.1.3 NUMERICAL INTEGRATOR

The numerical integral used algorithm only accepts the input data in the main directions of the bi-dimensional covariance, because the two sampling distances are adapted to the probability distribution of each main direction. Using this technique the algorithm's accuracy remains high while the computation time significantly decreases with respect to a numerical integral algorithm with only one sampling distance value.

Two auxiliary variables $(x_i, y_j)$are defined with the aim to sweep the entire surface in the encounter plane. The auxiliary variables are increased one unit of the previously computed sampling distances (Δd_j) after each step.

$$x_i = x_{i-1} + \Delta d_x\,, y_j = y_{j-1} + \Delta d_y \qquad \textbf{Eq. 56}$$

Then, the probability is computed with the following expression which is the bi-dimensional integral in numeric form.

$$prob_j = prob_{j-1} + maxw \cdot exp\left[\frac{1}{2}(\tilde{\rho} - \bar{\rho})^T P^{*-1}(\tilde{\rho} - \bar{\rho})\right] \cdot \Delta d_x \Delta d_y \qquad \textbf{Eq. 57}$$

3.1.4 DATA POST-PROCESS

Apart from the conjunction probability, the standard deviation of the miss distance and of the TCA as well as the principal axes of the bi-dimensional covariance and their orientation angles are going to be computed.

The procedure to find the uncertainty in the time of closest approach starts with the Taylor approximation of the relative position of the objects dismissing higher order terms.

$$\widetilde{\overrightarrow{\rho(\Delta t)}} = \widetilde{\overrightarrow{\rho_o}} + \tilde{\vec{v}} \cdot \Delta t \qquad \textbf{Eq. 58}$$

Being $\widetilde{\overrightarrow{\rho_o}}$ the uncertain initial relative position $\tilde{v}$ the initial uncertain velocity and Δt a small time variation. It is know that in the time of closest approach the derivate of the product of the relative position is zero:

$$\frac{d}{dt}(\tilde{\vec{\rho}} \cdot \tilde{\vec{\rho}}) = 0 \quad \text{Eq. 59}$$

$$2\tilde{\vec{v}} \cdot \tilde{\vec{v}}\Delta t_{ca} + 2\tilde{\vec{v}} \cdot \tilde{\vec{\rho}} = 0 \quad \text{Eq. 60}$$

$$\Delta t_{ca} = -\frac{\tilde{\vec{v}} \cdot \tilde{\vec{\rho}}}{\tilde{\vec{v}} \cdot \tilde{\vec{v}}} \quad \text{Eq. 61}$$

The uncertain relative position and the uncertain relative velocity are modeled as the addition of a mean $(\bar{\vec{x}})$ and a small perturbation$(\Delta\vec{x})$. After that the time of closest approach becomes:

$$\Delta t_{ca} = -\frac{\bar{\vec{\rho}}^T\bar{\vec{v}} + \bar{\vec{\rho}}^T\Delta\vec{v} + \bar{\vec{v}}^T\Delta\vec{\rho} + \Delta\vec{\rho}^T\Delta\vec{v}}{\bar{\vec{v}}^T\bar{\vec{v}} + 2\bar{\vec{v}}^T\Delta\vec{v} + \Delta\vec{v}^T\Delta\vec{v}} \quad \text{Eq. 62}$$

Where:

$$\bar{\vec{\rho}}^T\bar{\vec{v}} = 0\,,\ \Delta\vec{v}^T\Delta\vec{v} \ll \bar{\vec{\rho}}^T\Delta\vec{v}||\bar{\vec{v}}^T\Delta\vec{\rho}\,, 2\bar{\vec{v}}^T\Delta\vec{v}\ \&\&\ \Delta\vec{v}^T\Delta\vec{v} \ll \bar{\vec{v}}^T\bar{\vec{v}}. \quad \text{Eq. 63}$$

$$\Delta t_{ca} \approx -\frac{\bar{\vec{\rho}}^T\Delta\vec{v} + \bar{\vec{v}}^T\Delta\vec{\rho}}{\bar{\vec{v}}^T\bar{\vec{v}}} \quad \text{Eq. 64}$$

The variance in the time of closest approach is defined as:

$$\sigma_{tca}{}^2 = E[(t - E[t])^2] = E[\Delta t^2] \quad \text{Eq. 65}$$

If the one substitutes the time of closest approach expression in the previous equation:

$$\begin{aligned}\sigma_{tca}{}^2 &= \frac{1}{\left|\bar{\vec{v}}\right|^4}E\left[\left(\bar{\vec{\rho}}^T\Delta\vec{v}\right)\left(\bar{\vec{\rho}}^T\Delta\vec{v}\right) + \left(\bar{\vec{v}}^T\Delta\vec{\rho}\right)\left(\bar{\vec{v}}^T\Delta\vec{\rho}\right) + 2\bar{\vec{\rho}}^T\Delta\vec{v}\cdot\bar{\vec{v}}^T\Delta\vec{\rho}\right] = \\ &= \frac{1}{\left|\bar{\vec{v}}\right|^4}E\left[\bar{\vec{\rho}}^T\Delta\vec{v}\Delta\vec{v}^T\bar{\vec{\rho}} + \bar{\vec{v}}^T\Delta\vec{\rho}\Delta\vec{\rho}^T\bar{\vec{v}} + 2\bar{\vec{\rho}}^T\Delta\vec{v}\Delta\vec{\rho}^T\bar{\vec{v}}\right] = \\ &= \frac{1}{\left|\bar{\vec{v}}\right|^4}\left(\bar{\vec{\rho}}^TE[\Delta\vec{v}\Delta\vec{v}^T]\bar{\vec{\rho}} + \bar{\vec{v}}^TE[\Delta\vec{\rho}\Delta\vec{\rho}^T]\bar{\vec{v}} + 2\bar{\vec{\rho}}^TE[\Delta\vec{v}\Delta\vec{\rho}^T]\bar{\vec{v}}\right) = \\ &= \frac{1}{|v|^4}\left(\bar{\vec{\rho}}^TC_v\bar{\vec{\rho}} + \bar{\vec{v}}^TC_p\bar{\vec{v}} + 2\bar{\vec{\rho}}^TC_{pv}\bar{\vec{v}}\right)\end{aligned} \quad \text{Eq. 66}$$

Being respectively (C_p, C_v, C_{pv}) the position, velocity and mixed covariance. Once the time uncertainty is known then it is possible to proceed with the variance on the miss distance.

$$\widetilde{\overrightarrow{\rho(\Delta t_{ca})}} = \tilde{\vec{\rho}} + \bar{\vec{v}}\Delta t_{ca} \qquad \text{Eq. 67}$$

In the previous expression, the relative velocity has been directly considered totally know without any uncertainty because the extra terms that such consideration would produce are second order terms. Then, taking advantage of this expression the standard deviation of the miss distance can be deduced.

$$\begin{aligned} {\sigma_{\rho tca}}^2 &= E\left[\left(\widetilde{\overrightarrow{\rho(\Delta t_{ca})}} - E\left[\widetilde{\overrightarrow{\rho(\Delta t_{ca})}}\right]\right)^2\right] = \\ &= E\left[\left(\Delta\vec{\rho} + \bar{\vec{v}}\Delta t_{ca}\right)^T \cdot \left(\Delta\vec{\rho} + \bar{\vec{v}}\Delta t_{ca}\right)\right] = \\ &= E\left[\left(\bar{\vec{v}}\Delta t_{ca}\right)^T\left(\bar{\vec{v}}\Delta t_{ca}\right)\right] + E\left[2\Delta t_{ca}\bar{\vec{v}}^T\Delta\vec{\rho}\right] + E[\Delta\vec{\rho}^T\Delta\vec{\rho}] \end{aligned} \qquad \text{Eq. 68}$$

When analyzing the previous expression one can determine that the first term is the time variance multiplied by the velocity module, the third term is the trace of the positional covariance and finally the second term has to be developed using the previously found time of closest approach expression.

$$E\left[2\Delta t_{ca}\bar{\vec{v}}^T\Delta\vec{\rho}\right] = \frac{-2}{\left|\bar{\vec{v}}\right|^2}\left(\bar{\vec{\rho}}^T C_v\bar{\vec{\rho}} + \bar{\vec{\rho}}^T C_{pv}\bar{\vec{v}}\right) \qquad \text{Eq. 69}$$

Consequently, the variance of the miss distance becomes.

$${\sigma_{\rho tca}}^2 = \frac{1}{\left|\bar{\vec{v}}\right|^2}\left(\bar{\vec{\rho}}^T C_v\bar{\vec{\rho}} - \bar{\vec{v}}^T C_p\bar{\vec{v}}\right) + Tr\left(C_p\right) \qquad \text{Eq. 70}$$

3.2 MAXIMUM COLLISION PROBABILITY

The Maximum Collision Probability value is extremely important when the user suspects that the quality of the covariance data is poor or it even does not exist. That is why in this section three different algorithms have been developed to address this computation.

Before describing the algorithms it is important to proceed with a short overview about the Maximum Probability problem.

When looking for the maximum probability the configuration of the covariance which produces the highest probability value has to be found. So the only required parameters are the miss distance, the dimensions of the objects and finally the covariance aspect ratio (AR) which will be defined in the following paragraphs.

The starting point of the mathematical approach is the bi-dimensional expression described in section 2.3.2.6 Two-dimensional equation. Therefore, in order to fully understand the following explanation the reader should have understood the previously cited section.

$$P = \frac{1}{2\pi|p^*|^{1/2}} \int_{-COR}^{COR} \int_{-\sqrt{COR^2-x^2}}^{\sqrt{COR^2-x^2}} \exp(-S^*)\, dxdy \qquad \text{Eq. 71}$$
$$S^* = \frac{1}{2}(\tilde{\rho} - \bar{\rho})^T p^{*-1} (\tilde{\rho} - \bar{\rho})$$

Such expression states the probability distribution integration in the encounter plane over the combined object radius surface, centered on the chaser's relative position.

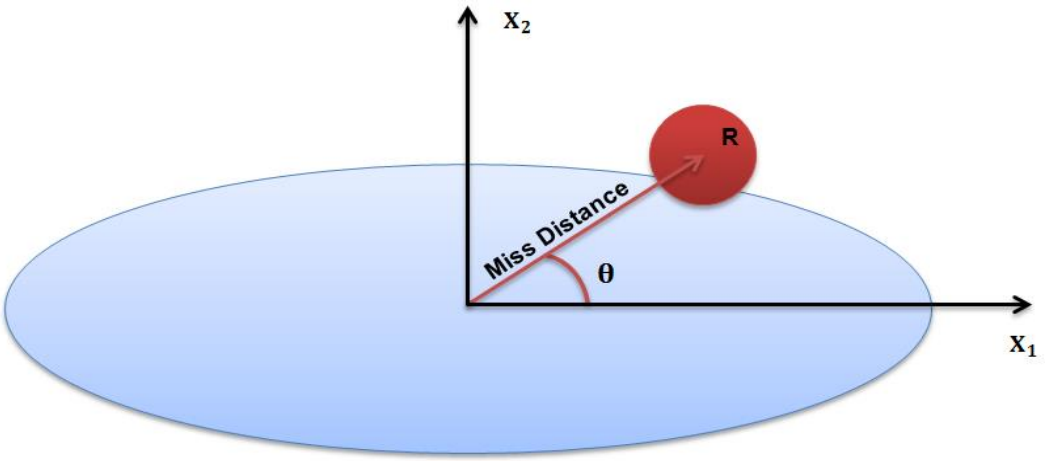

Figure 16: Bi-dimensional projection of the covariance and the combined object radius over the encounter plane.

Figure 16, provides the visual representation of a general projection of the covariance and combined object radius in the encounter plane. The used reference system follows the principal axes of the bi-dimensional covariance. Then the chaser position is expressed in polar coordinates with a Miss Distance value and a generic angle θ. It can be easily seen that the worst possible case would be when the relative position of the chaser coincides with the principal axis of the bi-dimensional covariance, in other words, when $\theta = 0$. That is why it is very convenient to work with the principal direction coordinates.

The relation between the major value of the bi-dimensional covariance and the minor value is the aspect ratio ($AR = \sigma_1/\sigma_2$).

Then, the covariance and the mean relative position become:

$$p = \begin{bmatrix} AR^2 \cdot {\sigma_2}^2 & 0 \\ 0 & {\sigma_2}^2 \end{bmatrix} \; and \; \bar{\rho} = [miss\ distance \quad 0] \qquad \textbf{Eq. 72}$$

Next, the relation that provides the (σ_2) that maximizes the value of probability can be found by:

$$\frac{dP}{d\sigma_2} = 0 \qquad \textbf{Eq. 73}$$

$$\frac{d\mathrm{P}}{d\sigma_2} = \frac{-1}{\pi |p(\sigma_2)^*|^{1/2} \cdot \sigma_2} \int_{-\mathrm{COR}}^{\mathrm{COR}} \int_{-\sqrt{\mathrm{COR}^2-\mathrm{x}^2}}^{\sqrt{\mathrm{COR}^2-\mathrm{x}^2}} \exp(-S(\sigma_2)^*)\,\mathrm{dxdy} + \frac{1}{{\sigma_2}^2} \int_{-\mathrm{R}}^{\mathrm{R}} \int_{-\sqrt{\mathrm{R}^2-\mathrm{x}^2}}^{\sqrt{\mathrm{R}^2-\mathrm{x}^2}} S(\sigma_2)^* \cdot \exp(-S(\sigma_2)^*)\,\mathrm{dxdy} = 0 \qquad \textbf{Eq. 74}$$

$$P(\sigma_2) \cdot {\sigma_2}^2 = \int_{-\mathrm{COR}}^{\mathrm{COR}} \int_{-\sqrt{\mathrm{COR}^2-\mathrm{x}^2}}^{\sqrt{\mathrm{COR}^2-\mathrm{x}^2}} S(\sigma_2)^* \cdot \exp(-S(\sigma_2)^*)\,\mathrm{dxdy} \qquad \textbf{Eq. 75}$$

3.2.1 ITERATIVE MAXIMUM PROBABILITY

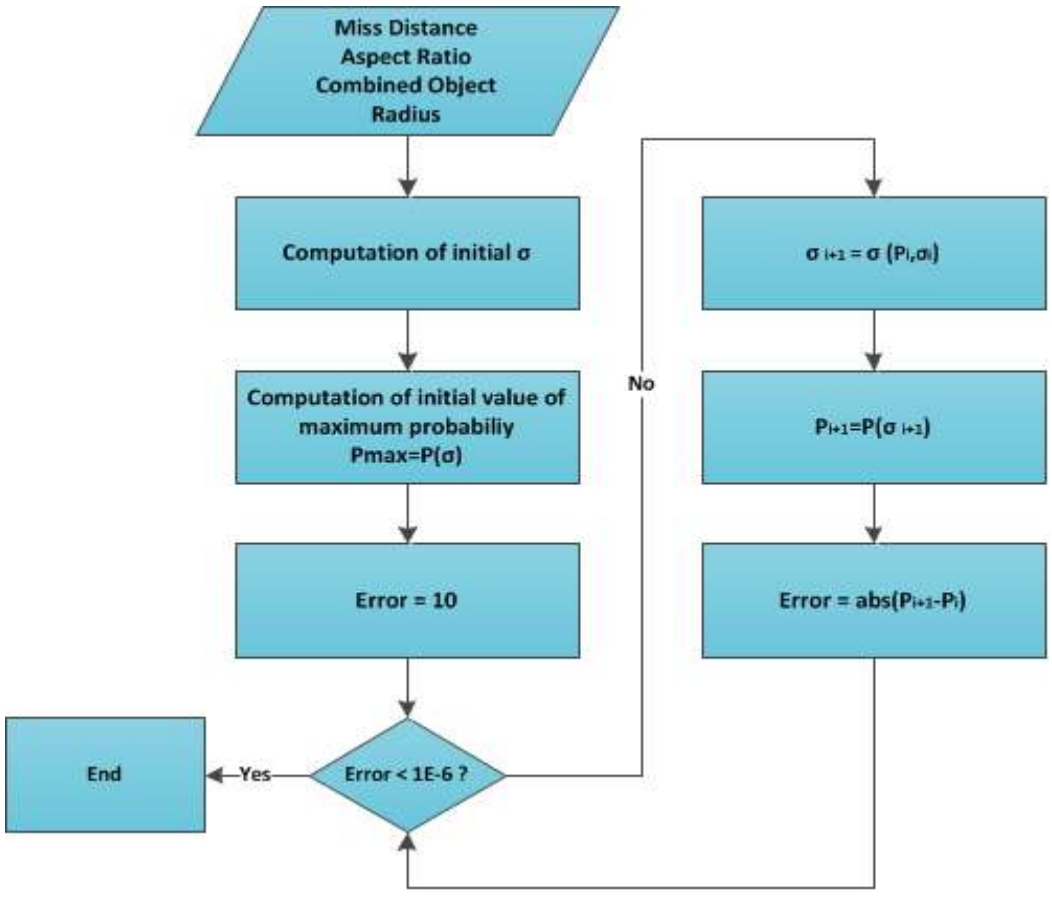

Figure 17: Flux diagram of the maximum Probability Iterative Algorithm.

A numeric iterative algorithm to compute the maximum collision probability has been developed to obtain high quality values of conjunction risk. The general working principle of the iterative algorithm is visually exposed in Figure 17.

Given as input values the miss distance, the AR and the combined object radius a first estimation of the (σ_2) value is computed based on the first order approximation found in [29].

$$\sigma_{20} = \sqrt{\frac{(AR^2+1)*COR^2 + 2\cdot\rho^2 + \sqrt{[(AR^2+1)*R^2]^2 + 4\rho^4}}{8\cdot AR^2}} \quad \text{Eq. 76}$$

On the other hand, the probability associated to such standard deviation is computed using the same integration method exposed in 3.1.3 Numerical Integrator.

Taking advantage of the two initial computed values the iteration process can be started, the standard deviation of each step can be computed using the following expression:

$$\sigma_{2i+1}(\sigma_{2i}, P_i) = \sqrt{\frac{1}{P_i}\int_{-\mathrm{COR}}^{\mathrm{COR}}\int_{-\sqrt{\mathrm{COR}^2-\mathrm{x}^2}}^{\sqrt{\mathrm{COR}^2-\mathrm{x}^2}} S(\sigma_{2i})^* \cdot \exp(-S(\sigma_{2i})^*)\,\mathrm{dxdy}} \quad \text{Eq. 77}$$

Each step a new value of standard deviation and maximum probability is computed until the user error requirements are satisfied.

This algorithm results are quite accurate (absolute error = 1E-6) and despite the fact that it is a numeric iterative process the computing times are less than one second.

3.2.2 Maximum Conjunction probability for infinite aspect ratio

As seen in the Literature review (section 2.3.3.6 Maximum Probability Assessment), Alfano determines a really simple analytic formula to determine the maximum collision probability for any conjunction assuming an infinite aspect ratio. Such configuration makes reference to the worst case possible and the maximum collision probability value will probably be overestimated. In [29] it is seen that only a 10% of the collisions have an aspect ratio greater than 15 and less than a 1% have an aspect ratio over 50.

When considering an infinite aspect ratio, the combined object radius is normalized with respect to the miss distance.

$$cor = \frac{COR}{mdis} \quad \text{Eq. 78}$$

Because the aspect ratio is infinite the probability associated with the minor axis is contained all into the combined object. Then the probability integral becomes one-dimensional:

$$P = \frac{1}{\sigma_u \sqrt{2\pi}} \int_{1-cor}^{1+cor} exp\left[\frac{-u^2}{2 \cdot {\sigma_u}^2}\right] du \quad \text{Eq. 79}$$

Again forcing:

$$\frac{dP}{d\sigma_u} = 0 \quad \text{Eq. 80}$$

The normalized standard deviation that maximizes the conjunction probability is:

$$\sigma_u = \sqrt{\frac{2cor}{ln\left[\frac{1+cor}{1-cor}\right]}} \quad \text{Eq. 81}$$

Considering that the probability equation can be expressed in an alternate form using error functions, when the maximized standard deviation is substituted the resultant expression is:

$$P_{max} = \frac{1}{2}\left[erf\left[\frac{cor+1}{2\sqrt{cor}}\sqrt{-ln\left[\frac{1-cor}{1+cor}\right]}\right] + erf\left[\frac{cor-1}{2\sqrt{cor}}\sqrt{-ln\left[\frac{1-cor}{1+cor}\right]}\right]\right] \quad \text{Eq. 82}$$

As appreciated in Figure 18 the previous equation is nearly linear, that is why it can be easily approximated to three significant figures with the equations:

$$\mathrm{P_{max}} = 0.48394 \cdot \mathrm{cor} \quad \text{when } \mathrm{cor} < 0.8 \quad \text{Eq. 83}$$

$$\mathrm{P_{max}} = 0.21329 \cdot \exp(1.01511 \cdot \mathrm{cor}) - 0.09025 \quad \text{when } 0.8 \leq \mathrm{cor} < 1 \quad \text{Eq. 84}$$

$$\mathrm{P_{max}} = 0.5 \quad \text{when } \mathrm{cor} = 1 \quad \text{Eq. 85}$$

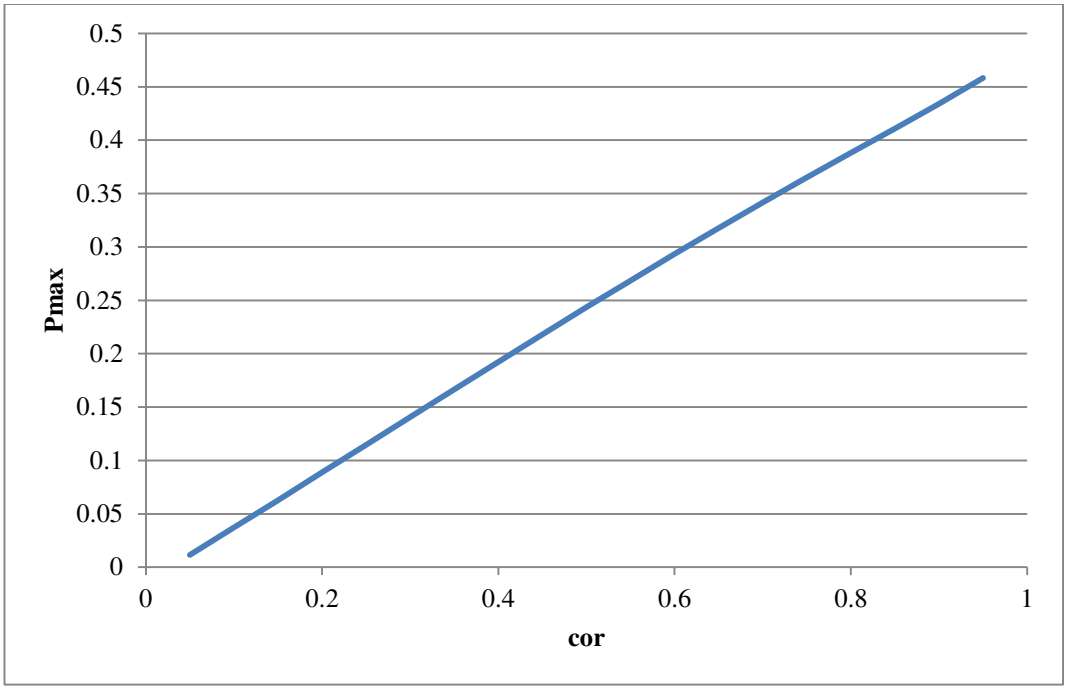

Figure 18: Maximum Probability computed with the error Function Expression.

3.2.3 MAXIMUM CONJUNCTION PROBABILITY LINEAR METHOD

Alfano, in [29], instead of performing the iterative method exposed at the beginning of this section, computes a set of numerical approximations that provide the maximum probability as a function of the miss distance, combined object radius and aspect ratio.

$$P_{max} = \frac{COR^2}{384[AR^5{\sigma_{max}}^6]} exp\left[\frac{-1}{2}\left[\frac{\rho}{AR \cdot \sigma_{max}}\right]^2\right] \cdot (A + B + C)$$
$$A = 192 \cdot AR^4 \cdot {\sigma_{max}}^4$$
$$B = (-24AR^4 \cdot R^2 - 24COR^2 \cdot AR^2) \cdot {\sigma_{max}}^2$$
$$C = (3AR^4 + 2AR^2 + 3) \cdot COR^4 + 24\rho^2 \cdot COR^2$$

Eq. 86

Where σ_{max} is:

$$\sigma_{max} = \sqrt{\frac{(AR^2 + 1) * COR^2 + 2 \cdot \rho^2 + \sqrt{[(AR^2 + 1) * COR^2]^2 + 4\rho^4}}{8 \cdot AR^2}}$$

Eq. 87

This equation provides maximum probability values a bit overestimated within the range 1<AR<50. This algorithm is only recommended if the time is critical and the maximum probability must be computed very fast.

3.3 MONTE CARLO

The Monte Carlo analysis is a computationally demanding algorithm; however in some situations it is the only available tool to address a given problem. In this project three different approaches of the Monte Carlo algorithm have been developed.

The general working principle of a Monte Carlo conjunction risk evaluation algorithm is visually expressed in Figure 19.

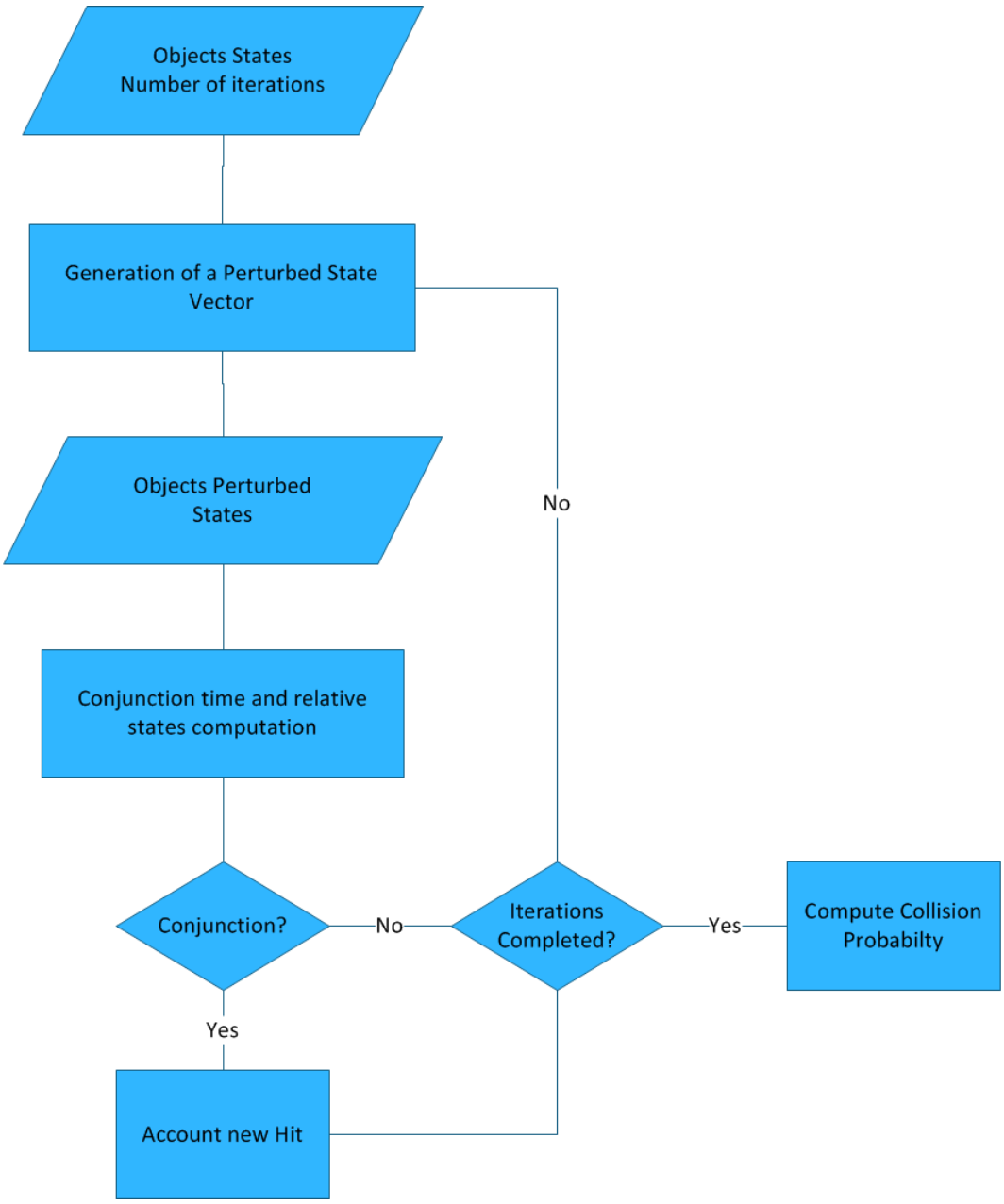

Figure 19: Flux diagram of the general Conjunction Probability Monte Carlo Approach.

Given two satellite states at the mean time of closest approach and a number of iterations established by the user, the general algorithm will generate a random perturbation based on the covariance of the objects, and will check the new time of closest approach and the new miss distance for the specific perturbation. If the miss distance is less than the combined object radius there is a collision for that case, the total collision probability is the fraction between all the noted collisions and the total number of cases analyzed. One remarkable advantage of the Monte Carlo method is that apart from providing the value of conjunction probability, because each case has been separately solved additional information can be extracted such as the miss distance histogram, the accumulative time probability plot and the standard deviation of the TCA and miss distance.

3.3.1 MONTE CARLO DATA POST PROCESS

As previously stated, because the Monte Carlo algorithm provides the miss distance and time of closest approach of each single conjunction case, a statistical analysis of them can be done in order to determine their standard deviation.

$$\sigma_{tca} = \sqrt{\frac{\sum_{i=0}^{N}(\mathrm{t_{ca}}^{i} - \overline{t_{ca}})^2}{N}} \qquad \textbf{Eq. 88}$$

$$\sigma_{\rho} = \sqrt{\frac{\sum_{i=0}^{N}(\vec{\rho}^{i} - \bar{\vec{\rho}})^2}{N}} \qquad \textbf{Eq. 89}$$

Where (N) is the number of analyzed trials, the (i) superindex makes reference to specific analysis case and the values without superindex are the mean values.

$$\overline{t_{ca}} = \frac{\sum_{i=0}^{N}\mathrm{t_{ca}}^{i}}{N} \; and \; \bar{\vec{\rho}} = \frac{\sum_{i=0}^{N}\vec{\rho}^{i}}{N} \qquad \textbf{Eq. 90}$$

3.3.2 LINEAR MONTE CARLO

The linear Monte Carlo has been designed with the aim to provide a detailed analysis of a conjunction within a reduced amount of time. It is limited to linear conjunction analyses which are the vast majority of the daily cases that a regular satellite operator has to deal with.

The followed approach is quite simple and it only requires a few steps to analyze a conjunction case. Once the initial chaser state has been perturbed following the Gaussian distribution given by the combined covariance matrix, the new time of closest approach is computed through its linear approximation.

$$t_{ca}{}^{i} = -\frac{\overrightarrow{r_r}^{i} \cdot \overrightarrow{V_r}^{i}}{\overrightarrow{V_r}^{i} \cdot \overrightarrow{V_r}^{i}} \qquad \text{Eq. 91}$$

The (i) superindex indicates that the term makes reference to a perturbed state case. After that the new relative position the time of closest approach is computed through:

$$\vec{\rho}^{i} = \overrightarrow{r_r}^{i} + \overrightarrow{V_r}^{i} \cdot (t_{ca}{}^{i} - t_{ca}) \qquad \text{Eq. 92}$$

Finally, as explained in the general description of the Monte Carlo algorithm if $\rho^{i} < COR$ a collision is accounted for that specific analysis case.

3.3.3 NUMERIC MONTE CARLO

This algorithm takes advantage of the numerical propagation module of the OREKIT library. It represents the most complete conjunction analysis of this project, because it is the approach with fewer simplifications.

Since the algorithm uses complex conjunction determination methods, the first step of the numeric Monte Carlo is to calculate the screening window, in other words the maximum and minimum time difference with respect to the mean time of closest approach, where the conjunction methods will look for a conjunction.

3.3.3.1 Screening window

The algorithm has two different conjunction assessment modes based on the way to determine the screening window. The first mode allows the user to select a screening interval and once defined, that interval will remain constant during all the conjunction analysis. That means that all the conjunctions that take place out of the time boundaries will be dismissed. In other words, this mode requires some user experience in order to select the right screening interval.

The second mode uses a default screening window and when no conjunction is found the window is automatically expanded. The default screening window is defined as three times the linear approximation of the standard deviation of the time of closest approach.

$$\Delta t = \mp 3 \cdot \sigma_{TCA} \qquad \text{Eq. 93}$$

The default multiplying factor is 3 and it comprehends the 99.7% of the linear cases, the (σ_{TCA}) is calculated through the linear approximation exposed in section 3.1.4.

3.3.3.2 *Propagation*

As previously noted the numerical propagation is performed thanks to the algorithms provided by the OREKIT library. The library contains several different kinds of orbital propagators. However, not all were suitable to perform an accurate collision analysis for LEO satellites, due to the high level of orbital perturbations in such altitudes.

3.3.3.2.1 Integrator

When using the numerical propagator for the Monte Carlo analysis is important to understand that the numerical propagator takes advantage of a mathematical integrator. The one used in this project is the DormandPrince853Integrator, which is an embedded Runge-Kutta integrator of order 8 (5, 3). The integrator uses 12 functions evaluations per step for integration and 4 evaluations for interpolation. Nevertheless, since the first interpolation evaluation is the same as the first integration evaluation of the next step the resultant evaluation cost per step is 12 evaluations.

In OREKIT there is a built in class that automatically sets the Dormand-Prince 853 Integrator, the method that is used for such functionality only requires three parameters, which are the position tolerance, the maximum and minimum integration step.

The maximum and minimum integration step has time units (s), while the positional tolerance determines the positional error in (m).

3.3.3.2.2 Force Models

The gravitational model used in the numerical propagator is the Holmes Featherstone Attraction Model described in [30]. This model directly uses normalized coefficients and stable recursion algorithms so it is more suited for high degree gravity fields. The Holmes and Featherstone algorithm features a good behavior in the poles of the gravitational object.

3.3.3.3 Conjunction Determination

The conjunction determination is achieved through a process of three steps that is thought to minimize the computational time spent in each conjunction determination.

In the first step, taking advantage of the equations found in section 2.3.2.3 a linear approximation of the time of closest approach is computed using:

$$t_{ca0} = -\frac{\vec{\tilde{\rho}} \cdot \overrightarrow{V_r}}{\overrightarrow{V_r} \cdot \overrightarrow{V_r}} \qquad \text{Eq. 94}$$

In the second step, with the ephemeris of the chaser and target provided by the numerical propagations, the state vectors of the two objects are computed by interpolation. Then the relative velocity $\overrightarrow{V_r}$ and the relative position $\vec{\rho}$ vector are determined to check if at that specific time instant the two objects are approaching or moving away. With the relative speed and position, it is possible to compute $f(t)$ which has been previously defined in section 2.2.1. When $(f(t_0) > 0)$ the two objects are moving away which means that the real time of closest approach is backwards in time $(t_{ca} < t_0)$. On the other hand if $(f(t_0) < 0)$ then $(t_{ca} > t_0)$. Once the time direction of the TCA is known $f(t)$ is evaluated every six seconds as recommended in [7], following the previously determined time direction until the expression $sign(f(t_n)) \neq sign(f(t_{n-1}))$ is fulfilled.

Then in the third step, with the previously found time interval the Regula-Falsi[15] algorithm is applied to found the TCA with the level of accuracy established by the user.

3.3.4 *FINITE DIFFERENCES TRANSITION MATRIX APPROACH*

The most important drawback of the numeric propagation Monte Carlo algorithm is the high computational cost leading to large time periods to achieve a significant result. This is why an alternative propagator has been developed with the aim to reduce significantly the computational cost but at the same time preserve the accuracy of the numerical propagator.

The fundamental concept of the new approach is to compute more efficiently the orbits resulting from the perturbation of the initial state. The idea is to determine the ephemeris of an orbit resulting from an initial state perturbation taking advantage of a well-known ephemeris of an orbit that results from the unperturbed initial state.

To achieve this objective the first step is to take into consideration the state vector of the spacecraft known as a function of time and the initial state $(\vec{X}(t, \vec{X}_0))$. In our case using the first order Taylor approximation it is possible to compute a new state vector as a function of time $(\vec{X}_i(t))$ of the same spacecraft but with a slightly different initial state vector.

[15] See section: Regula-Falsi Root Finder 2.2.2 for more information about the Regula-Falsi algorithm.

$$\vec{X}_i(t,\vec{X}_{0i}) \simeq \vec{X}_{ref}(t,\vec{X}_{0ref}) + \frac{d\vec{X}_{ref}(t,\vec{X}_{0ref})}{d\vec{X}_{0ref}} \cdot \Delta\overrightarrow{X_i} \quad \text{Eq. 95}$$

$$\vec{X}_i(t,\vec{X}_{0i}) \simeq \vec{X}_{ref}(t,\vec{X}_{0ref}) + \frac{d\vec{X}_{ref}(t,\vec{X}_{0ref})}{d\vec{X}_{0ref}} \cdot (\vec{X}_{0i} - \vec{X}_{0ref}) \quad \text{Eq. 96}$$

The first two terms in the right side of the equation describe the orbit of the object that turns out from the unperturbed initial state. The second term is the product of the initial perturbation vector and the transition matrix. The OREKIT library does not incorporate the ability to compute such data, which is why the transition matrix will be computed by finite differences along this approach.

The transition matrix will be referred as φ where a component of it is defined the following way:

$$\varphi_{xy}(t,\vec{X}_{0ref}) = \frac{dX_x(t)}{dX_{0ref-y}(tca)} \quad \text{Eq. 97}$$

The finite differences expression of the previous equation is:

$$\varphi_{xy}(t,\vec{X}_{0ref}) = \frac{X_x(t,X_0 + \Delta X_y) - X_{xref}(t,X_0)}{\Delta X_y} \quad \text{Eq. 98}$$

The interpretation of the previous equation is that the transition matrix can be computed as a function of time, if previously seven ephemerides are calculated. First of all the reference orbit ephemerid is required, but at the same time it is also necessary to compute of a set of ephemerides that contain the orbit evolution with a small perturbation in the initial state in each dimension of the state vector. Since the state vector is a six dimensional vector, six ephemerides of the orbit with an initial small perturbation are required.

For instance if component 1,2 needs to be computed, then it is necessary to subtract the first component of the state vector, generated by the propagation of the initial state with a small perturbation in the second component, and the state vector generated by the propagation of the initial unperturbed state. The result of such subtraction is then divided by the size of the small perturbation used in the initial state.

3.3.4.1 Finite Differences Propagator

Considering the previous theoretical approach, a propagator will be implemented to apply the previous simplifications, and it will be used in the Monte Carlo algorithm.

The propagator will internally compute the ephemeris of the reference initial state, and for each stored state it will couple a transition matrix. After that, given a perturbation of the initial state using the following expression, it will be able to compute the new ephemeris.

$$\vec{X}_i(t, \vec{X}_{0i}) \simeq \vec{X}_{ref}(t, \vec{X}_{0ref}) + \varphi_{xy}(t, \vec{X}_{0ref}) \cdot \left(\vec{X}_{0i} - \vec{X}_{0ref}\right) \quad \textbf{Eq. 99}$$

Since the only required operation to compute the new ephemeris is a set of matrix products, the resulting computational time it is expected to be significantly lower[16] than a standard numerical propagation.

3.3.5 PLOTS

One interesting feature of the Monte Carlo algorithms is that a concrete close approach is solved in each iteration. That means that for each conjunction interesting data can be recorded for its subsequent statistical analysis. In this report three plots based on any kind of Monte Carlo analysis are computed: the distributed probability histogram, the conjunction probability vs. combined object radius and the accumulative probability plot.

The previous three noted plots are based in two characteristic parameters that are extracted from each close approach assessment: the miss distance and the conjunction date.

3.3.5.1 Distributed probability histogram

To generate the distributed probability histogram, the first step is to define a miss distance range and divide it in constant intervals. When the Monte Carlo analysis is started every close approach is classified in one of the previous defined intervals. After a reasonable number of iterations the result is that for each miss distance interval, several close approaches have been recorded. Then, if the number of close approaches of a determined interval is divided by the total number of trials, the result is the probability of the miss distance to be comprehended between the two values that form the interval. And even more, if that concrete probability is divided by the magnitude of the interval, then the distributed probability along the miss distance is obtained. However, it is obtained in a discrete form, since infinite Monte Carlo trials would be required to obtain a continuous distribution.

$$\mu(x_i) = \frac{n(x_i)}{N \cdot x_i} \; [m^{-1}] \quad \textbf{Eq. 100}$$

[16] Check section 6.7 Algorithms Computational Performance improvement rate quantification.

Where $(\mu(x_i))$ is the distributed discrete probability function (x_i) is a specific miss distance interval $(n(x_i))$ is the number of recorded miss distances for a given miss distance interval, and finally (N) is the total number of recorded miss distances.

3.3.5.2 Conjunction probability vs. combined object radius

If the previous function is integrated along the miss distance, the result is the total conjunction probability for a given combined object radius.

$$P(COR) = \int_0^{COR} \mu(x)dx = \sum_{i=0}^{N} \mu(x_i) \cdot x_i \qquad \text{Eq. 101}$$

Where (I) is the index of the miss distance interval that equals the desired explored value of combined object radius.

This plot can result very useful when the dimensions of the objects are unknown because it can help to determine if an increment in the combined object radius is critical for that concrete close approach. Generally, the relation between the combined object radius and the conjunction risk is mostly linear, however as it could be seen in the previous sections, in some particular objects relative approaches the relation can be nonlinear.

3.3.5.3 Cumulative probability plot

On the other hand, since the date of all conjunctions can be calculated with the Monte Carlo analysis, the conjunction probability density function can be expressed as a function of time if there is a reasonable amount of recorded conjunctions. This plot follows a parallel approach from the previous one; the only difference is that in this case $(\mu(t))$ is the distributed probability density along time.

$$P(t) = \int_0^{t} \mu(t)dt = \sum_{i=0}^{N} \mu(t_i) \cdot t_i \qquad \text{Eq. 102}$$

CHAPTER FOUR: SPECIFICATIONS

Before starting the software design phase of the probability calculator software it is essential to determine and clarify the specifications that the software must fulfill. The following sections are a summary of the table that can be found at the end of the current chapter.

4.1 FUNCTIONAL REQUIREMENTS

The main aim of the software is to compute the collision probability of a conjunction of two orbiting objects. To achieve that objective, the algorithms that build up the software should be able to ingest as an input the exact date of the two object's closest approach, the state vectors, covariances and their span.

The algorithms that will be used to compute the probability shall be Akella and Alfriend's, Alfano's Maximum Probability and a Monte Carlo method. As explained in the previous section 2.3.5 Conjunction problem conclusions those have been considered the most suitable for the general purpose of the project. The algorithm that will be used in each case will be selected by means of configuration (e.g., through a user interface) and in any situation the software will consider the objects as perfect spheres.

For the Monte Carlo method, the software should be able to perturb the state vector of the target and chaser, propagate their orbits forward and backward and find the new TCA associated to the perturbed state. This shall be repeated a number of trials necessary to achieve an accurate result for the collision probability.

Finally, the software should be able to handle different reference system as the: J2000, GRCF, EME2000, ITRF from the IERS 96 and IERS 2003 conventions[17].

4.2 INTERFACE REQUIREMENTS

The input data of the software will be provided as a CSM from JSpOC or as a CDM[18] defined by the CCSDS[19]. Such information should be provided in HTML in

[17] IERS conventions are detailed explained in section 2.4 Reference Frames.

[18] CDM: is the abbreviation of Conjunction Data Message. It is an information standard proposed by CCSDS to make easier the information exchange between different space entities.

[19] CCSDS is the abbreviation of: Consultative Committee for Space Data Systems. It is a multinational forum for the development of communications and data systems standards for spaceflight founded in 1982 by the major space agencies of the world.

the case of CSM and in XML in the case of the CDM. On the other hand, the output will be a standard CDM in XML format.

For the proper internal operation of the library when making reference system transformations, the software should be able to accept as an input IERS 03 and IERS 96 files.

All the inputs and outputs paths should be able to be settled by means of configuration.

4.3 PERFORMANCE REQUIREMENTS

The software should be able to make the probability computation using Akella and Alfriend, and Maximum Probability algorithms in less than 5 seconds. Nevertheless, the time of the Monte Carlo method will not be limited, because one of the objectives of this project is to test the Java code performance for high demanding algorithms.

4.4 VALIDATION REQUIREMENTS

Akella and Alfriend's algorithm implementation will be validated using existing software owned by GMV named ***closeap*** and implemented in FORTRAN 95[20]. On the other hand, a parallel validation will be done comparing the results between the linear and Monte Carlo algorithms.

4.5 DESIGN CONSTRAINTS

The software will be designed as a modular library taking advantage that the Java language is object oriented; it will contain a main class that will make use of the entire library.

4.6 IMPLEMENTATION CONSTRAINS

The software will be implemented in Java 2 Standard Edition, under the Eclipse Integrated Development Environment. It will be built nightly with Hudson and the configuration control will be made through Subversion[21].

---

[20] FORTRAN: is a General-purpose, imperative programming language that is especially suited to numeric computation and scientific computing. It was developed by IBM in the 1950s and after half a century it has Become One of the most popular languages in the area of high-performance computing.

[21] Subversion: is a software versioning and revision control system distributed under an opens source license. It's most frequent use is to maintain current and historical versions of files such as source code, web pages, and documentation.

4.7 REUSED LIBRARIES

The development of the software in Java language involves several advantages; one key advantage is the great number of available ready-to-use open source libraries. This fact simplifies the programing task considerably. In this section a brief explanation of all the libraries to be reused will be done.

4.7.1 OREKIT LIBRARY

The Orbit Extrapolation Kit is a Space Flight Dynamics Java Library that provides a quite complete set of low level classes that enable the user to handle orbits, dates, frames, attitudes and to perform conversions, propagations and other tasks.

During the past years OREKIT has suffered a quick evolution and has gained widespread recognition. It first started as a closed-source product developed by a French company, but just after 2008 it switched to a permissive open-source license. Three years later it even became more open and a collaborative site was opened to let the public have direct visibility of its development. Finally, nowadays it is opening its governance, based in the Apache Software Foundation, involving representatives from different space field actors. The library is now been used by spacecraft manufacturers, satellite operators, academics, software industry and independent experts.

In conclusion, OREKIT is a well-recognized robust library that fits perfectly for the development of the collision probability software.

4.7.2 LOG4J LIBRARY

It is an Apache Software Foundation Project library for logging messages from the code.

It is an Apache Software Foundation Project dedicated to produce a logging library for Java.

4.7.3 HTMLPARSER LIBRARY

The HTML Parser is a Java library used to extract or transform HTML code in either linear or nested fashion. It is a robust, fast and well tested package that will be used principally to extract the information from the CSMs.

4.7.4 APACHE MATH LIBRARY

Another library from the Apache Software Foundation, it contains the basic mathematics and statistics components to address the most common problems that are not available in the Java language.

4.7.5 JAMA MATRIX LIBRARY

The JAMA library is a basic package to make the most common algebraic operations, in a very intuitive way.

4.8 SPECIFICATIONS TABLE

Software requirements speciation		
Req. ID	**Requirement description**	**Comment**
1	**Functional requirements**	
SRD-0100	The software shall be able to compute the collision probability of a conjunction	
SRD-0105	The software shall be able to ingest as inputs the time of closest approach (TCA), state vectors and covariance at TCA for both objects	
SRD-0110	The software shall be able to use Akella and Alfriend's algorithm for collision risk evaluation	
SRD-0115	The software shall be able to use the Maximum Probability algorithm for collision risk evaluation	
SRD-0120	The software shall be able to use a standard Monte-Carlo method for collision risk evaluation	
SRD-0125	The software shall allow to choose the method to use for collision risk evaluation by means of configuration	
SRD-0130	The software shall handle the various reference frames and IERS conventions under consideration (J2000, GRCF, EME2000, ITRF; IERS 96 and IERS 2003) in a consistent way	
SRD-0135	The software shall be able to propagate the orbits of target and chaser based on initial state vector and covariance at a given initial state	
SRD-0140	The software shall be able to perturb the conditions at the original TCA based on the position and velocity covariance provided for both objects in support of the Monte-Carlo analysis	
SRD-0145	The software shall be able to find the perturbed TCA associated to the perturbed conditions described in SRD-0140	

SRD-0150	The software shall consider both target and chaser objects as spherical objects	This implies that the attitude of the objects is irrelevant for the collision risk analysis
2	**Interface requirements**	
SRD-0200	The software shall accept as inputs a Conjunction Summary Message (CSM) from JSpOC or a Conjunction Data Message (CDM) as defined by the CCSDS	The version of the CDM to be implemented is the latest version available as of 15/04/2013
SRD-0205	The software shall accept as input files CSMs in html (and xml optionally) formats	
SRD-0210	The software shall accept as input files CDMs in xml (and ASCII optionally) formats	
SRD-0215	The software shall generate as output files CDMs in xml (and ASCII optionally) formats	
SRD-0220	The software shall accept as input files the leap seconds file and EOPs files (IERS 2003 and IERS 96)	
SRD-0225	The software shall allow to define the paths of input and output file by means of configuration	
SRD-0230	The software shall respect the interface defined for applications to be integrated in the ***focus*** infrastructure	Any application to be executed within the ***focus*** must respect the interface used by ***focus*** in order to
SRD-0235	The software shall generate standard error and output with a summary of the progress of the execution to be integrated in ***focus***	
3	**Performance requirements**	
SRD-0300	The software shall be able to compute the collision risk in less than 5 seconds for one conjunction in a standard PC in case of using Akella and Alfriend's algorithm or the maximum probability algorithm	
SRD-0305		
4	**Operational requirements**	
	None are identified	

5	**Validation requirements**	
SRD-0500	The software shall be validated against ***closeap***	
SRD-0505	The software shall be validated for consistency between Akella and Alfriend's method and the Monte Carlo analysis	
SRD-0510	The random generation algorithm shall be validated in order to obtain an effective Monte Carlo algorithm	
6	**Design constraints**	
SRD-0600	The software shall be designed in modular way	A clear UML class diagram and package diagram shall be created as part of the design process
SRD-0605	The software shall be designed as a library	This library shall be completely agnostic to the ***focus*** interface
SRD-0610	The software shall contain a main class (or application) making use of the library defined in SRD-0605	This main class shall handle all aspects related to the interface with ***focus***
SRD-0615	The software shall be designed such that the information between the main application defined in SRD-0610 and the library defined in SRD-0610 is done through Java objects (i.e., no file-based interfaces)	
7	**Implementation constraints**	
SRD-0700	The software shall be implemented in Java 2 Standard Edition (J2SE)	
SRD-0705	The software shall be implemented under the Eclipse Integrated Development Environment	
SRD-0710	The software shall be kept under configuration control using Subversion	
SRD-0715	The software shall be built nightly with Hudson	
8	**Quality requirements**	
SRD-0800	The software shall respect the metrics defined at GMV for SSA projects	
SRD-0805	The software metrics shall be checked with **Checkstyle**, **PMD** and **findbugs**	The configuration of these files is provided

		by GMV based on SSA projects with ESA
SRD-0810	The software shall be validated with unit tests with a **coverage** greater than 80%	
SRD-0815	The software coverage shall be checked with **Cobertura**	
SRD-0820	The software shall have a cyclomatic complexity number below 15 for all classes	
SRD-0825	The software shall have a nesting index below 8 for all classes	
9	**Reuse requirements**	
SRD-0900	The software shall reuse the library **OREKIT** 6.0-SNAPSHOT as of 15/04/2013 as low level flight dynamics library	
SRD-0905	The software shall reuse the ***focusJava standalone*** product for the Human Machine Interface	
SRD-0910	The software shall reuse the library **log4j** for the generation of the standard error and output	
SRD-0915	The software shall reuse the library **hmltparser** for the parsing of html files	
SRD-0920	The software shall reuse the **JAXB** framework for the parsing of xml files	
SRD-0925	The software shall reuse the **apache math** library for mathematical functions	The version of apache math library shall be the same as used by OREKIT
SRD-0930	The software shall be built with **maven** 3 and the corresponding plugins for checkstyle, PMD, findbugs, JAXB and cobertura	
SRD-0935	The software build process shall generate automatically Javadoc, cobertura, checkstyle, pmd and findbugs documentation	
SRD-0940	The software tests shall be executed with the **jUnit** framework	
10	**Security requirements**	
	None are identified.	***focus*** HMI already provides security measures (authentication/authorization) and thus no special measures need to be taken to this respect

11	**Reliability requirements**	
SRD-1100	The software shall be robust against format errors in the inputs	
SRD-1105	The software shall report errors in the inputs and exit gracefully	
12	**Monitoring and maintenance requirements**	
	None are identified	

Software optional requirements speciation		
Req. ID	**Requirement description**	**Comment**
1	**Functional requirements**	
SORD-0105	The Monte Carlo method could provide the TCA and Miss distance with their relative standard deviations.	
SORD-0110	The Akella method could provide the TCA and Miss distance with their relative standard deviations.	
SORD-0115	The Monte Carlo method could include the functionality to consider or dismiss the correlation of the covariance.	
SORD-0120	The Monte Carlo method could generate a real time plot showing error-iterations.	
SORD-0125	Akella Method could provide a graphical representation of the projection of the n-shell and the combined object radii in the encounter plane with the angle between the relative position and the principal axis of the combined covariance projection.	
SORD-0130	Akella Method could require an error input value for the two dimension integral accuracy.	
SORD-0135	The Monte Carlo method could require an error value for the global probability computation.	
SORD-0140	The Akella Method could have a special warning when the covariance shell is much larger than the miss distance.	
SORD-0145	The Akella and Total Probability method could provide a warning when the collision is not linear (relative speed below 10m/s).	
9	**Reuse requirements**	
SORD-0905	The software could reuse the JAMA library for the mathematical matrix operations.	*b*

CHAPTER FIVE: SOFTWARE DESIGN

The Java conjunction assessment library developed in this project has been implemented following object oriented programming techniques. Such techniques arrange the code in a modular structure making it easier to write, read and modify.

The basic elements that are defined in the oriented object techniques are: packages, classes, attributes and methods. The conceptually most important element is the class; it is a self-contained code composed by its own attributes (variables) and methods (functions). In other words, when following object orientation techniques methods and attributes are encompassed in a single unit called class. Nevertheless, the greatness of the technique is that once the class has been defined several objects from a single class can be declared. That makes the code really simple and easy to understand.

A library is a set of classes that can be called and used from a main routine; those classes are generally arranged in package units. The package content is quite open to the programmer choice, however the general criteria is to arrange all the classes that have a general functionality in common.

It is important to introduce the inheritance concept; it is also useful to simplify the code implementation. The inheritance allows creating new classes based in existing ones, which simplifies the previously developed code reutilization. As an example, if two classes have some parts in common it is possible to define a parent class that contains the common items and two child classes that inherit the common attributes and methods and only cover the different items.

Java does not admit the space character for class names declarations. However, for the reader's convenience in this report all the class names will be written in cursive with spaces.

The conjunction probability calculation library is composed by six packages: model, business, dataio, configuration, exceptions and main. The **model** package comprehends all the classes in charge of holding the information required by the second package (**business**), which encompasses the algorithmic part. The **dataio** (data Input-Output) package contains the classes used to transform data, in other words, in charge to interpret or write the input and output data. There is also the **configuration** package which includes management modules of the general program configuration. And finally, the **exception** package that, as its name indicates, contains the specific Java exceptions of the conjunction probability library. Finally, there is a **main** module that comprehends a general class that allows the general usage of the library.

In this section graphic UML2[22] class diagrams will be used to allow the reader visually understand the general software design and operation.

In Figure 20 the global package distrubution of the probability computation library is exposed with all the subclasses of each package. Since the bussines package contains a large number of classes it has been internally divided in subpackages.

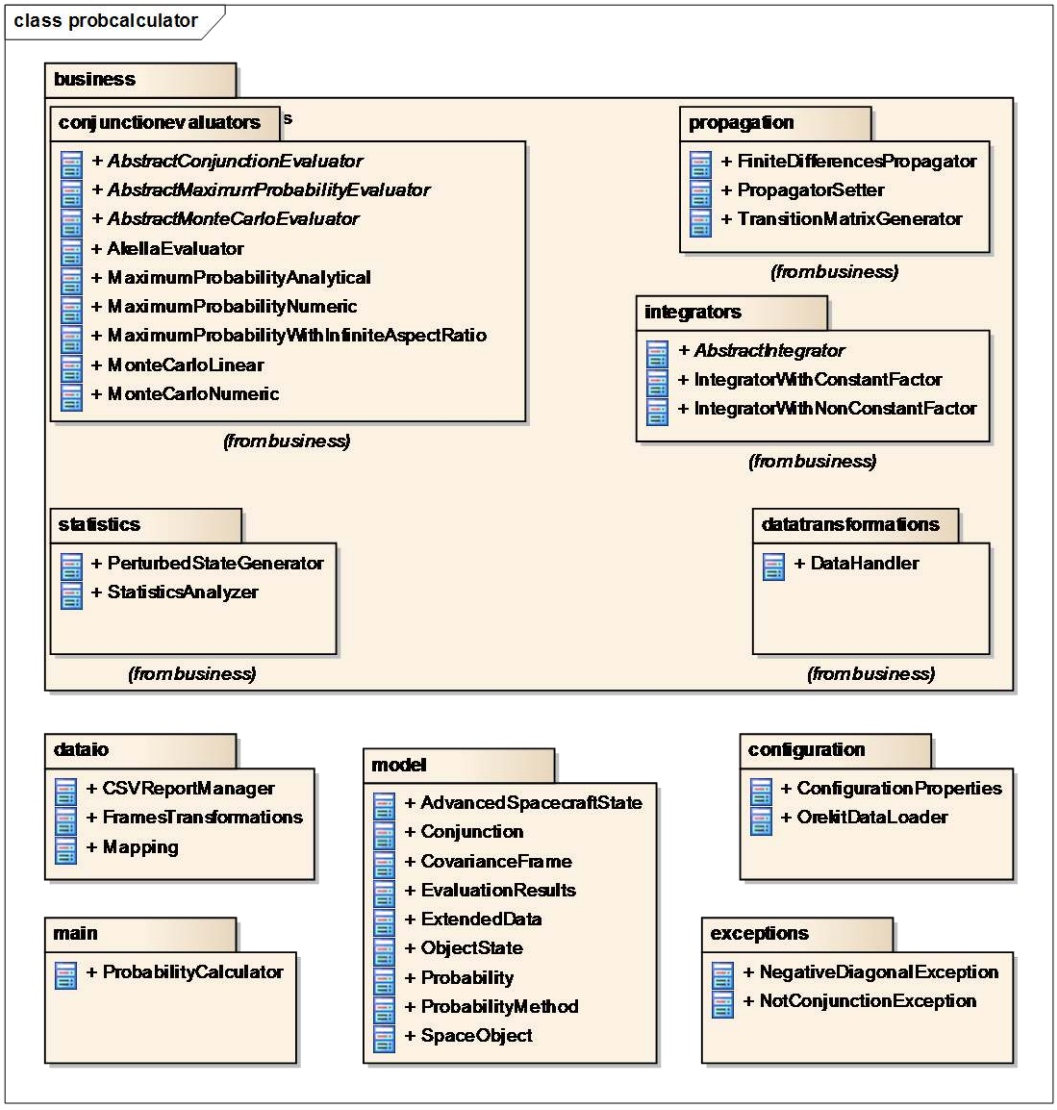

Figure 20: UML2 diagram of the Package distribution of the probability computation library.

5.1 Model Package Architecture

The model package, as mentioned before, is composed by those classes that will be used as data containers for the different algorithms to perform the conjunction

[22] UML2: acronym of Unified Modeling Language, it includes a set of graphic notation techniques to create visual model of objects-oriented of software systems.

analysis. As exposed in Figure 21, the model package is formed by nine classes: *Evaluation Results, Extended Data, Conjunction, Space Object, Object State, Probability, Probability Method* and finally *Extended Spacecraft State*.

- ***Evaluation Results:*** this class is the upper data container of all the library, it only has two attributes: a *Conjunction* object that holds all the necessary data to characterize a risky close approach and an *Extended Data* object which contains some extra data resultant from the conjunction risk evaluation process.

Extended Data: this class contains all the data that cannot be stored by the *Conjunction* object, in other words all that data that results from the conjunction risk evaluation and cannot be mapped into a Conjunction Data Message. Its content is a set of arrays that define some interesting plots that could be plotted by third party applications. Currently, the plots that have been implemented are: the cumulative conjunction probability, the distributed probability histogram and the total conjunction risk vs. the combined object radius. Examples of these plots can be found in

- CHAPTER SIX: Validation and Results.
- ***Conjunction:*** this is the fundamental class of the conjunction probability library; it contains all the information to fully specify a close approach. The main idea of this class is to be the node between the data in and out algorithms and the logic algorithms that compute the conjunction probability. For this reason, a *Conjunction* object contains all the data required to compute the collision probability, but at the same time it is prepared to hold all the data provided by the previous mentioned logic algorithms. It follows a very similar structure than the Conjunction Data Messages, since it has been designed to be the only required object to comprise all the information to print a CDM (or CSM).

  The *Conjunction* class comprehends the date of the closest approach, the miss distance, their respective standard deviations, the collision probability and the characterization of the target and chaser.

- ***Space Object:*** it is the class that characterizes an orbiting object. It contains data regarding the object's name, the name of the catalog where it belongs, its designator for that specific catalog. It also comprehends information about the maneuverability of the object, its aim and finally, information about its state at the time of closest approach.
- ***Object State:*** class that encompasses the state information of a space object at a specific time, concretely the time of closest approach. It provides the state vector, covariance matrix, the radius of the object, and the frames of the state vector and covariance matrix. There is a conceptually similar class in the OREKIT library, but it has not been used because it does not have access methods to its internal data.
- ***Probability:*** this class contains the value of the risk of conjunction and it also specifies with which method the probability has been computed. The probability method is specified through an enumeration class called *Probability Method*.
- ***Extended Spacecraft State:*** it is a special class only used by the *Finite Differences Propagator*; it is an improvement of the *Spacecraft State* class already implemented in the OREKIT library. This class, in addition of defining the state of a spacecraft also contains its related transition matrix.

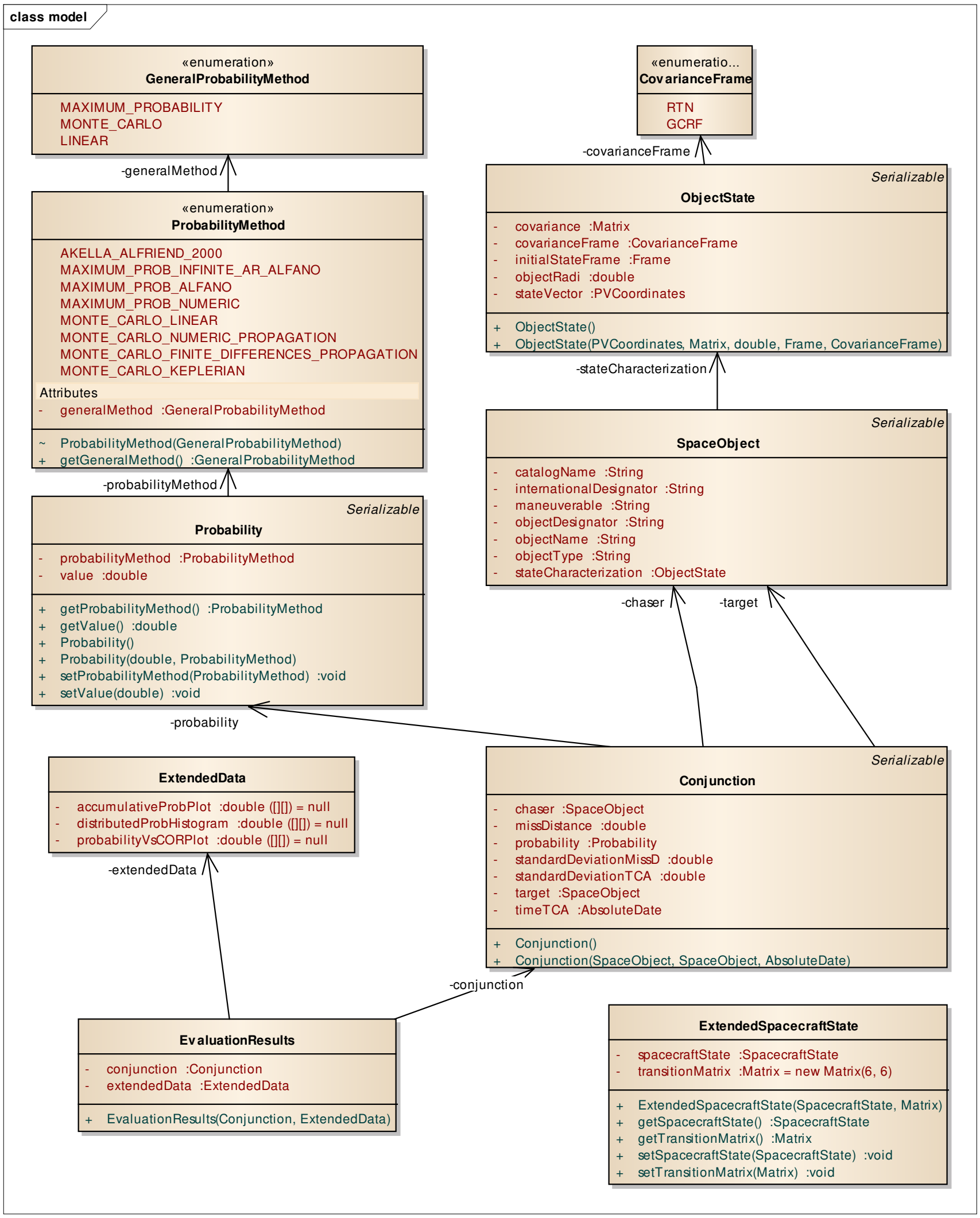

Figure 21: UML2 class diagram of the model package.

5.2 BUSINESS PACKAGE ARCHITECTURE

The business package is the most complex because it covers all the algorithms required for the conjunction risk assessment and plots computation. It encompasses a set of classes to compute the collision risk taking advantage of seven different algorithms. The package is composed by five sub packages: conjunction evaluators, integrators, propagation, statistics, and data transformation.

5.2.1 CONJUNCTION EVALUATORS

- ***Abstract Conjunction Evaluator:*** this class is the parent class of all probability assessment algorithms. It has a principal method that returns an *Evaluation Results* object with all the information regarding the conjunction assessment. Since it is an abstract class the definition of its method is done through its children: *Akella Evaluator*, *Abstract Maximum Probability Evaluator* and *Abstract Monte Carlo*.
- ***Akella Evaluator:*** it extends from the *Abstract Conjunction Evaluation* class; it can mainly do three operations. On one hand, it can calculate the conjunction risk taking advantage of the linear Akella and Alfriend 2000 algorithm, but it also is capable to compute the standard deviation of the miss distance and time of closest approach making use of the expressions developed in this report.
- ***Abstract Maximum Probability Evaluator:*** it extends from the *Abstract Conjunction Evaluation* class. It consists of the common attributes and methods of their child classes the: *Maximum Probability Numeric*, *Maximum Probability Analytical* and *Maximum Probability Infinite Aspect Ratio*.
- ***Abstract Monte Carlo Evaluator:*** it also extends from the *Abstract Conjunction Evaluation* class and as well as the previous described class it is composed by the common code of their child classes *Monte Carlo Linear* and *Monte Carlo Numeric*. It has methods to generate the Monte Carlo plots, methods to calculate the conjunction probability and methods to generate an output conjunction object.
- ***Maximum Probability Numeric:*** it extends from the *Abstract Maximum Probability Evaluator* and it computes the maximum conjunction probability through an iterative algorithm developed in this report in section 3.2.1 Iterative Maximum Probability. This class and the *Akella Evaluator* class make use of the integrators found in the business package.

- ***Maximum Probability Analytic:*** it is a child class of the *Abstract Maximum Probability Evaluator* and it is used to compute the maximum conjunction probability as a function of the combined covariance aspect ratio making use of an analytical formula developed by Alfano [20].
- ***Maximum Probability Infinite Aspect Ratio:*** it is also a child class of the *Abstract Maximum Probability Evaluator* and it is also used to compute the maximum conjunction risk when the combined covariance aspect ratio is infinite.
- ***Monte Carlo Linear:*** extends from *Abstract Monte Carlo Evaluator* and it overwrites some of their methods to compute the conjunction risk and to save the required data for the Monte Carlo plots.
- ***Monte Carlo Numeric:*** extends from *Abstract Monte Carlo Evaluator*, this class is the only one that takes advantage of orbital propagators to perform a conjunction risk assessment. This is why it is able to perform two different conjunction assessments depending on the propagators used to initialize the class. In this report only two propagators have been used but the class is designed to run with any kind of OREKIT propagator or extension of them. If propagations are carried out with a numerical propagator then the conjunction risk assessment used method is the Numeric Monte Carlo. However, if the propagations are carried out with a Finite Differences propagator then the method is the Finite Differences Monte Carlo.

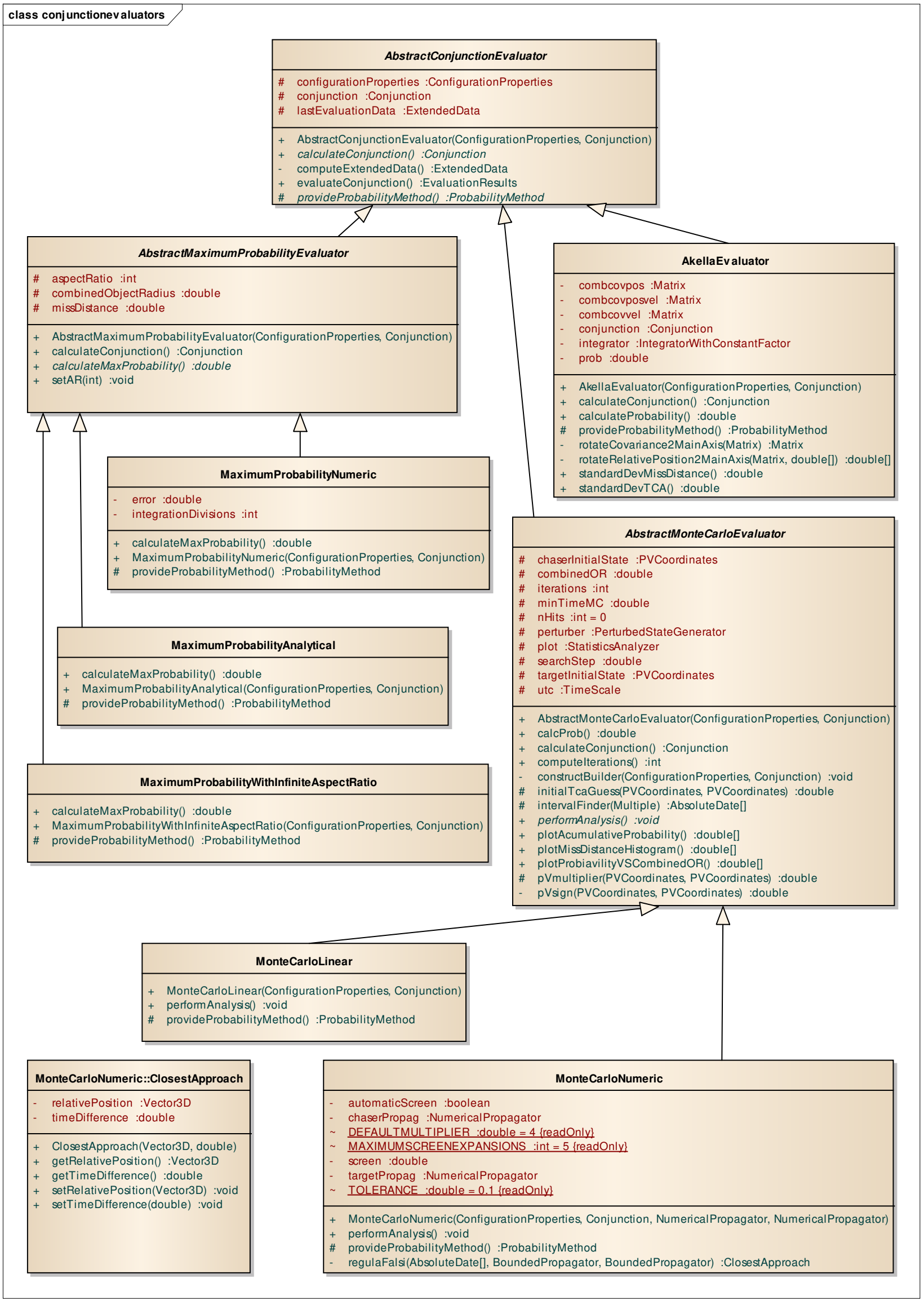

Figure 22: UML2 class diagram of the 'Conjunction Evaluators' sub package.

5.2.2 PROPAGATION

This package contains three classes that are somehow related to the propagation process. The *Transition Matrix Generator*, *Finite Differences Propagator* and finally the *Propagator Setter*.

- ***Transition Matrix Generator:*** it is a class used to compute mainly the transition matrix of a spacecraft at the required time instant. However, before being able to compute the transition matrix, it is necessary to define a maximum and minimum access date to fix the lower and upper time bounds for transition matrix computation. Then the class performs seven internal propagations that are stored as internal attributes before being able to compute the transition matrix of the space object. Although the name of this class is *Transition Matrix Generator* it returns an *Extended Spacecraft State* which contains a *Space Craft State* object and its transition matrix.

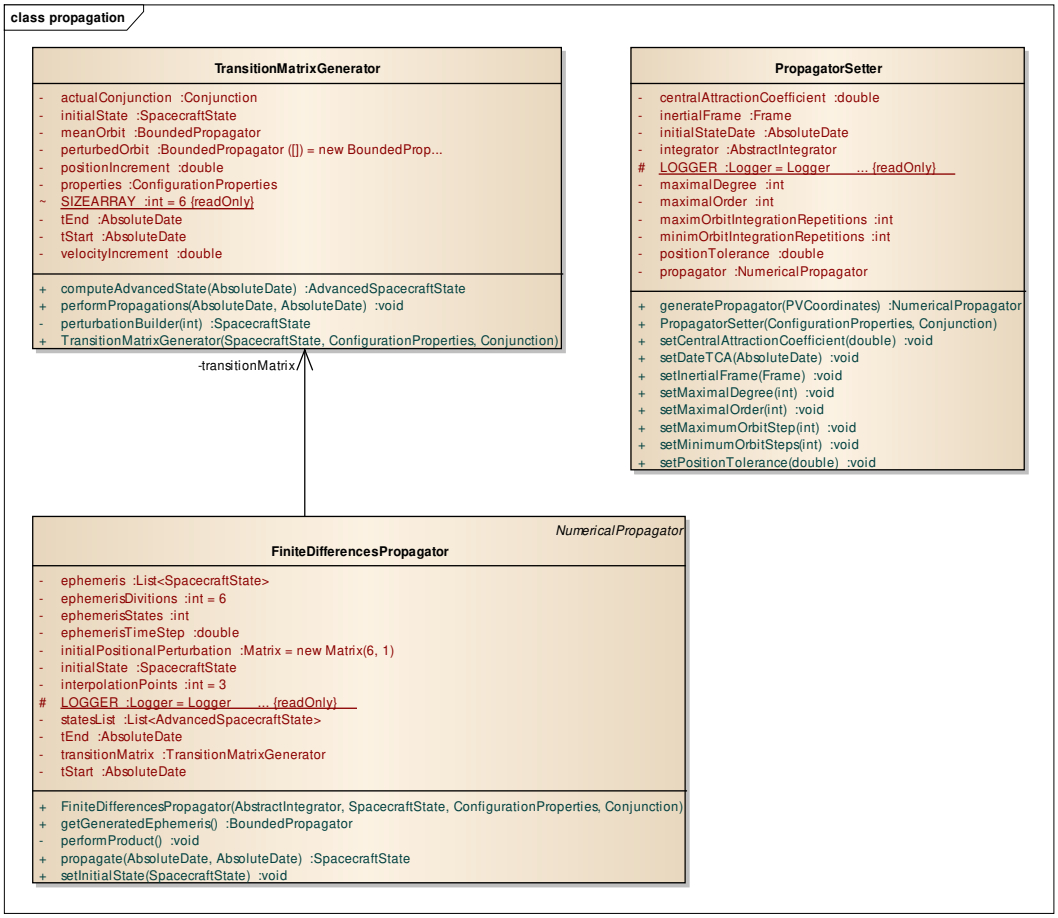

Figure 23: UML2 class diagram of the Propagation sub package of the Business package.

- ***Finite Differences Propagator:*** this innovative propagator makes use of a *Transition Matrix Generator* object to calculate and store an internal list of *Extended Spacecraft States*. Then, given an initial perturbation the class is able to compute an ephemeris of the spacecraft orbit.
- ***Propagator Setter:*** class used to create a *Numeric Propagator* from the OREKIT library with the configuration determined by the user of the conjunction probability library.

5.2.3 INTEGRATORS

The Akella and Alfriend 2000 and the Maximum Numeric Probability algorithms depend on the solution of two quite similar bi-dimensional integrals. The Integrators sub package contains three classes in charge of the numerical solution of such integrals. The *Abstract Integrator* class has the common code of the two integrals and then its children; *Integrator with Constant Factor* and *Integrator with Non Constant Factor* have the code that differs from the two integrals.

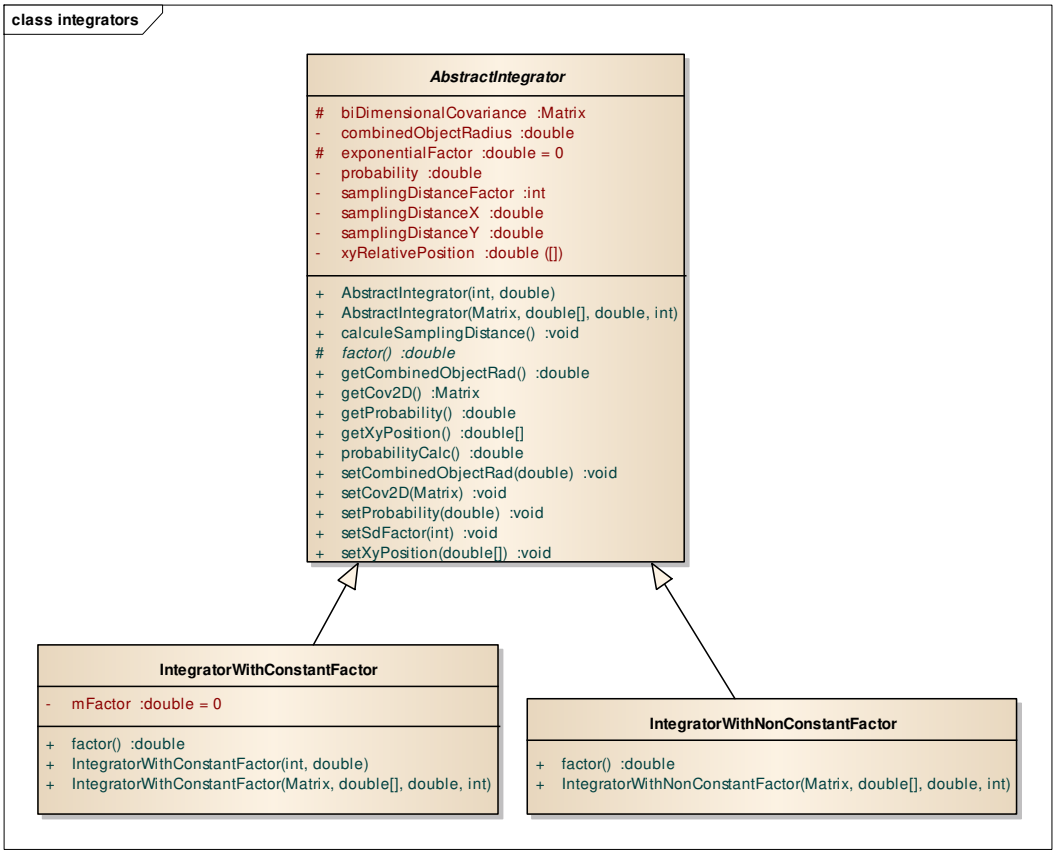

Figure 24: UML2 class diagram of the 'Integrators' sub package of the Business package.

5.2.4 STATISTICS

The statistics subpackage only contains two classes that have the common particularity to create and capture random Gaussian distributed populations.

- ***Perturbed State Generator:*** it is a class that given a six dimension covariance matrix it is able to return a six dimension random vector that follows the Gaussian population distribution specified by the initial covariance matrix.
- ***Statistics Analyzer:*** complex class that allows to record specifics events during a Monte Carlo analysis such as the time of closest approach of a specific conjunction, or the miss distance for a specific close approach. Then, after the analysis has been completed it is able to compute a set of plots that provide important information regarding that analysis.

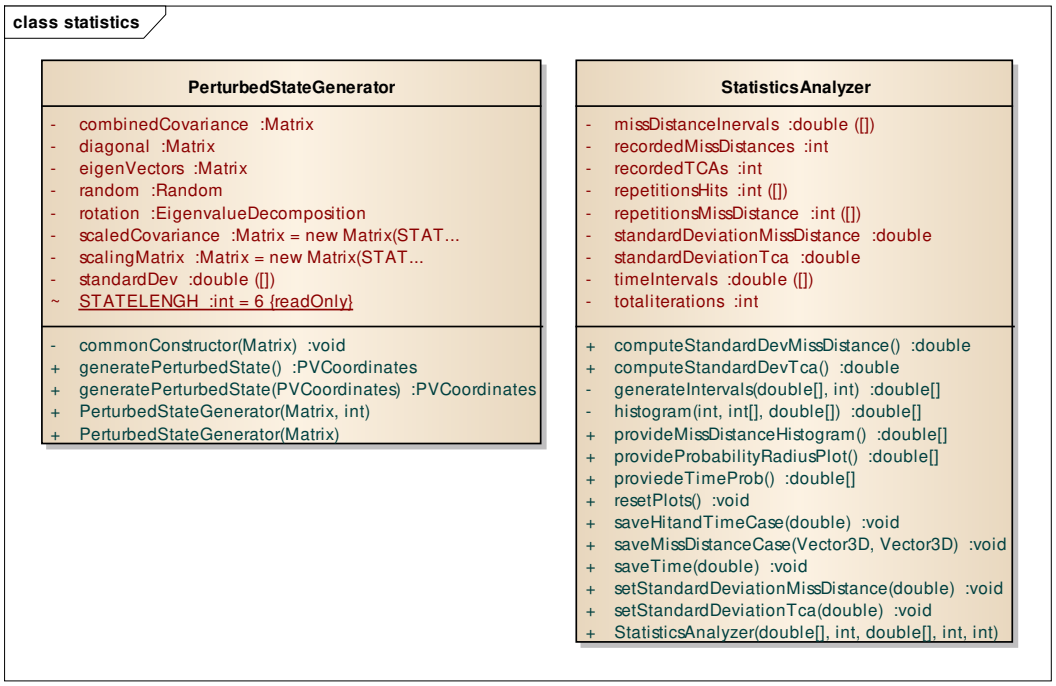

Figure 25: UML2 class diagram of the Statistics sub package of the Business package.

5.2.5 DATA TRANSFORMATIONS

This package is composed by a single class called *Data Handler* that contains a set of static methods to transform data objects from the different used libraries. This class was designed with the single aim to simplify the code of the conjunction evaluation library.

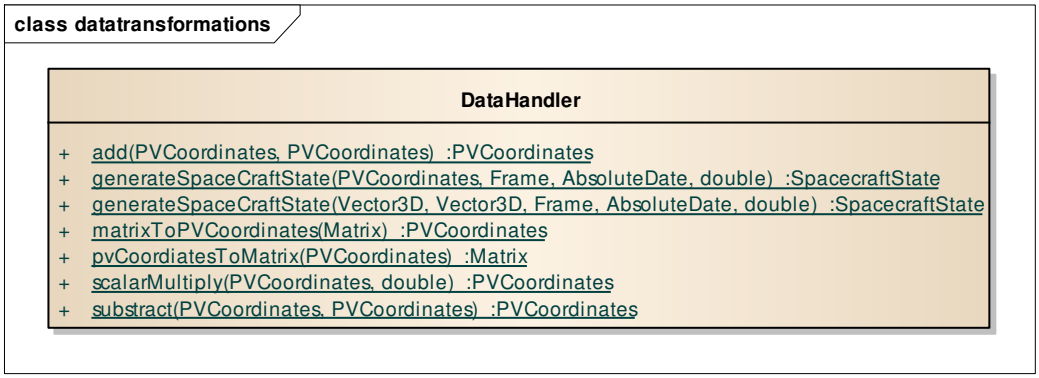

Figure 26: UML2 class diagram of the 'Data Transformations' sub package of the Business package.

5.3 DATAIO PACKAGE ARCHITECTURE

As it is established in CHAPTER FOUR: Specifications, the library has to be able to handle input and output Java objects. These objects are created by another project that parses the XML files of a CDM or a CSM and transform them into JAVA objects that follow a parallel structure from the one defined in the XSD[23] of these two different standards.

When the library receives one of these objects created by an external project, the Mapping class is in charge of transforming these objects into a well-defined *Conjunction* object. At the same time, it makes use of the *Frames Transformations* class to perform the proper frames transformations of the input conjunction to GCFR frame which is the one used by all the algorithms of the conjunction probability library.

- ***Mapping:*** this class is able to transform a CDM or CSM Java objects to a *Conjunction* object, or a *Conjunction* object to a CDM object.
- ***Frames Transformations:*** it is used to transform from the reference frames used in the CDM and CSM standards to the GCFR frame used in the conjunction probability library and vice versa.
- ***CSV Report Manager:*** class able to create CSV[24] files in order to export the plots data.

[23] XSD (xml schema definition): Is an XML schema language published as a W3C recommendation in May 2001. It is used to express a set of rules to which an XML must conform in order to be considered valid according to that schema.

[24] CSV (coma separated values): is a data format that consists on strings separated by comas.

Figure 27: UML2 class diagram of the 'dataio' package.

5.4 CONFIGURATION PACKAGE ARCHITECTURE

This package is composed by only two classes: *Configuration Properties* and *OREKIT Data Loader*. Both classes are in charge of providing the correct configuration for the conjunction probability library and the OREKIT library.

- ***Configuration Properties:* this class is used by practically all the other classes of the library to access to the library's configuration parameters.**
- ***OREKIT Data Loader:* class used to set the EOPs and gravity field data for the OREKIT library. The class allows the user to specify whether to load a default data set or to load a specific data set.**

5.5 MAIN PACKAGE ARCHITECTURE

This package is composed by a single class; such class allows using the library in a very simplified way. The *Probability Calculator* class has a principal method that, given a *Conjunction* and a *Probability Method* object, performs the whole analysis with the proper method and it returns an *Evaluation Results* with all the results of the computation.

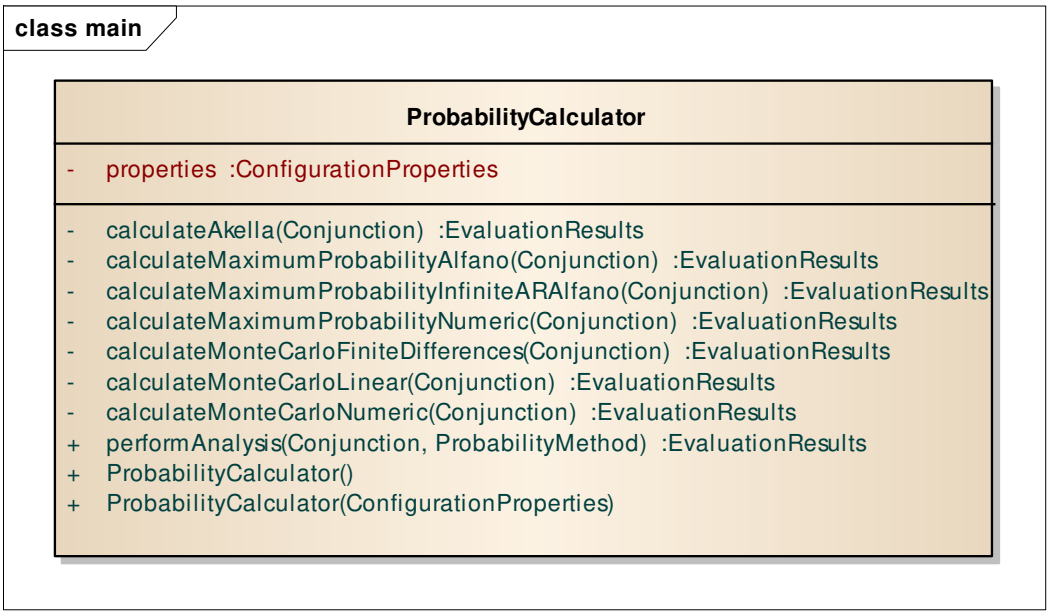

Figure 28: UML2 class diagram of the main package.

CHAPTER SIX: VALIDATION AND RESULTS

This section covers all the implemented algorithms to prove they work properly. The validation methodology may vary along the algorithms list, because it has not been possible to find reference outputs for all the algorithms. When no reference data is found, the algorithms are validated comparing their results against the results of different algorithms form the same library.

6.1 AKELLA AND ALFRIEND 2000 VALIDATION

The validation of the Akella and Alfriend 2000 algorithm has been done by contrasting the algorithm's results against the Conjunction Prediction Service, CPS[25], developed by GMV[26]. It computes the conjunction risk using a very similar algorithm from the one that has been validated.

Cases Summary				
Case	**DEC [Km]**	**Miss Distance [m]**	**Vr [m/s]**	**TCA**
1	7174	602.5	14863.4	2013-07-16T19:34:35.033
2	7250	630.4	14804.2	2013-07-19T14:55:36.581
3	7015	8.9	15045.1	2013-07-19T04:26:21.192
4	7142	306.7	14945.3	2013-07-16T04:12:56.494
5	7009	222.0	15065.7	2013-07-20T15:58:18.533
6	7159	894.4	13477.1	2013-07-16T11:10:37.434
7	6998	299.3	15127.8	2013-07-17T13:47:10.767
8	7153	88.2	14887.5	2013-07-16T01:30:29.588
9	7235	995.9	14813.9	2013-07-22T14:10:58.958

Table 3: Summary table of the nine conjunctions selected. DEC (Distance to the Earth Center), Vr (Relative Speed), TCA (Time of Closest Approach).

In Table 3, nine of the potential conjunctions during the dates 16/07/2013 and 22/07/2013 have been selected with the aim to validate among others the Akella

[25] Conjunction Prediction Service: service under development, nowadays it is in the SSA Preparatory Program phase. There is a testing online unit available in: https://sst.ssa.esa.int/cwbi/index.xhtml

[26] GMV: is a privately owned technological business group with an international presence. Founded in 1984, GMV offers its solutions, services and products in very diverse sectors: Aeronautics, Banking and Finances, Space, Defense, Health, Security, Transportation, Telecommunications, and Information Technology for Public Administration and large corporations.

and Alfriend algorithm. The table contains some relevant information regarding the cases selected such as the miss distance, the relative speed, the TCA and the distance of the objects to the center of the earth in the closest approach position. As it can be easily seen the relative speed in all cases is very high, to ensure perfect linear approach in all cases. These cases have been selected following the criteria of highest conjunction risk, and then the results of both tools have been directly compared.

In Table 4 the probability provided by the library and the CPS are compared considering the CPS results as reference values.

Akella and Alfriend-2000 Conjunction Risk				
Case	**Aspect Ratio**	**Reference Value**	**Computed**	**Relative Error**
1	83211	3.060E-05	3.058E-05	8.073E-04
2	429500	2.137E-05	2.134E-05	1.530E-03
3	297975	1.799E-05	1.798E-05	6.388E-04
4	12293	1.630E-05	1.629E-05	8.804E-04
5	19616	1.171E-05	1.170E-05	1.061E-03
6	557075	1.143E-05	1.142E-05	1.121E-03
7	526425	9.995E-06	9.987E-06	8.432E-04
8	267136	9.261E-06	9.253E-06	8.428E-04
9	95274476	5.780E-07	5.771E-07	1.554E-03
			Mean	9.899E-04
			Maximum	1.554E-03

Table 4: Validation table of the Akella and Alfriend 2000 algorithm. The 'Reference value' is the conjunction probability value computed by the CPS, while the 'Computed' field is the value computed by the algorithm implemented in this report.

The validation results for the Akella and Alfriend algorithm are exceptionally satisfactory since the mean relative error is below 0.10% and the maximum relative error is 0.16% for all nine tested cases.

6.2 Maximum Probability

The validation of the maximum probability algorithms is more complicated than the previous one, because there are no available reference values. There is an online

service called SOCRATES[27] that provides the maximum conjunction probability of all possible conjunctions predicted through the TLE states propagation. However, such data cannot be used for validations purposes because there are two drawbacks.

In the first place, the service uses a non-public database to load the catalog objects' dimensions, which means that there is no way to know which combined object radius is using the algorithm.

In second place the SOCRATES tool downloads the TLE information once a day and it uses such information to perform the all versus all conjunction assessment. On the other hand, the CPS uses the same working principle but it downloads the TLE data in a different moment along the day. That means that the predicted conjunctions are slightly different between the two tools, so even if it would be possible to have the object radii the compared results would differ because they would have been computed considering slightly different conjunctions.

Consequently, the validation of the maximum probability algorithms will be partially validated comparing their results among them for consistency.

6.2.1 Maximum Probability Infinite Aspect Ratio Alfano Validation

Maximum Conjunction Probability with infinite Aspect Ratio			
Case	**Aspect Ratio**	**Computed Akella**	**Maximum Probability**
1	83211	3.05753E-05	2.86632E-03
2	429500	2.13373E-05	2.73931E-03
3	297975	1.79785E-05	1.93297E-01
4	12293	1.62856E-05	5.63114E-03
5	19616	1.16976E-05	7.77869E-03
6	557075	1.14172E-05	1.93077E-03
7	526425	9.98657E-06	5.76910E-03
8	267136	9.25319E-06	1.95782E-02
9	95274476	5.77102E-07	1.73399E-03

Table 5: Maximum Conjunction Probability with infinite aspect ratio results.

The first test does not prove that the solution obtained by the Maximum Probability algorithm with infinite aspect ratio is correct but at least it proves that is not wrong.

[27] SOCRATES (Satellite Orbital Conjunction Reports Assessing Threatening Encounters in Space): is a service offered by the Center for Space Standards & Innovation (CSSI) that provides regular information on pending conjunctions over the coming week to help satellite operators to avoid the catastrophic consequences of a conjunction.

The results provided by such algorithm are compared against the results provided by the Akella and Alfriend 2000 algorithm in Table 5.

It is appreciated that all the maximum probability results are higher than the Akella results, which could indicate that the algorithm is finding an upper bound for the conjunction risk.

6.2.2 MAXIMUM PROBABILITY NUMERIC

It is appreciated that all the maximum probability results are higher than the Akella results, which could indicate that the algorithm is finding an upper bound for the conjunction risk.

For the Numeric Maximum Probability algorithm the conjunction risk will be computed for a range of aspect ratios and it will be demonstrated that if the aspect ratio is increased the numeric solution converges to the value computed with the previous algorithm.

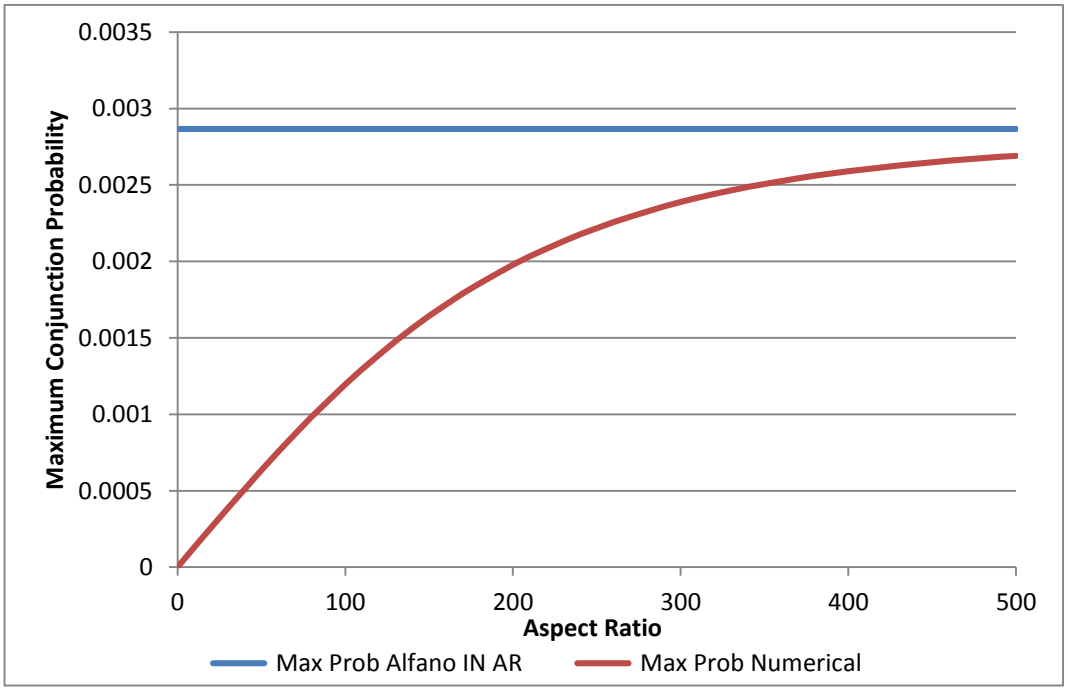

Figure 29: Numeric Maximum Conjunction Probability of the CASE 1 Conjunction VS Aspect Ratio. Max Prob. Alfano IN AR (Maximum probability with Infinite Aspect Ratio).

As it can clearly be appreciated in Figure 29 the maximum probability value obtained that depends on the aspect ratio converges to the maximum conjunction probability value with infinite aspect ratio. This is not a conclusive proof that both algorithms are working properly, but it is a very relevant result because the two

algorithms internally are really different but despite that, they converge to the same result.

6.2.3 MAXIMUM PROBABILITY ALFANO

The analytic Alfano approach to the maximum conjunction probability seems not to be providing significant accurate results. Figure 30 is a representative case of the behavior of the algorithm. For low aspect ratios, it returns higher probability values than the ones provided by the numeric algorithm. However, for higher aspect ratios the solution converges to zero instead to the maximum probability value. For all the cases tested the algorithm presents a similar behavior, so this algorithm is only recommended to be used for low aspect ratios to get a solution in the safe side.

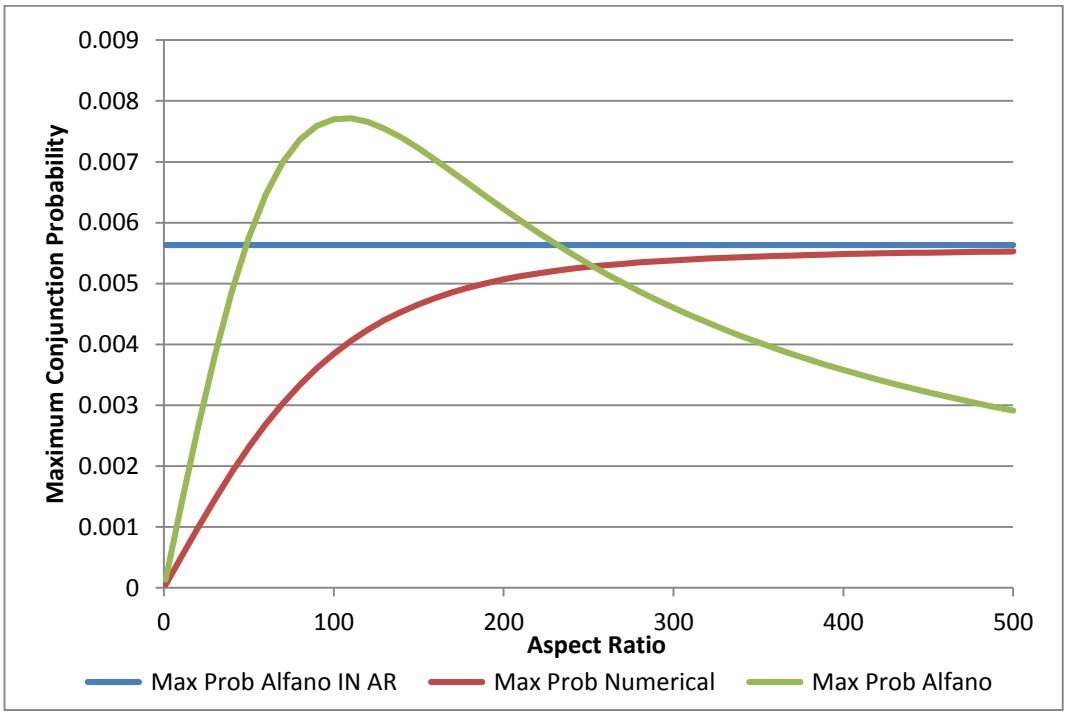

Figure 30: Numeric Maximum Conjunction Probability of the Case 4 Conjunction vs. Aspect Ratio. Max Prob. Alfano IN AR (Maximum probability with Infinite Aspect Ratio).

6.3 MONTE CARLO LINEAR

The Monte Carlo Linear is an algorithm that is in between the linear algorithms and the complex Monte Carlo algorithms with real propagation methods. It is between them in terms of computational cost and results reliability.

In Table 6 the nine cases used to validate the Akella and Alfriend algorithm have been analyzed using the Linear Monte Carlo algorithm with 10^9 trails with a mean computation time of three minutes for each case.

Monte Carlo Linear 1E9				
Case	Aspect Ratio	Reference	Computed Value	Relative Error
1	83211	3,06E-05	3,03E-05	1,11%
2	429500	2,14E-05	1,03E-06	95,18%
3	297975	1,80E-05	1,72E-05	4,45%
4	12293	1,63E-05	1,58E-05	3,37%
5	19616	1,17E-05	1,35E-05	15,46%
6	557075	1,14E-05	1,16E-05	1,22%
7	526425	1,00E-05	9,96E-06	0,35%
8	267136	9,26E-06	9,03E-06	2,49%
9	95274476	5,78E-07	5,00E-08	91,35%

Table 6: Monte Carlo Linear Validation Table against CPS Results.

It can be appreciated that in most cases the Linear Monte Carlo algorithm returns a result quite similar to the one computed by the CPS used as reference value. However, there are three cases where the relative error is higher than a 5%. These cases have been carefully analyzed with the other Monte Carlo algorithms and the results are closer to the Linear Monte Carlo than the reference values of the CPS. However, it has been seen that the covariance of these problematic cases is really large. Consequently, during the Monte Carlo analysis some trials are dismissed because one of the space objects collides with the Earth, what indicates that maybe the orbit determination is not good enough to perform a successful conjunction risk assessment.

6.3.1 STANDARD DEVIATION ANALYTIC FORMULAS

In section 3.1.4 two analytical expressions were developed to calculate the standard deviation of the TCA and miss distance in a simple and easy way without the need to perform complex Monte Carlo assessments. Due to the fact that no attempts to analytically compute these values have been found in the reviewed literature, in this section, those formulas are going to be validated against the values provided by the linear Monte Carlo algorithm.

In Table 7, the validation has been done through the analysis of the nine real cases already used for the validation of the Akella and Maximum probability algorithms.

When the Linear Monte Carlo algorithm was being tested it was seen that the convergence of the standard deviation values was higher than the convergence of the collision probability value. That means that the accuracy of the standard deviation values is above the accuracy of the conjunction probability value.

Case	σ_{tca}[s]			σ_{ρ} [m]		
	Analytic	Monte Carlo	Relative Err.	Analytic	Monte Carlo	Relative Err.
1	5.358	5.358	1.610E-05	7736.296	7736.946	8.402E-05
2	422.033	422.054	4.897E-05	13985.294	14257.341	1.908E-02
3	21.493	21.494	4.539E-05	13707.637	13708.720	7.895E-05
4	3.431	3.432	4.534E-05	2871.509	2871.601	3.211E-05
5	40.292	40.293	4.524E-05	4647.852	4647.556	6.354E-05
6	3.197	3.197	3.538E-05	20356.945	20356.619	1.602E-05
7	18.082	18.083	4.759E-05	17452.495	17451.342	6.607E-05
8	12.131	12.132	4.159E-05	15656.327	15658.140	1.158E-04
9	627.673	627.703	4.735E-05	326788.856	326857.476	2.099E-04
		Mean	3.967E-05		Mean	1.234E-04
		Maximum	4.897E-05		Maximum	1.908E-02

Table 7: Validation of the analytical expressions of the standard deviation of the TCA and miss distance against the values provided by the Linear Monte Carlo Algorithm with 10E7 trials.

It is important to take into account the previous statement when analyzing the results shown in Table 7 because the error of the analytical formula against the values computed with the 10E7 Monte Carlo analysis are of 0.001% for the standard deviation of the TCA and 0.01% for the standard deviation of the miss distance. This result satisfactorily proves that the analytic formulas and their underlying hypothesis are correct.

Finally, it is important to underline that the two previous analytic expressions have been developed for linear conjunctions cases, so good accuracy levels cannot be guaranteed for nonlinear approaches.

6.4 OREKIT PROPAGATORS

OREKIT is an open source high quality library with great specifications. Nevertheless, it has some design drawbacks that are going to be addressed in this section. Some of the propagators that have been used for the conjunction risk evaluation tool do not provide much visibility to the internal behavior. That means that in some situations it is difficult to understand how the algorithms that are being used work. That is why in order to guarantee acceptable quality levels of the tool some testing of those algorithms has also been done with the aim to understand its operation.

6.4.1 NUMERICAL PROPAGATOR

Basically, in OREKIT the propagation accuracy depends on three parameters that characterize the integrator that is being used. These three parameters are the position tolerance and the maximum and minimum integration step. Of which, the most restrictive ones are the position tolerance and the maximum integration step.

To find out the correct configuration of the numerical propagator, a high accuracy reference propagation, computed with a numerical propagator using a position tolerance of 1mm and a maximum integration step of 1s, has been compared with several propagation with different configurations. It has been tested in the worst case scenario which is a LEO, with a Holmes Featherstone Attraction Model[28] of 30th order and degree for six hours propagation.

In the conjunction evaluation tool the maximum and minimum integration step values are relativized from time units to fraction of the orbital period. That way a single configuration is acceptable for multiple orbiting regimes.

Position Deviation 6h propagation a=6,88E6				
		Position Tolerance [m]		
		1	0.1	0.01
Maxim Step	30	2.50E-02	3.78E-02	4.27E-02
	40	4.12E-05	4.49E-04	1.37E-03
	50	2.56E-05	1.63E-05	1.49E-04
	60	1.41E-05	1.25E-05	9.95E-06
Velocity Deviation 6h propagation a=6,88E6				
		Position Tolerance [m]		
		1	0.1	0.01
Maxim Step	30	1.84E-05	3.20E-05	3.48E-05
	40	6.96E-08	4.85E-07	1.52E-06
	50	2.47E-08	1.49E-08	1.63E-07
	60	1.48E-08	1.31E-08	1.04E-08

Table 8: Propagation optimization test results.

Table 8 contains the results of the Numerical Propagation test. Since the propagation time of the orbit is considerably short, the maximum allowed position deviation has been fixed to 1mm and the maximum velocity deviation to 0.1mm/s.

[28] Holmes Featherstone Attraction Model: see more information in section 3.3.3.2.2 Force Models.

The green values are those that meet the precision requirements while the red ones are those which do not.

Considering that the lower the Position Tolerance and the higher the maximum orbital period fraction the slower the propagation is, in Figure 31 the blue block represents the best configuration, since the resulting positional deviation is below the previously established threshold and at the same time it involves the lowest possible computational load.

Finally the Numeric Propagator is going to be used with an orbit period fraction of 40 and a position tolerance of 0.1m. Since these parameters are going to be user configurable it is highly recommended to follow the recommendations of this section.

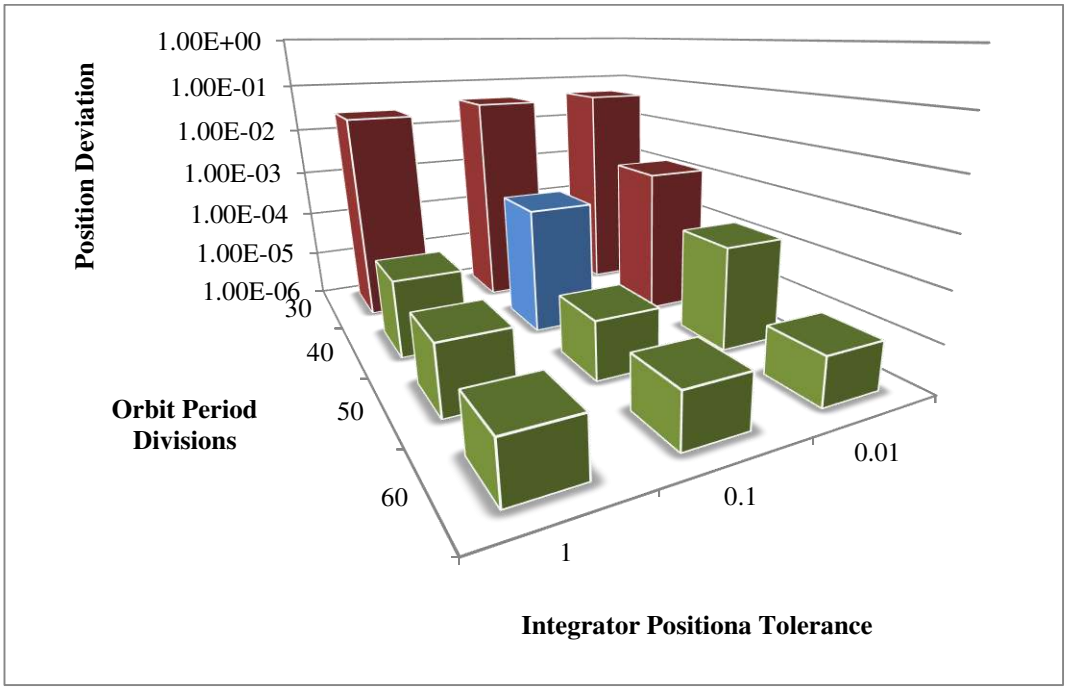

Figure 31: Graphic Position Deviation of a 6h LEO Numerical Propagation vs. Orbit period divisions and Position Tolerance of the Dormand and Prince 856 Integrator.

It is interesting to see how the final position deviation changes with the maximum orbital period fraction of the integrator when the Position Tolerance is fixed to 0.1m. Figure 37 shows how the position deviation remains around 1m when the orbital period divisions are lower than 30. Between 30 and 45 orbital period divisions the final position deviation decreases five orders of magnitude and after 45 the position deviation stabilizes to 1E-5m.

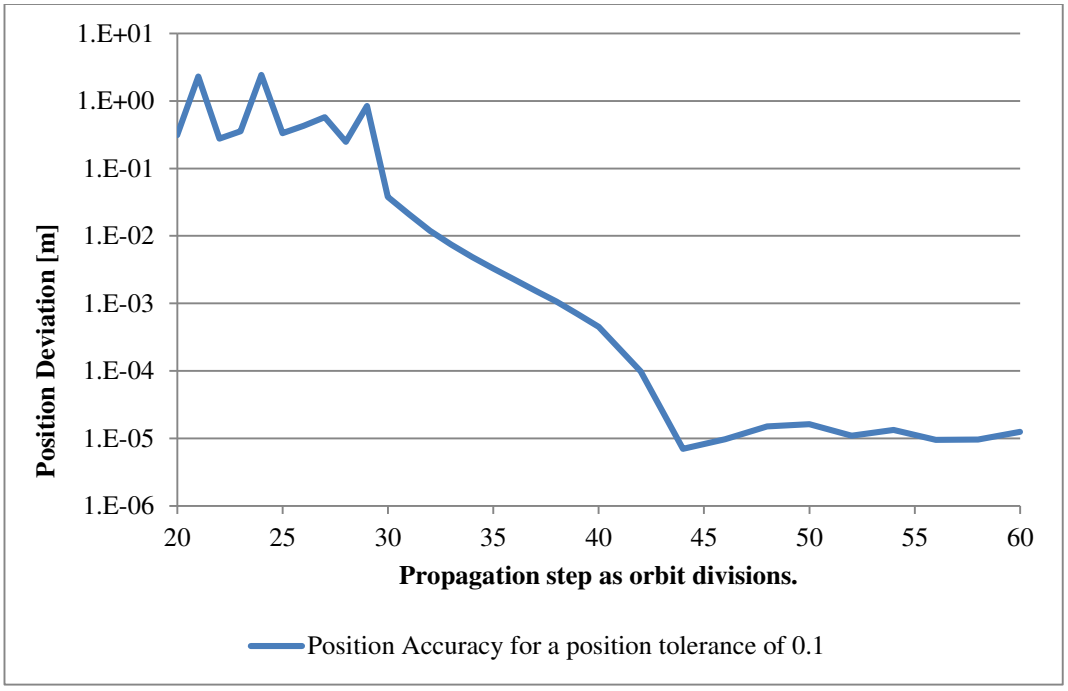

Figure 32: Position deviation evolution of a 6h LEO Propagation vs. the maximum orbit Period Fraction of the Dormand and prince Integrator.

This result is quite coherent, because as remarked before the geopotential model that is being used is of 30th order and degree. That means that the maximum integration step to capture its effects is a thirtieth fraction of the orbital period and that is exactly what is reflected in Figure 32.

6.4.2 EPHEMERIS INTERPOLATION

The most important drawback of the OREKIT library is that when the orbital ephemeris are generated there is no information about the time difference between its internal states, and the number of points that are being used for interpolation of the state vectors.

Following the previous testing case of six hours propagation of a LEO satellite with a position tolerance of 0.1m and a maximum integration step of a 40th fraction of orbit, another test is carried out. In this case an ephemeris of such propagation has been created to compare every 1s the interpolated state of the ephemeris with a high accuracy reference propagation. Since the obtained data seems to have coupled noise caused by the interpolation method, an additional plot of the position deviation with noise reduction has been computed in order to detect possible longer period perturbations.

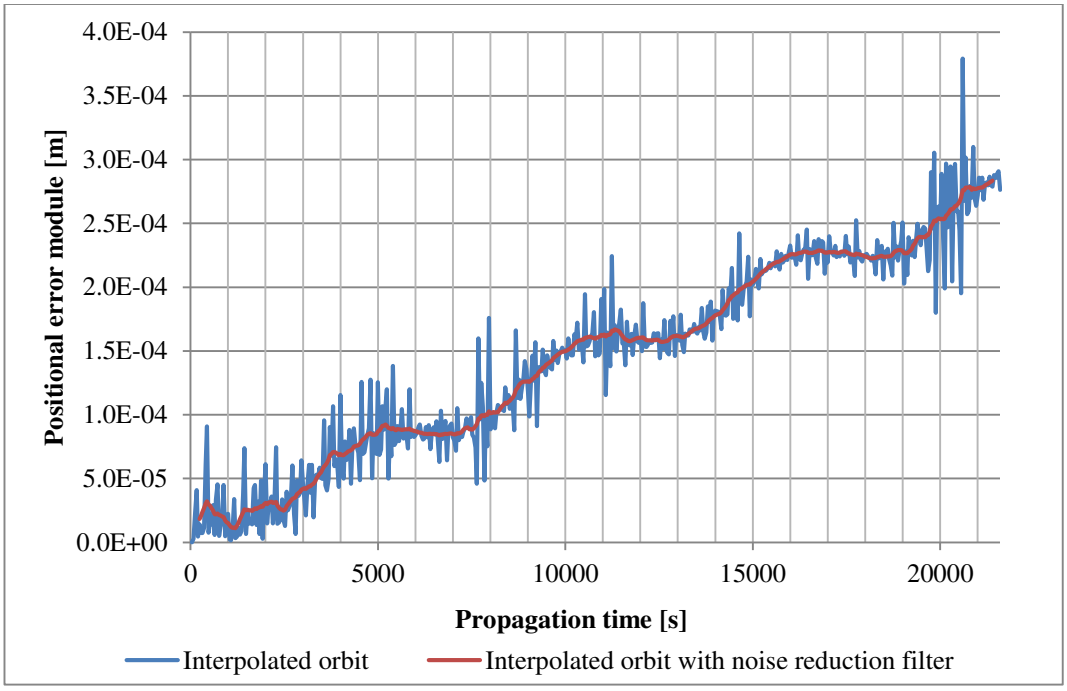

Figure 33: Position deviation between the interpolated states of a 6h Ephemeris and a high accuracy Reference Propagated orbit For a Leo Satellite with a Geopotential Field of 30th order and degree.

Figure 33 clears some doubts about the internal operation of the numerical propagators of OREKIT library. Firstly, it is possible to see how the accumulative propagation error increases along time. But what is more interesting is that the positional deviation follows a sinusoidal tendency with a period that is exactly the orbital period. That means that there are some regions of the orbit where the positional deviation is higher than in some other regions.

Finally the noise magnitude has been evaluated through:

$$Noise = \sqrt{\frac{(PosDev^i - LowNoicePosDev^i)^2}{Nsamples}} = 1.68 \cdot 10^{-5} m \qquad \text{Eq. 103}$$

Such noise level is acceptable for the accuracy requirements established in the previous section. So it can be concluded that when the numerical propagators of the OREKIT library generate an ephemeris, it is properly arranged to fulfill the precision requirements when the integrator is configured as exposed in the previous section.

However, the finite differences propagator returns ephemerides that are not automatically generated by OREKIT and its internal configuration is defined by the user of the conjunction evaluation tool. That is why it is also important to find out

which is the proper number of interpolation points and time difference between the internal states of an OREKIT ephemeris.

Again, a similar test than section 6.4.1 Numerical Propagator is carried out, but now the parameters that are being optimized are the number of interpolation points and the time difference between the internal states of the ephemerides relativized again as orbital period divisions. In this test the mean positional and velocity deviation are computed by comparing the vector states generated by a reference orbit, computed with a numerical propagator that has a positional tolerance of 1mm and a maximum integration step of 1s, and an ephemeris based on the previous orbit but generated with the parameters to optimize.

For the interpolation test the threshold for the positional deviation is 0.1mm and 0.01mm/s for the velocity deviation. Table 9 and Figure 34 show the results of the Test and final ephemeris parameters that meet the established requirements and are also more computationally efficient. The higher the number of used interpolation points and lower the time difference between internal states the higher the computational load will be.

LEO ephemeris orbits quality (Case 5 Alfano 6h propagation)

Positional deviation

Orbital P. divisions	Interpolation Points						
	2	3	4	5	6	7	8
30	2.198E+01	7.526E-02	4.712E-03	4.512E-03	3.293E-03	4.202E-03	1.379E-02
60	1.404E+00	1.236E-03	7.428E-05	4.518E-05	3.816E-05	3.594E-05	3.578E-05
90	2.716E-01	1.095E-04	2.847E-05	2.761E-05	2.768E-05	2.745E-05	2.765E-05
120	8.412E-02	2.840E-05	2.167E-05	2.169E-05	2.164E-05	2.167E-05	2.166E-05
150	3.595E-02	1.761E-05	1.620E-05	1.665E-05	1.645E-05	1.668E-05	1.660E-05

Velocity deviation

Orbital P. divisions	Interpolation Points						
	2	3	4	5	6	7	8
30	4.025E-01	7.526E-02	4.712E-03	4.512E-03	3.293E-03	4.202E-03	1.379E-02
60	5.114E-02	4.685E-05	2.269E-06	1.129E-06	6.313E-07	5.729E-07	5.591E-07
90	1.492E-02	6.126E-06	9.044E-07	8.962E-07	8.944E-07	9.033E-07	9.418E-07
120	6.194E-03	1.848E-06	1.185E-06	1.196E-06	1.193E-06	1.199E-06	1.199E-06
150	3.273E-03	1.590E-06	1.499E-06	1.516E-06	1.513E-06	1.522E-06	1.517E-06

Table 9: Mean position and velocity deviation Between a Self-configured Ephemeris and a reference orbit vs. The Number of interpolation points and the Time Step of the internal states of it (Orbital Period divisions).

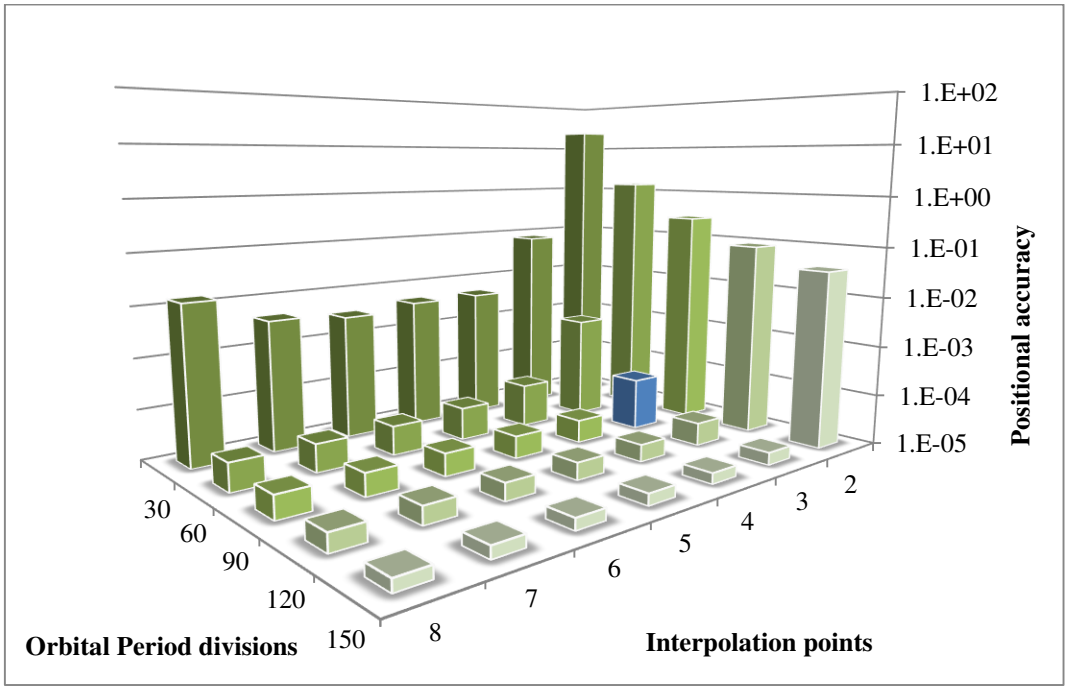

Figure 34: Graphic representation of the Mean Position Deviation between a Self-Configured Ephemeris and a Reference Orbit. The Blue Block is the One That Meets the Accuracy Requirements and it is also the Most Computationally Efficient.

Finally, it is concluded that 90 orbital period divisions and 3 interpolation points is the best choice to ensure an accurate ephemeris states interpolation.

6.5 FINITE DIFFERENCES PROPAGATION

In this section the accuracy levels of the Finite Differences Propagator are going to be tested. This test is also done with the worst case scenario with a LEO and a geopotential field of 30th order and degree. Then the Finite Differences Propagator is settled with all the previously determined parameters, and it is tested with increasing initial position perturbations from 1 to 50m, divided in along-track, cross-track and radial perturbations. For each perturbation a 6h propagation is done with the Finite Differences Propagator and a high precision Numerical Propagator, and then the final positional error is recorded.

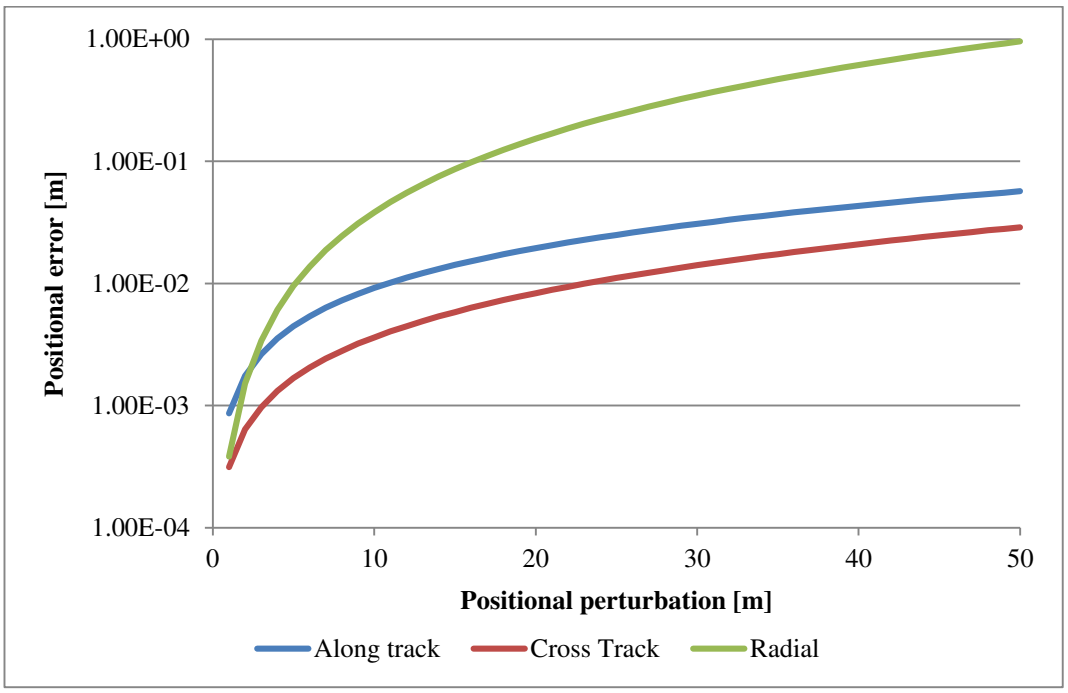

Figure 35: Positional Error vs. Initial Position perturbation module of the finite Difference Propagator.

As it can be appreciated in Figure 35 the radial initial position perturbations generate a final positional error two magnitude orders greater than the cross track and along track perturbations. The positive aspect is that as described in [27] during orbit determination the error in radial direction is the smallest, while the error in the cross track and along track directions is higher. That means that in the Monte Carlo tests, the magnitude of the perturbations generated in radial direction will normally be smaller than in the remaining two directions.

It can be concluded that the accuracy levels of the Finite Difference Propagator are relatively acceptable since with a 50m along track perturbation the algorithm determines the position of the space object with an error less than 6cm. Considering that a reasonable satellite's diameter is 4m, the collision can be

satisfactorily determined. The velocity deviation follows the same behavior than the positional deviation but with a 0.006mm/s error for a 50m initial positional along track perturbation.

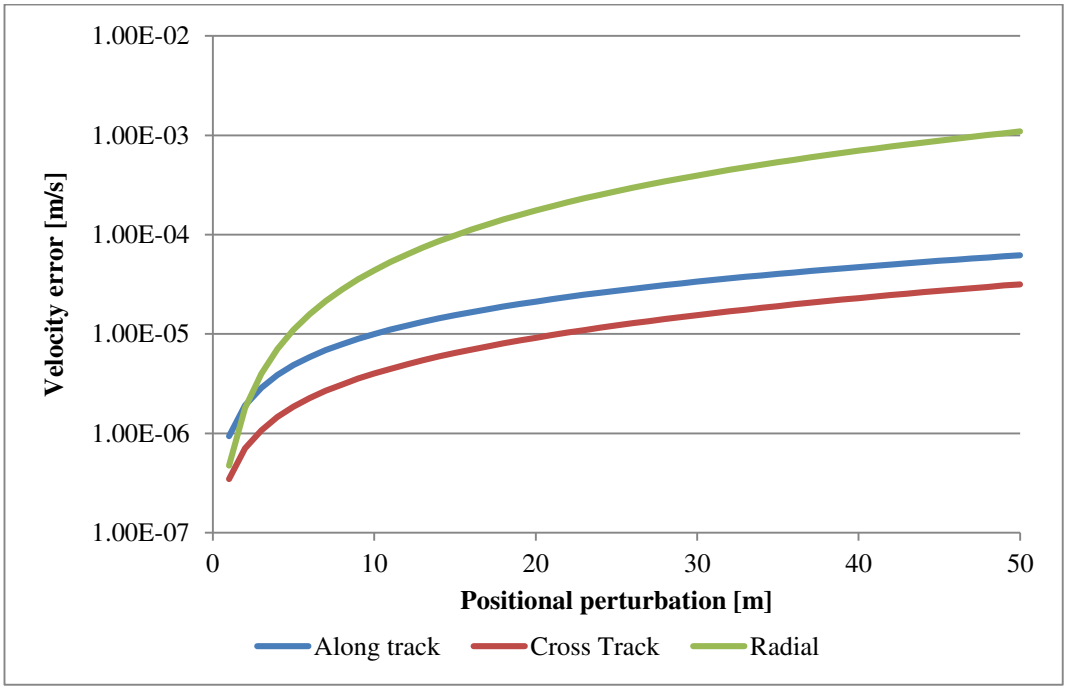

Figure 36: Velocity Error vs. Initial Position perturbation module of the finite Difference Propagator.

6.6 ALFANO CASES

In [13] Salvatore Alfano defines and analyses 12 conjunction cases to perform a Keplerian Monte Carlo Analysis. This article is really interesting because it provides the Mont Carlo collision probability of each case with the collision probability of some linear and nonlinear methods.

Since some of the data of the Alfano's report is missing, case 6 and 10 have been dismissed. Table 10 provides a global summary of the comparison of the results from Alfano's article and the algorithms implemented in this report. It can be seen that the results are quite satisfactory because most of the cases have a relative error lower than 2% with the exception of case 12 that will be carefully discussed in section 6.6.10 Case 12. It is also appreciable that the Numeric and Finite Differences Monte Carlo analysis, despite being different algorithms provide a really similar solution. That is the reason why in all the following presented plots,

the results of the Numerical and Finite Differences Monte Carlo algorithms are overlapped.

Alfano Cases Results Summary Table							
Case	Alfano E8	Linear	Numeric	Fin. Diff.	Linear Err.	Numeric Err.	Fin. Diff. Err.
1	0.2175	0.2071	0.2146	0.2146	0.0479	0.0131	0.0132
2	0.0157	0.0066	0.0154	0.0154	0.5800	0.0239	0.0239
3	0.1008	0.0993	0.0993	0.0993	0.0155	0.0155	0.0155
4	0.0731	0.0861	0.0723	0.0723	0.1783	0.0109	0.0109
5	0.0445	0.0433	0.0433	0.0433	0.0272	0.0272	0.0272
7	0.0002	0.0002	0.0002	0.0002	0.0091	0.0091	0.0091
8	0.0353	0.0343	0.0353	0.0353	0.0280	0.0004	0.0001
9	0.3651	0.3554	0.3642	0.3641	0.0267	0.0026	0.0028
11	0.0033	0.0030	0.0034	0.0034	0.1047	0.0215	0.0215
12	0.0026	0.0032	0.0035	0.0035	0.2442	0.3850	0.3862

Table 10: Comparative table of the Alfano (Keplerian) Monte Carlo 1E8 and the implemented Linear, Numeric and Finite Differences Monte Carlo Algorithms with 1E5 iterations. Red relative error painted values are those that overpass a 5% of relative error, hence are not acceptable.

For each close approach case two different plots are computed. On one hand there is the distributed probability plot that expresses which miss distance values are more probable to happen. In the same plot there is also represented through a secondary axis the integration of the distributed probability density, which expresses the conjunction risk as a function of the combined objects radius. On the other hand for each close approach case, there is also the cumulative probability plot, which shows the conjunction risk as a function of time.

6.6.1 CASE 1

Case 1 involves nonlinear relative motion (relative velocity 0.014m/s) of two GEO satellites where the mean miss distance is less than the combined object radius (15m).

Despite being a nonlinear case, in Figure 37 it can be appreciated that the Linear Monte Carlo provides a really similar result than the other more accurate algorithms. The plot clearly shows that it is not a linear case because in such situations the probability distribution is homogenous and the slope of the conjunction probability vs. combined object radius curve is constant.

The Cumulative Probability plot (Figure 38) shows the conjunction risk along a screen of 11h around the mean TCA. This is a really special case where the

collision probability increases in two segments. The Numerical and Finite Differences algorithms provide the same solution while the linear algorithm has errors in the prediction of the far approaches because they occur about 3h after the mean TCA. Obviously, the linear hypothesis does not fit for a 3h period. That is why the second approach prediction is not as good as the first approach with the Linear Algorithm.

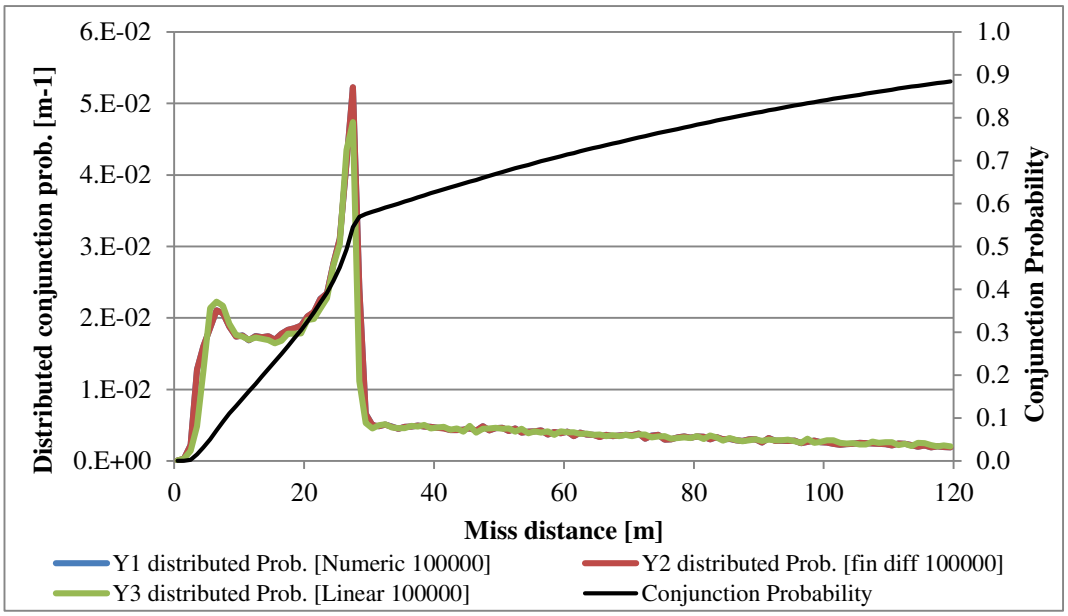

Figure 37: Plot of the probability distribution along the miss distance computed with the three different Monte Carlo algorithms of Alfano's case 1. There is also (In black) the Conjunction probability value as a function of the initial Combined Object Radius.

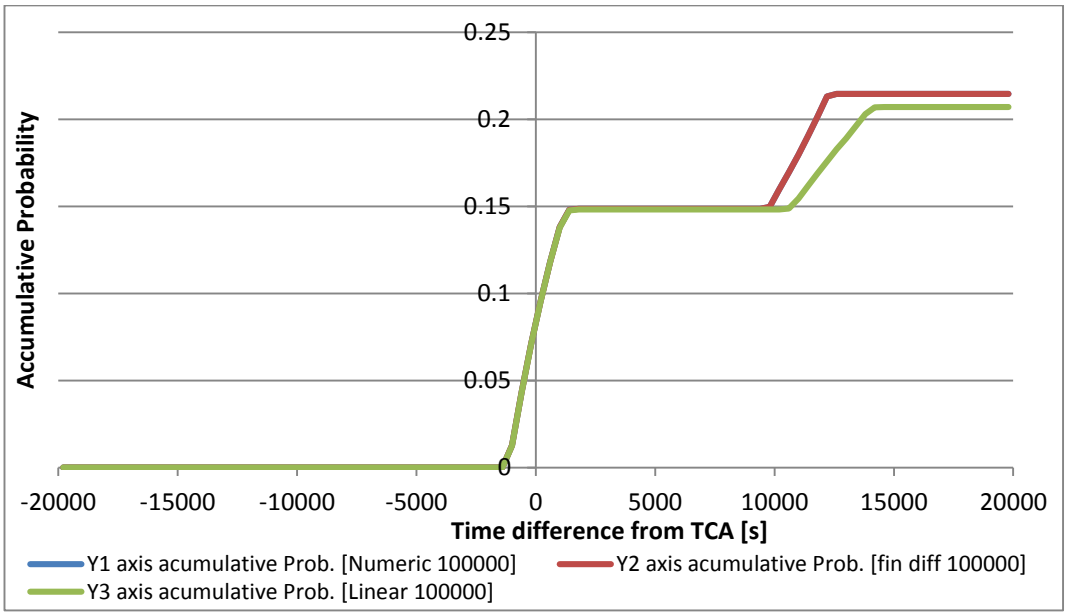

Figure 38: Conjunction probability as a function of time near the mean TCA of Case 1.

6.6.2 CASE 2

The second case is the exact same case as the previous one (Case 1) but with the exception that the combined object radius is smaller (4m). The distribution probability plot is not exposed because it does not depend on the combined object radius and it would be exactly the same as the one of previous section.

Nevertheless, the cumulative probability plot has been considerably modified with respect to the previous one. In this case, the probability of far conjunctions increases while the probability of near conjunction decreases. This fact deteriorates the Linear solution as clearly can be appreciated in Figure 39 where the second slope is barely predicted.

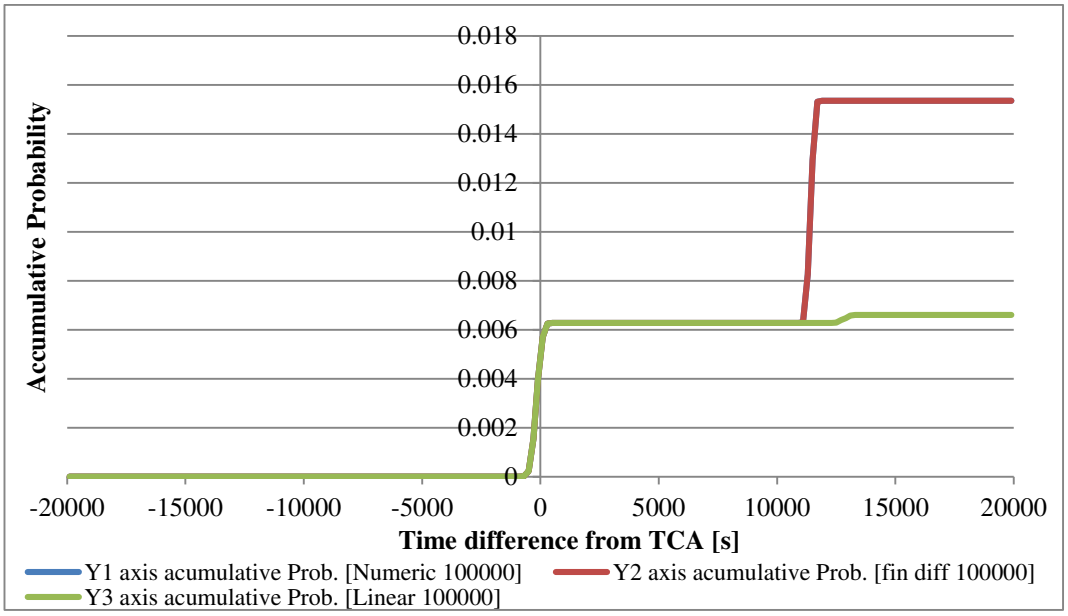

Figure 39: Conjunction probability as a function of time near the mean TCA of Case 2.

6.6.3 CASE 3

This case is a linear relative motion approach with a relative velocity at TCA of 16m/s. In this case the linear algorithm and the numerical algorithms provide exactly the same results in both cases. This case validates the linear algorithm, and shows that for linear cases the solution is completely reliable.

Figure 41 shows the time cumulative conjunction probability for Case 3 within a screening window of less than two hours. As it is a linear relative motion approach the accumulative probability plot presents an abrupt slope very near from the mean TCA.

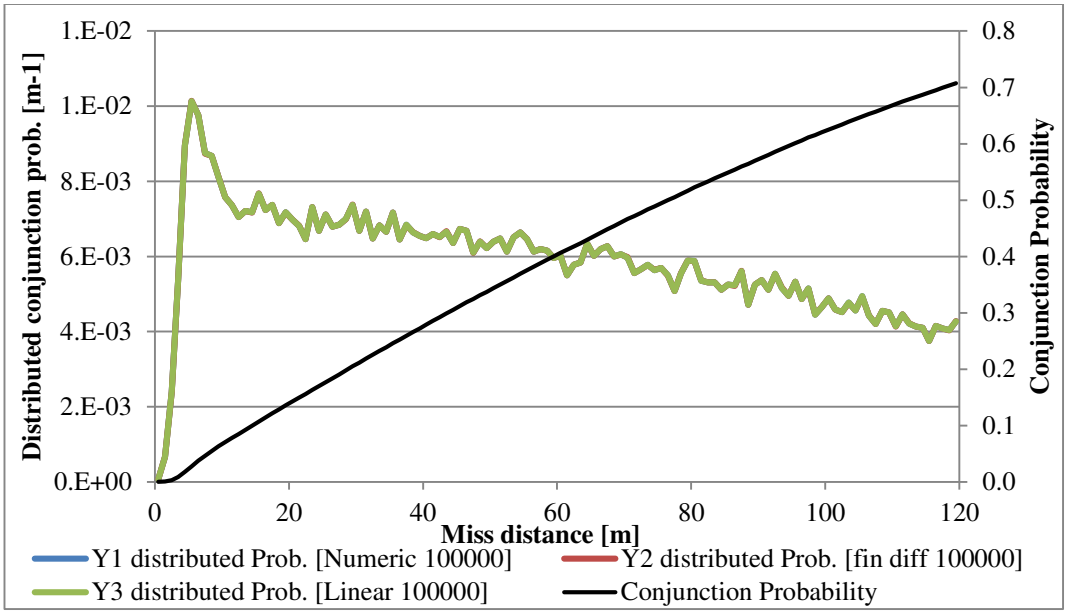

Figure 40: Plot of the probability distribution along the miss distance computed with the three different Monte Carlo algorithms of Alfano's case 3. There is also (In black) the Conjunction probability value as a function of the initial Combined Object Radius.

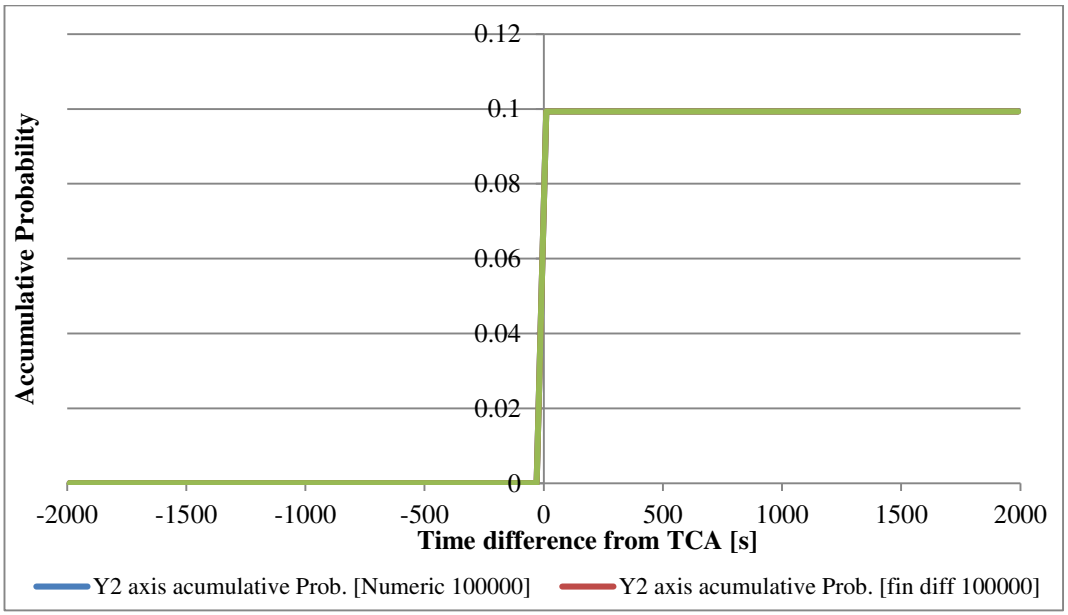

Figure 41: Conjunction probability as a function of time near the mean TCA of Case 3.

6.6.4 CASE 4

This case involves nonlinear relative motion for two geosynchronous satellites where the miss distance is greater than the combined object radius (15m) and a relative velocity in the TCA of 0.019m/s.

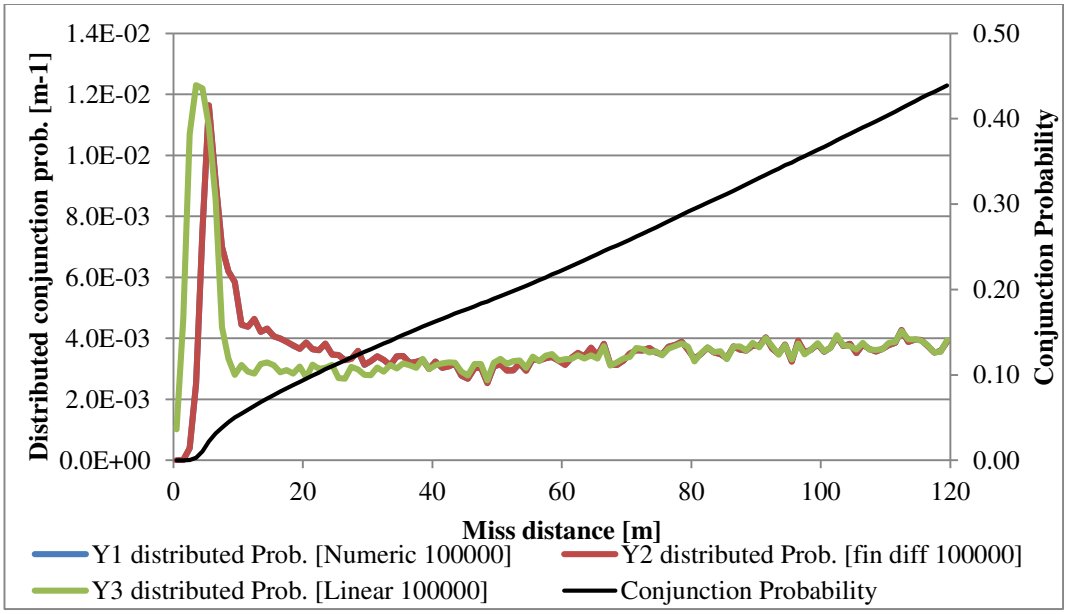

Figure 42: Plot of the probability distribution along the miss distance computed with the three different Monte Carlo algorithms of Alfano's case 4. There is also (IN Black) the Conjunction probability value as a function of the initial Combined Object Radius.

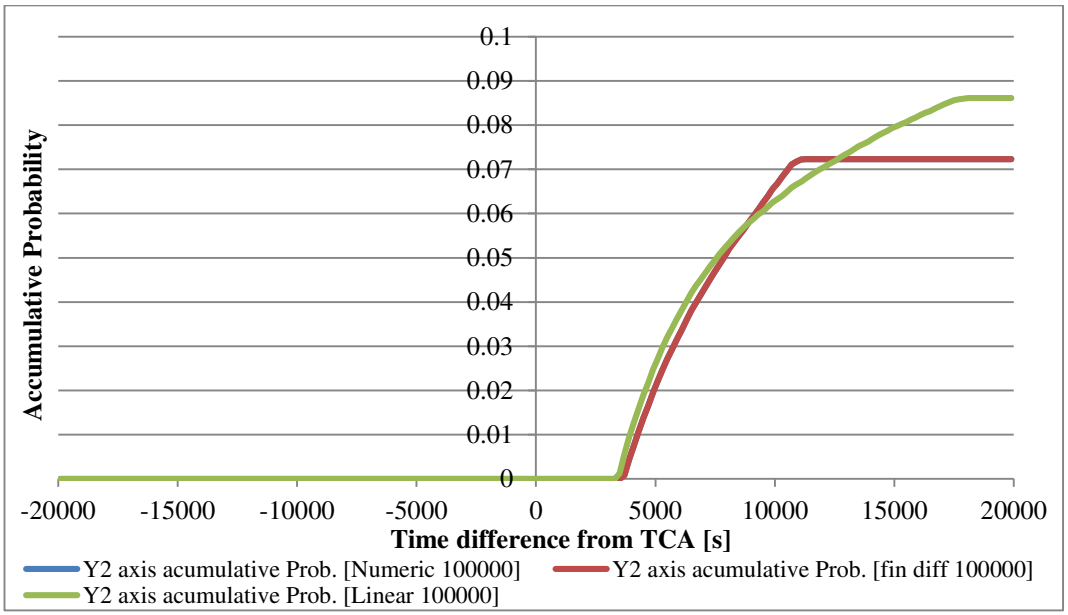

Figure 43: Conjunction probability as a function of time near the mean TCA of Case 4.

The covariance ellipsoids have been arranged in a specific way to set back the accumulative probability slope about 3000s after the mean TCA. As it is seen in both Figure 42 and Figure 43, this case is clearly unfavorable for the linear algorithm because all the potential conjunctions are far from the TCA where the linearity hypothesis is not anymore valid.

6.6.5 CASE 5

Case 5 is quite similar to Case 3 (linear motion approach) with the main difference that the satellites are in a LEO. The conjunction probability along the miss distance follows a semi rectilinear path, which means that the probability slope is practically linear. The interpretation is that this case is easily scalable for different combined object radius values.

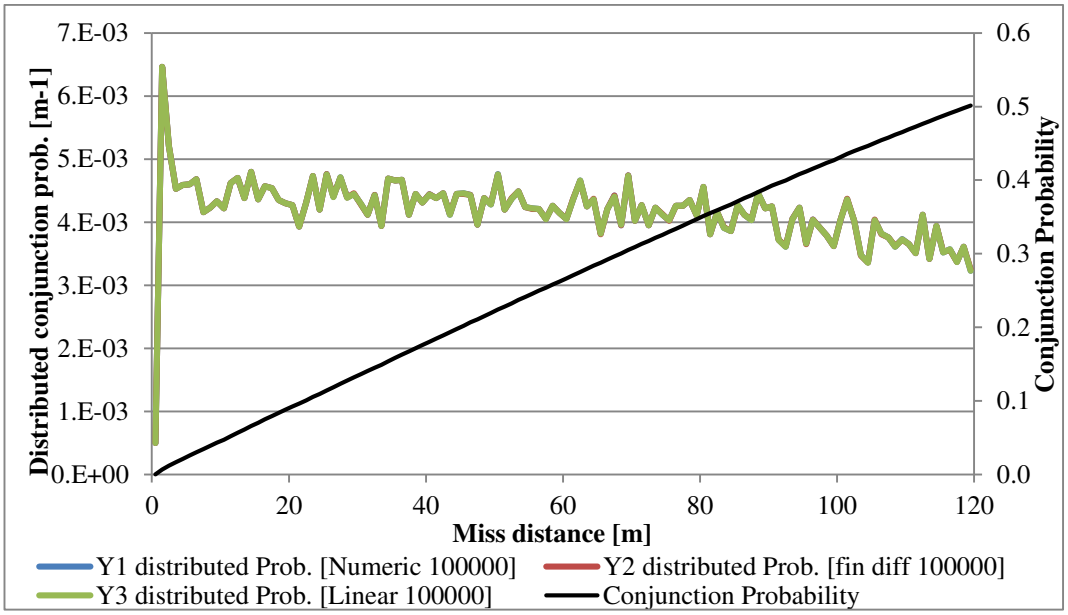

Figure 44: Plot of the probability distribution along the miss distance computed with the three different Monte Carlo algorithms of Alfano's case 5. There is also (IN Black) the Conjunction probability value as a function of the initial Combined Object Radius.

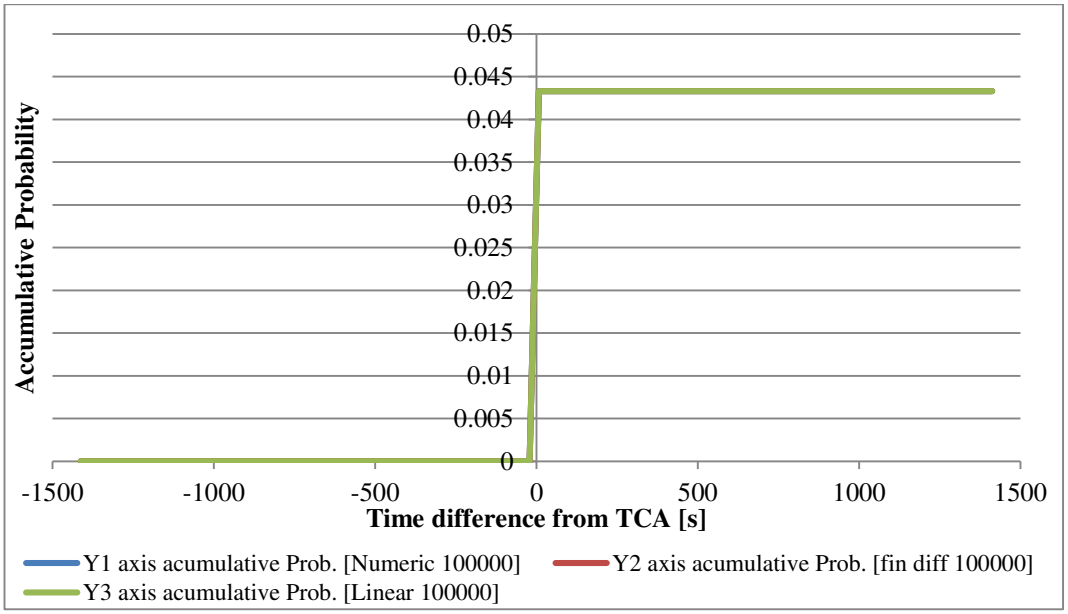

Figure 45: Conjunction probability as a function of time near the mean TCA of Case 5.

Again the results of the numerical a linear algorithms match since the case is a linear relative velocity approach.

6.6.6 CASE 7

This case is a nonlinear approach of two LEO satellites with the peculiarity that the conjunction risk is below 0.001. This case is analyzed with the aim to check how a low number of Monte Carlo iterations affects to the results.

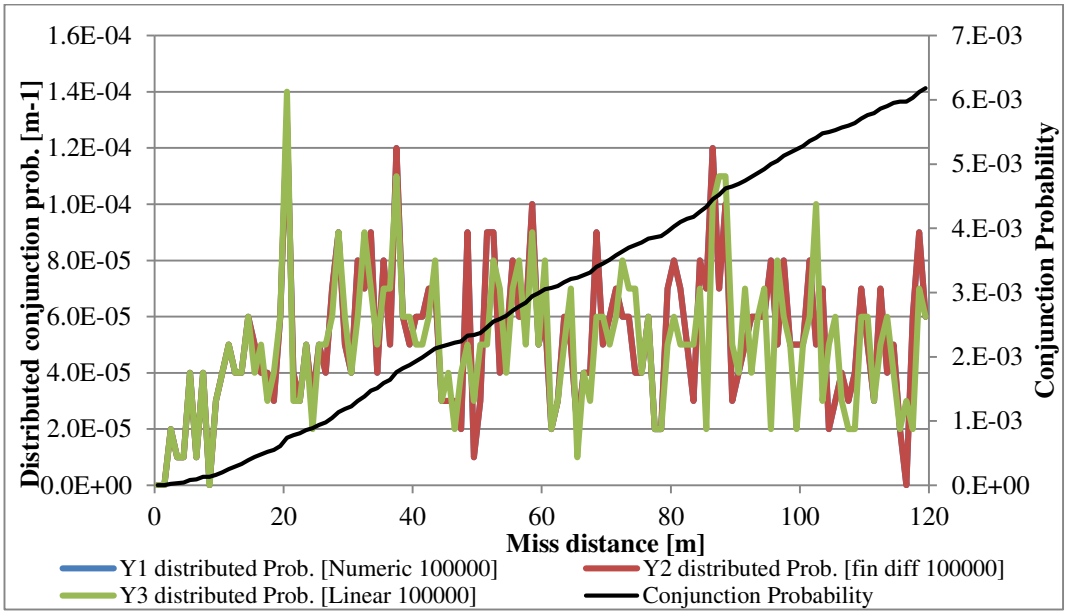

Figure 46: Plot of the probability distribution along the miss distance computed with the three different Monte Carlo algorithms of Alfano's case 7. There is also (In black) the Conjunction probability value as a function of the initial Combined Object Radius.

In this case the conjunction probability has a magnitude order of 1E-4 and the number of iterations has been settled to 1E5. A good indicator of a non-adequate number of iterations is Figure 46. When the points of the probability distribution plot do not follow a smooth curve it means that the number of tested cases is not enough.

Figure 47 shows an abrupt slope typical of a linear approach; however the reason for the abrupt slope is because not enough conjunctions have been recorded to capture a smooth plot curve.

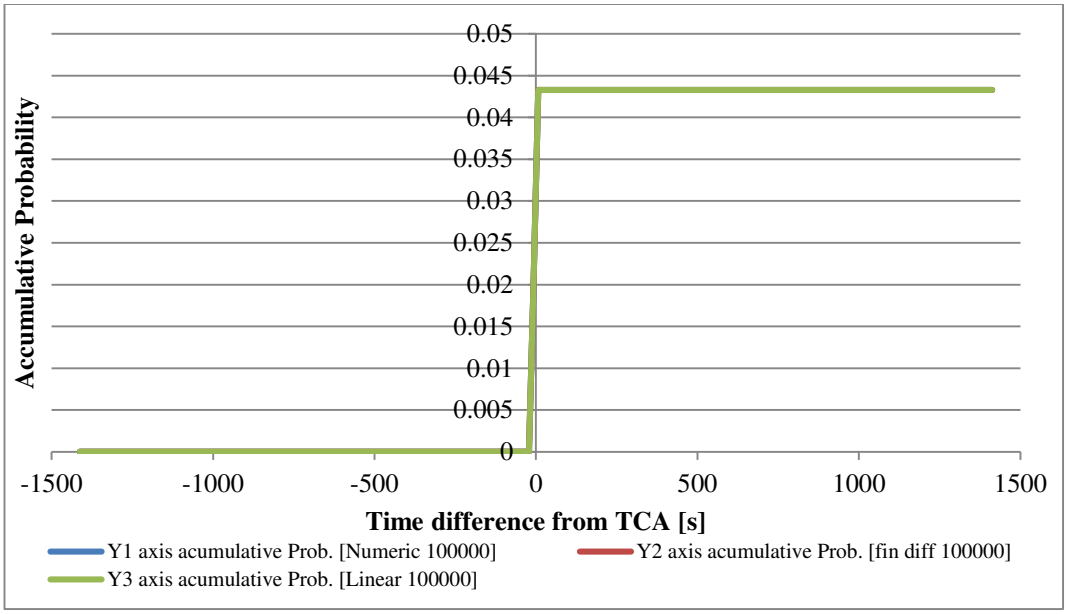

Figure 47: Conjunction probability as a function of time near the mean TCA of Case 7.

6.6.7 CASE 8

This case is a nonlinear approach of two satellites MEO with a really low relative velocity at the TCA of 8.9E-4m/s. The miss distance is less than the combined object radius.

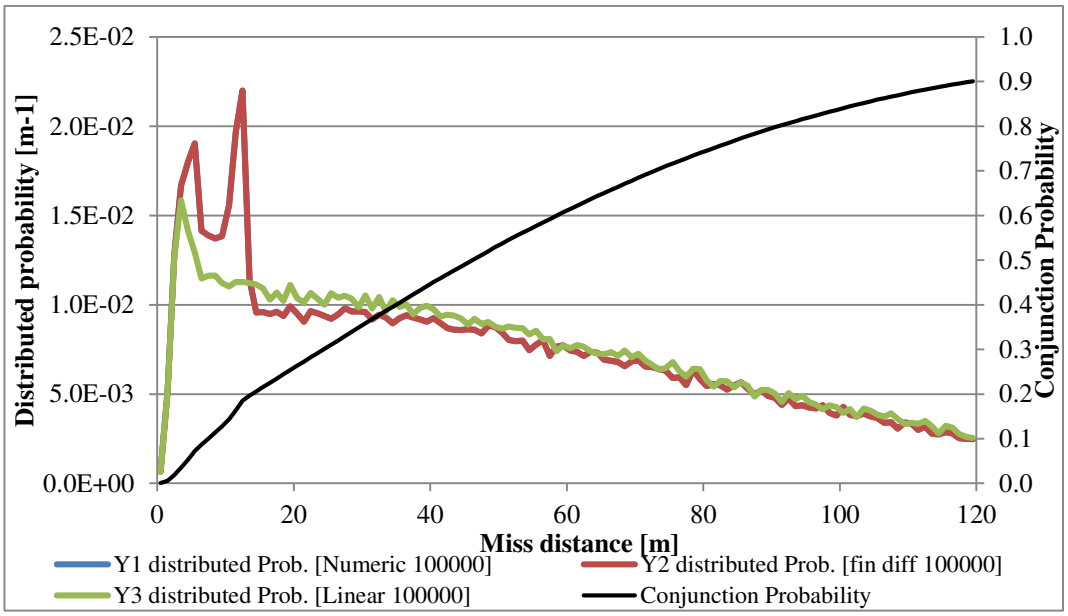

Figure 48: Plot of the probability distribution along the miss distance computed with the three different Monte Carlo algorithms of Alfano's case 8. There is also (IN Black) the Conjunction probability value as a function of the initial Combined Object Radius.

The probability distribution plot confirms that this is a non-linear approach since the larger is the combined object radius the less the conjunction probability risk increases. Despite Figure 48 shows different results between the numeric and linear algorithms in the probability distribution plot (Figure 48), the cumulative probability predicted by the linear algorithm only has a 2% relative error with respect to the Alfano's reference value tested for a 1E8 Monte Carlo.

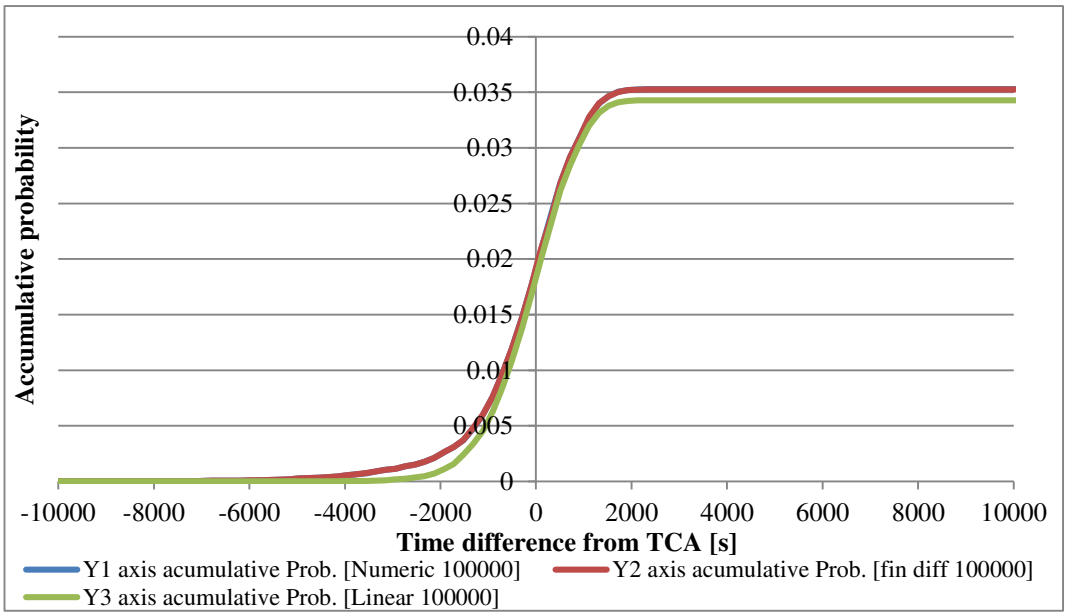

Figure 49: Conjunction probability as a function of time near the mean TCA of Case 8.

6.6.8 CASE 9

This case is a nonlinear approach of two highly-eccentric orbits satellites; it is a very stressing case due to tight turns in the relative trajectory coupled with low relative velocity. All the algorithms present a similar behavior providing a final probability value very close to the reference value of the Alfano's paper.

The probability distribution plot (Figure 50) proves that this case is quite particular because when the combined object radius is larger than 40m an increment of it does not increases the conjunction risk. This fact also proves the high non-linearity of this case.

Nevertheless, the shape of the accumulative probability slightly differs from the one computed by Alfano because, according to Alfano, the slope starts at -13000s and in Figure 51 it starts in -10000s. These small differences could be caused by the fact that the propagation methods used in this report and the Alfano's paper are not exactly the same.

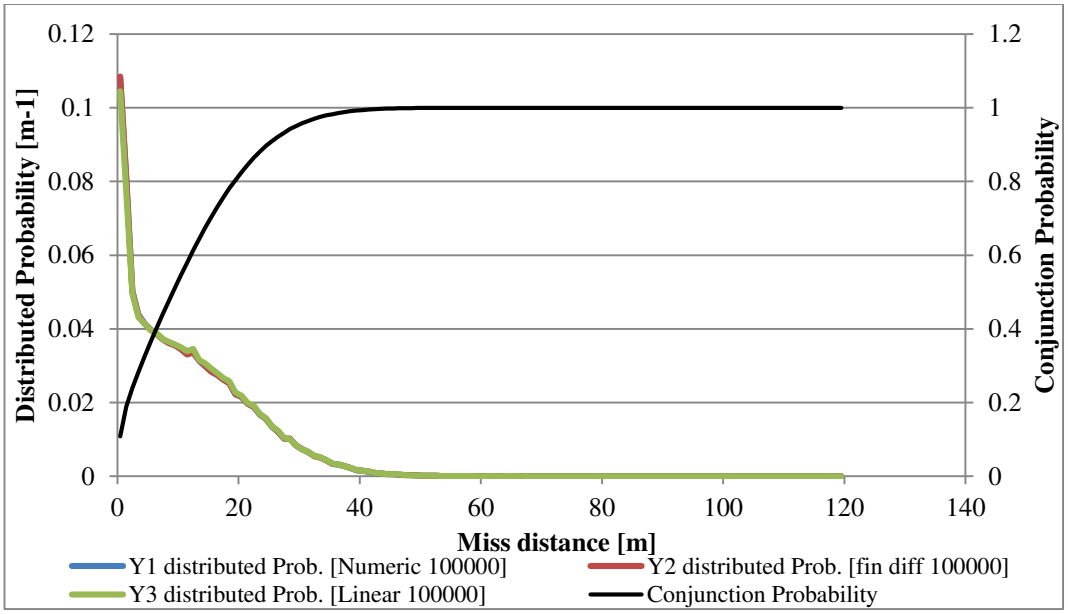

Figure 50: Plot of the probability distribution along the miss distance computed with the three different Monte Carlo algorithms of Alfano's case 9. There is also (In black) the conjunction probability value as a function of the initial combined object radius.

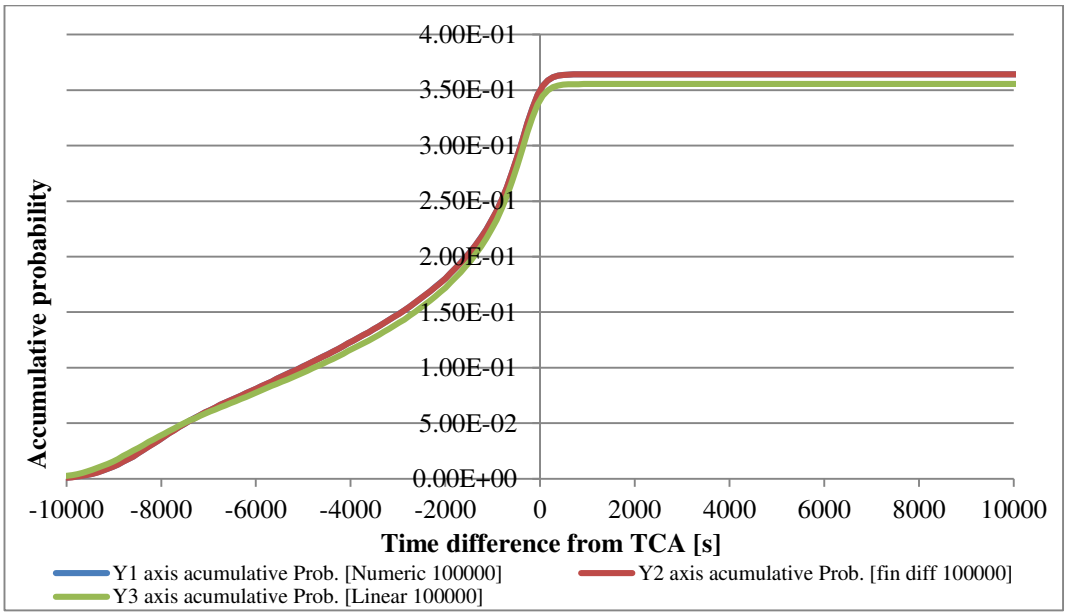

Figure 51: Conjunction probability as a function of time near the mean TCA of Case 9.

6.6.9 CASE 11

This case involves two LEO satellites in leader-follower formation where the two satellites fly in the same orbital path separated only by mean anomaly. Since the relative velocity is zero, the TCA has been arbitrarily chosen.

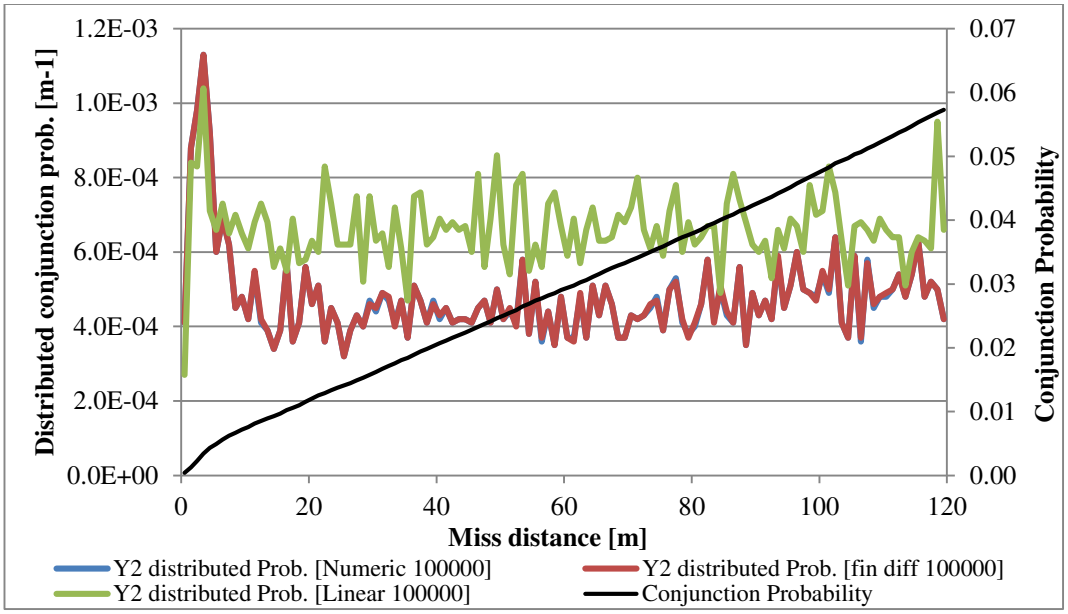

Figure 52: Plot of the probability distribution along the miss distance computed with the three different Monte Carlo algorithms of Alfano's case 11. There is also (In black) the Conjunction probability value as a function of the initial Combined Object Radius.

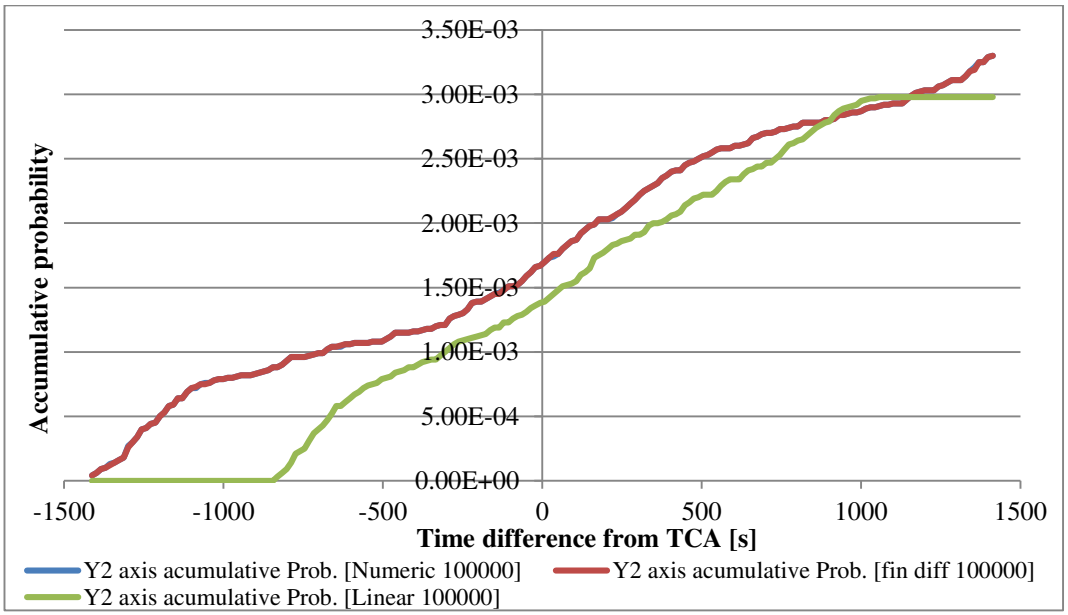

Figure 53: Conjunction probability as a function of time near the mean TCA of Case 11.

Figure 54 shows how the accumulative probability grows over time as the positional uncertainty of the two objects also gets larger with time. In this case the linear approximation predicts a similar solution but with the difference that no conjunctions farther than +-1000s are predicted, as a consequence the total probability value of the linear algorithm is a 10% lower than the value provided by the numeric algorithm.

6.6.10 CASE 12

Finally, this case is the same case as case 11, with the two objects in the exact same position. This means that as the miss distance has been reduced to zero the total collision probability should be at least slightly larger than the total probability computed in case 11.

The finite differences algorithm computed a conjunction probability of 0.0034 for case 11 and 0.0035 for case 12. However, in Alfano's paper the conjunction probability for case 11 is 0.0033 and 0.0026 for case 12. Such results do not have any physical sense, furthermore the accumulative probability plot of both cases do not match with the total computed probability. That is why it could be concluded that the results extracted by Alfano in case 11 and 12 are erroneous.

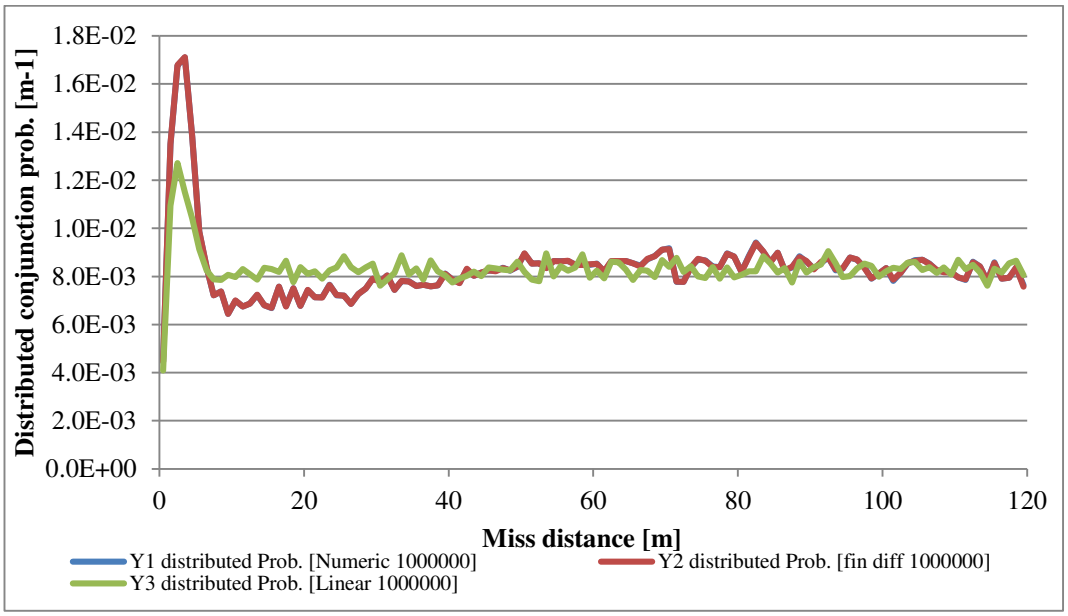

Figure 54: Plot of the probability distribution along the miss distance computed with the three different Monte Carlo algorithms of Alfano's case 12. There is also (In black) the Conjunction probability value as a function of the initial Combined Object Radius.

Case 12 was settled to be computed with 1E6 iterations, one order of magnitude over all previous tests. This is why Figure 55 and Figure 53 follow almost the same curve but with the difference that the second plot is smoother because it has been computed with a larger number of samples.

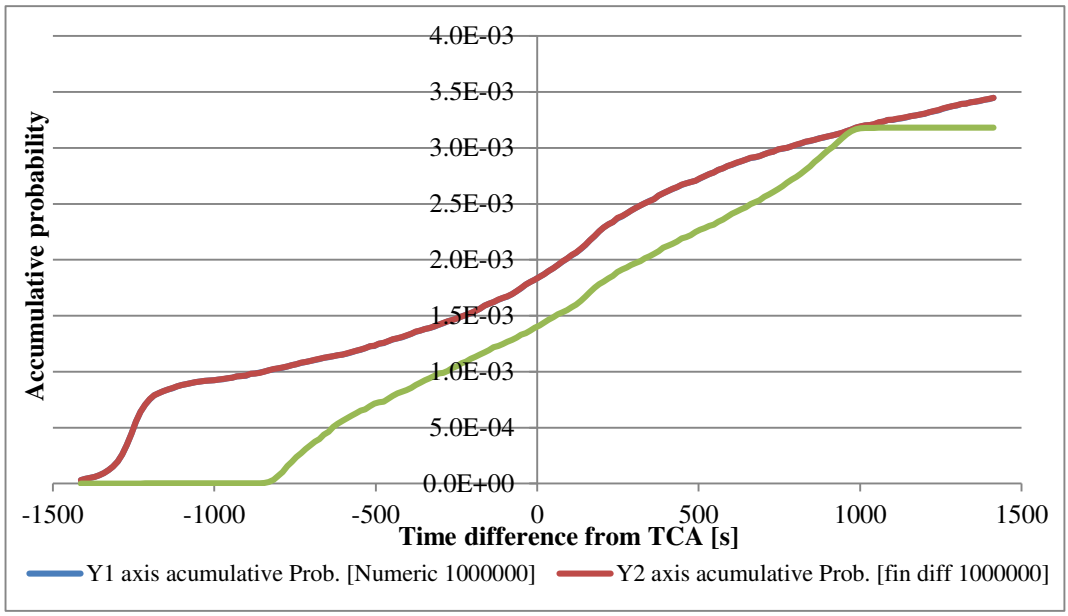

Figure 55: Conjunction probability as a function of time near the mean TCA of Case 12.

6.7 ALGORITHMS COMPUTATIONAL PERFORMANCE

The aim of the Finite Differences algorithm was to provide very similar results than the numeric Monte Carlo algorithm but with a better performance.

	Computation time [s]		
Case	Numeric	Finite Differences	Improvement
1	11128	517	0.046
2	11057	517	0.047
3	4403	31	0.007
4	10935	218	0.020
5	9362	58	0.006
7	5643	535	0.095
8	14783	3599	0.243
9	20103	136	0.007
11	7872	972	0.123
12	7851	971	0.124
		Minimum times faster	4
		Mean times faster	14
		Maximum times faster	161

Table 11: Computational performance table for the numeric and finite differences Monte Carlo algorithms; all cases with 1e5 trials.

During the Alfano validation section it has been proven that both algorithms provide quite the same solution, so the first objective of the Finite Differences algorithm has been fulfilled.

The next step is to quantify the new algorithm's computational performance; Table 11 shows the required time to run all 10 Alfano cases with 1E5 iterations. In all cases the Finite Differences algorithm is faster than the numeric; however the improvement rate is not constant.

The worst improvement rate is for case 8 where the Finite Differences algorithm only computes the solution four times faster than the numerical algorithm; on the other hand there is case 5 where the new algorithm finishes the computation 161 times faster. The mean improvement rate of the Finite Differences algorithm is 14 times faster, this is, one order of magnitude less than the numeric algorithm.

Project Planning

The organization of the project was structured from the beginning to follow a parallel project procedure than the organization followed in ESA projects. ESA organizes its software engennering projects in five phases: requirements engineering, design, implementation, validation and approval.

This structure is the one that has been folowed along all the project, Figure 56 sows the first project planning that was done before starting the project.

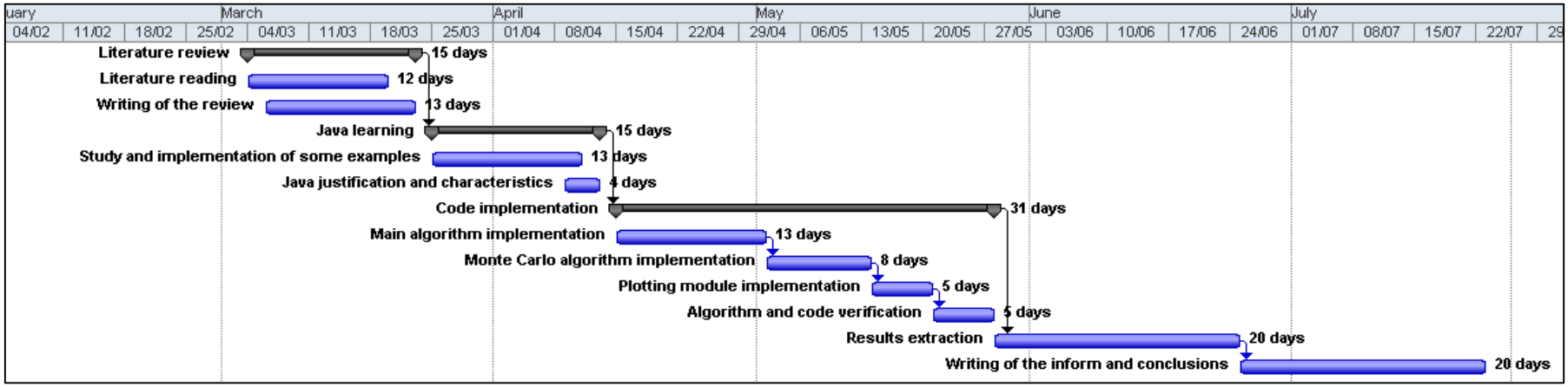

Figure 56: Initial Gantt diagram of the project planning.

During the progress of the project several meetings were scheduled in order to review and discuss the evolution state of the project, in all the situations the progress was mostly as scheduled. However, it is important to underline that due to a lack of experience in this kind of

projects many new tasks have been detected during the course of the project. That is why in Figure 57 (the real project evolution) several new activities have been added.

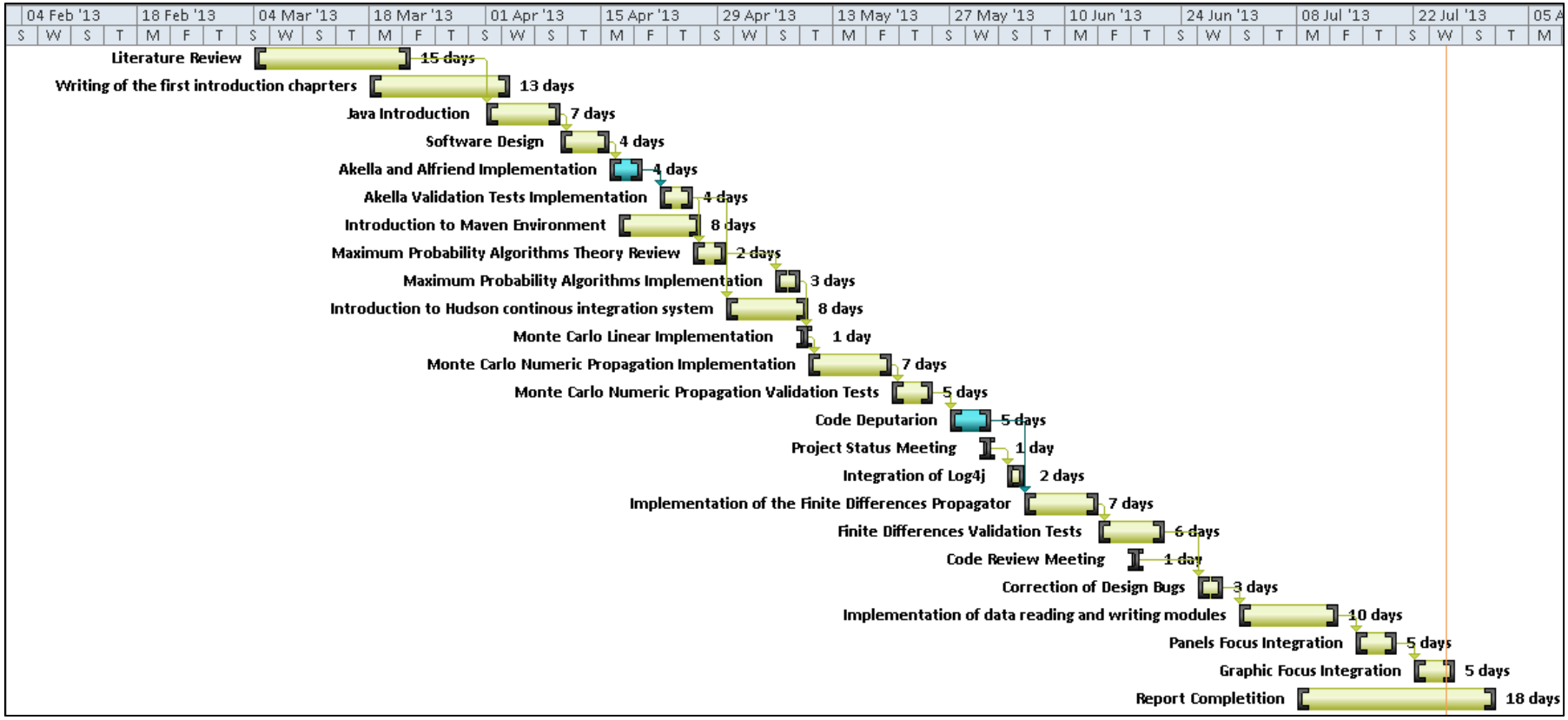

Figure 57: Final Gantt diagram of the real undertaken tasks during the project.

ENVIRONMENTAL IMPACT

The development of this project has represented a minimum environmental impact. Since it is a software development project the three main sources of environment pollution produced during its course are: the energy used for daily transport to the office, the energy consumed in the office considering the acclimatization system and all the paper used for the confection of the project report.

Despite this minimum environmental impact, this study can contribute to the prevention of large environmental disasters. For instance, from a space collision of two manmade objects hundreds of uncontrolled fragments can be produced leading to the disablement of some space regions. If one of the objects is carrying a toxic or radioactive payload a conjunction could put Earth living organisms' integrity under risk.

BUDGET

Table 12 shows the budget of the project, which has been divided in for main fields: hardware, software, engineer salary and UPC administration fees. The most important expense is the salary of the engineer followed by the cost of the hardware. However, considering that the hardware can be used for several projects its real cost is below the estimated cost of the table. It is also important to underline that the in the case that the software licenses are corporate licenses, then its cost is also significantly reduced.

Project Budget		
Hardware	Computer	€ 500,00
	Continuous integration server	€ 800,00
Software	Microsoft Office	€ 100,00
	Eclipse	€ -
	Enterprise Architect	€ 240,00
Engineer salary	8,7€/h	€ 7.800,00
UPC Administration fees	14,8% of engineer salary	€ 1.154,00
Total		€ 10.594,00

Table 12: Most important expenses of the project.

CONCLUSIONS AND FURTHER WORK

The aim of this study was to respond to the actual necessities of the European space operators by characterizing the probability of collision between the objects orbiting in near Earth altitudes. A study of the available techniques for collision risk assessment of space objects has been done, and some of these techniques have been implemented in Java to build a consistent conjunction risk assessment tool.

A total of seven collision risk assessment algorithms including the linear Akella and Alfriend 2000, three algorithms to compute the maximum collision probability, and three Monte Carlo methods, have been implemented to determine their advantages and drawbacks.

The Akella and Alfriend algorithm is the fastest and the most suitable for an operational use, since very low computational times are required to asses thousands of potential conjunctions every day. It is important to underline that its results are only valid under linear relative velocity conditions. Nevertheless, low relative speed (<10m/s) approaches take place in very limited occasions. Also the Numeric Maximum probability algorithm developed in this report is appropriate to be used with an aspect ratio not larger than 40, as mentioned in [20], for operational purposes since it is the best option when no covariance data is available and at the same time is accurate and fast. The other two maximum probability algorithms are not very recommended because the Maximum Probability with infinite Aspect Ratio algorithm provides a too large safety margin and the Maximum Analytic Probability has been proven to have short validity ranges.

On the other hand, the Monte Carlo algorithms remain for research purposes or special case studies, despite the great performance improvement that has been achieved with both the Finite Differences and Linear Monte Carlo innovative Algorithms. The Numeric Propagation Monte Carlo algorithm has been a good tool to validate the Finite Differences Monte Carlo, but since the results of the second algorithm are obtained about 14 times faster with the same accuracy there is not a strong reason to be used by the future users of the developed library.

Java and its object orientation techniques have been a key factor for the development of this project in terms of flexibility and third party libraries reuse. However, it is not the best option when the best computational performance is a primary specification, because one of the key features of Java is that it runs in a virtual machine that can be migrated easily to multiple platforms. This is at the same time one of its strongest weaknesses because it makes the code somehow slow.

Another purpose of the project was to evaluate the OREKIT library, which despite having small drawbacks discussed along the reports it is a quite complete flight dynamics library with a low learning cost. It can be recommended for both didactical and commercial uses.

Regarding the software development platform, eclipse is an extremely powerful tool that simplifies considerably the day to day development work, and at the same time offers a perfect frame to incorporate the necessary plugins. On the other hand, Maven has proved to be a useful software project management tool that when combined with a continuous integration system such as Hudson, the project maintenance is highly simplified.

Finally, it would have been interesting to implement some extra perturbation models such as air drag, solar pressure and moon gravity perturbation to compare the results of a Monte Carlo that takes all the previous perturbations into account with a simple Keplerian Monte Carlo algorithm. Such results would be useful for validation purposes and to indicate if the extra perturbation models suppose a key factor for the conjunction risk assessment.

REFERENCES

[1] H. Klinkrad, Space Debris Models and Risk Analysis, Chichester, UK: Praxis Publishing Ltd, 2006.

[2] "CNES," [Online]. Available: http://debris-spatiaux.cnes.fr/english/risques_debris_eng.html. [Accessed 08 April 2013].

[3] ESA, "FFG Forschung Wirkt," 2008 November 12. [Online]. Available: www.ffg.at/getdownload.php?id=4467. [Accessed 2013 April 3].

[4] E. S. Team, "Space Situational Awareness - Space Surveillance & Tracking Customer Requirements Document," 2011.

[5] S. Aida and M. Kirschner, "Collision Risk Assessment and Operational Experiences For Leo Satellites at GSOC," in *SpaceOps Conference*, Huntsville,Alabama, US, 2010.

[6] F. Bonaventure and A. Giequel, "Collision Risk Management in Alstrium Satellites," in *European Space Surveillance Conference*, Madrid, SP., June 2011.

[7] W. James, V. Coppola and F. Stoner, "A Description of Filters for Minimizing the Time Required for Orbital Conjunction Computations," 2010.

[8] G. M, S. N and B. M, "Analysis of Collision Risk & Avoidance Maneuvers," Madrid, 2000.

[9] S. Alfano, "Determining Satellite Close Approaches, Part II," vol. 42, no. 2, 1994.

[10] R. P.Brent, "Algorithms for Minimization Without Derivatives," in *Algorithms for Minimization Without Derivatives*, Yorktown Heights, New York, Prentice-Hall, 1973.

[11] R. C. Frigm, "A Single Conjunction Risk Assessment Metric: The f-Value," *Advances in the Astronautical Sciences Volume 135.,* 2010.

[12] A. Salvatore, "Review of Conjunction Probability Methods for Short-term Encounters," in *AAS/AIAA Spaceflight Mechanics Meeting*, Sedona, Arizona, USA, February 2007.

[13] A. Salvatore, "Satellite Conjunction Monte Carlo Analysis," in *AAS/AIAA Spaceflight Mechanics Meeting*, Savannah, Georgia, USA., February 2009.

[14] R. P. Patera, "General Method for Calculating Satellite Collision Probability," *Journal of Guidance, Control, and Dynamics, Vol. 24, No. 4 ,* pp. 716-722, 2001.

[15] V. T. Coppola, J. Woodburn and H. Richard, "Effects of Cross-Correlated Covariance on Spacecraft Collision Probability," in *AAS/AIAA Spaceflight Mechanics Meeting*, Maui, Hawaii, USA., 2004.

[16] A. Kauderer, "NASA," 23 October 2010. [Online]. Available: http://www.nasa.gov/mission_pages/station/news/orbital_debris.html. [Accessed 2013 March 15].

[17] K. Chan, "Short-Term vs Long-Term Spacecraft Encounters," in *AIAA/AAS Astrodynamics Specialist Conference and Exhibit*, Providence, Rhode Island, USA., August 2004.

[18] M. R. Akella and K. T. Alfriend, "Probability of Collision Between Space Objects," *Journal of Guidance, Control, and Dynamics, Vol. 23, No. 5,* pp. 769-772, 2000.

[19] S. Alfano, "A Numerical Implementation of Spherical Object Collision Probabiliry," *The Journal of the Astronautical Sciences, Vol.53 No.1,* pp. 103-109, Jaunary-March 2005.

[20] A. Salvatore, "Method for detemining maximum conjunction probability of rectangular-shaped objects". Unated States Patent US 7,383,153 B, 3 June 2008.

[21] J.-C. Dolado, X. Pena, R. Garmier, B. Revelin and P. Legendre , "Satellite collision probability computation for long term encounters," in *AAS/AIAA Astrodynamics Specialist Conference*, Girdwood, Alaska, USA., July 2011.

[22] S. Alfano, "Addressing Nonlinear Relative Motion For Spacecraft Collision Probability," in *AIAA/AAS Astrodynamics Specialist Conference*, Keystone, Colorado, August 2006.

[23] R. P. Patera, "Satellite Collision Probability for Nonlinear Relative Motion," *Journal of Guidance, Control and Dyanamics Vol.26, No. 5,* October 2003.

[24] M. David, "Development of a Nonlinear Probability of Collision Tool for the Earth Observing System," in *AIAA/AAS Astrodynamics Specialist Conference and Exhibit*, Keystone, Colorado, Agust 2006.

[25] S. Alfano, "Beta Conjunction Analysis Tool," in *2007 AAS/AIAA Astrodynamics Specialist Conference*, August 2007.

[26] V. Copplola, "Including Velocity Uncertainty in the Probability of Collision Between Space Objects," in *AAS/AIAA Spaceflight Mechanics Meeting*, Charleston, South Carolina, USA, February, 2012.

[27] O. Montenbruck, Satellite Orbits, Berlin: Springer Heidelberg, 2012.

[28] J. Seago and D. Vallado, "Coordinate Frames of the U.S. Space Object Catalogs," in *AIAA/AAS Astrodynamics Specialist Conference*, Denver CO, 2000.

[29] S. Alfano, "Relating Position Uncertainty to Maximum Conjunction Probability," *The Journal of the Astronautical Sciences,* pp. 193-205, 2005.

[30] W. E. F. S. A. Holmes, "A unified approach to the Clenshaw summation and the recursive computation of very high degree and order normalised associated Legendre functions," vol. Journal of Geodesy, no. 76, 2002.

[31] J. Alarcón, "Independent Orbit Determination for Colision Avoidance," in *Proceedings of the Fourth European Conference on Space Debris*, Darmastadt, GE., April 2005.

[32] G. L. Slater, S. M. Byram and T. W. Williams, "Collision Avoidance for Satellites in Formation Flight," *Journal of Guidance, Control, and Dynamics Vol.29 No.5,* September-October 2006.

[33] N. Bérend, "Estimation of the probability of collision between two catalogued orbiting objects," *Advances in Space Research, Volume 23, Issue 1,* pp. 243-247, 1999.

[34] K. T. Alfriend, M. R. Akella, J. Frisbee, J. L. Foster, D.-J. Lee and M. Wikins, "Probability of Collision Error Analysis," *Space Debris, Volume 1, Issue 1,* pp. 21-35, 1999.

APPENDIX

1.1 MAXIMUM PROBABILITY RESULTS

In this section contains the comparison of the three maximum probability algorism of all the analyzed cases in section: 6.2.

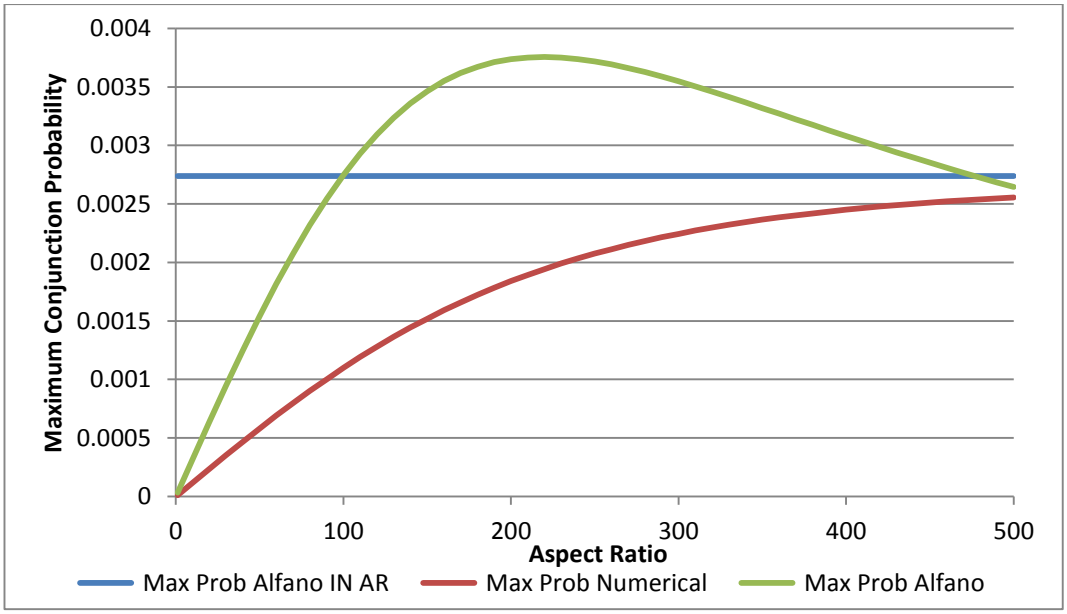

Figure 58: Numeric Maximum Conjunction Probability of the CASE 2 Conjunction VS Aspect Ratio. Max Prob. Alfano IN AR (Maximum probability with Infinite Aspect Ratio).

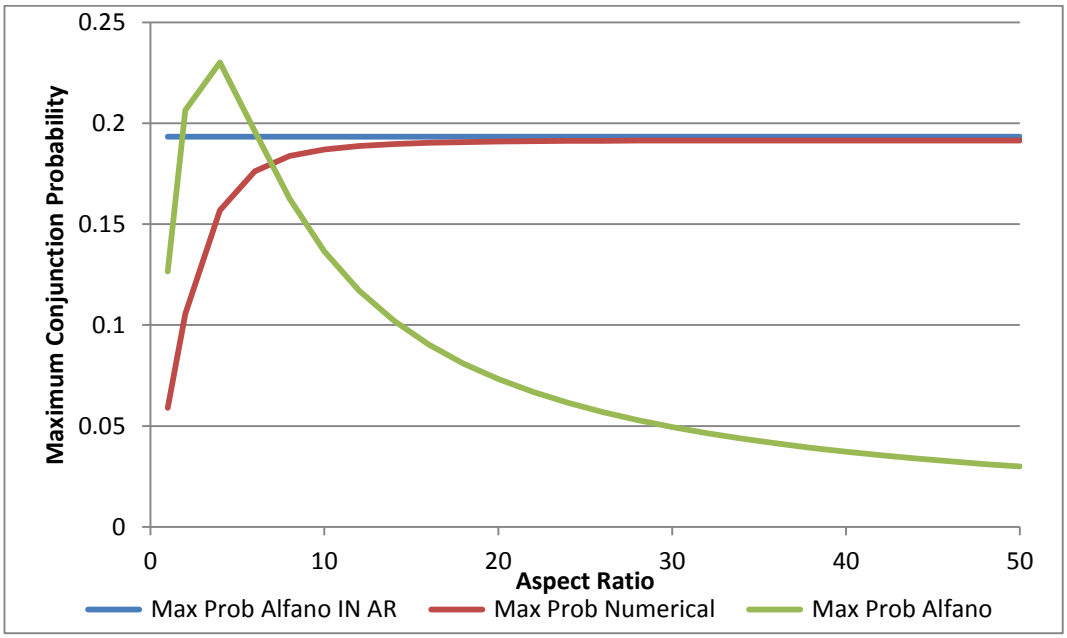

Figure 59: Numeric Maximum Conjunction Probability of the CASE 3 Conjunction VS Aspect Ratio. Max Prob. Alfano IN AR (Maximum probability with Infinite Aspect Ratio).

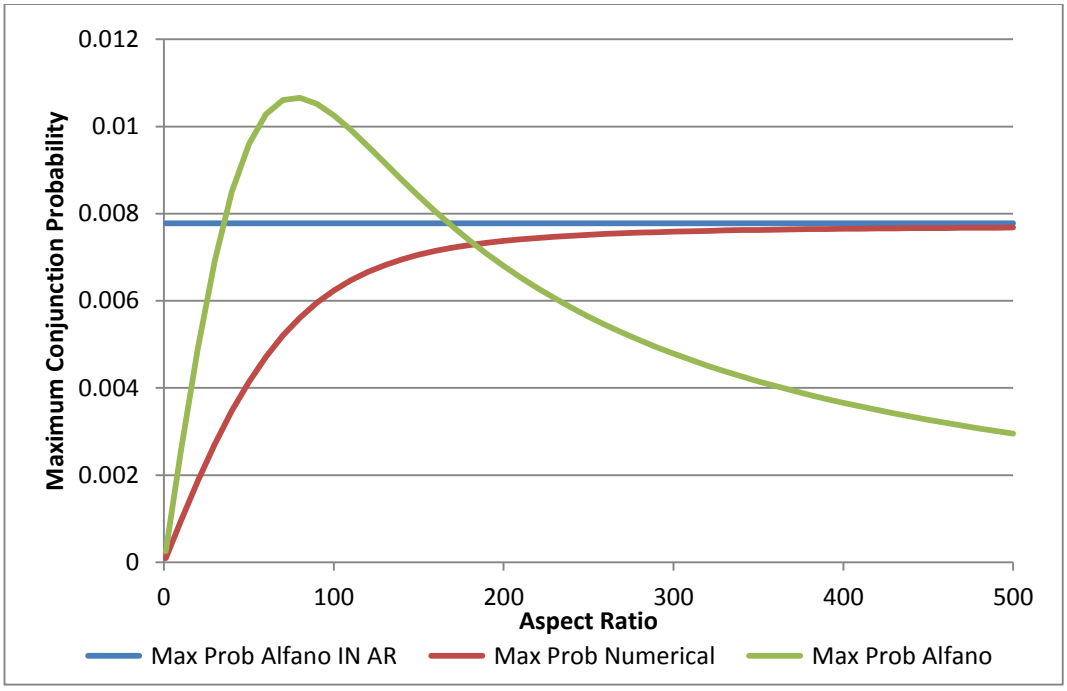

Figure 60: Numeric Maximum Conjunction Probability of the CASE 5 Conjunction VS Aspect Ratio. Max Prob. Alfano IN AR (Maximum probability with Infinite Aspect Ratio).

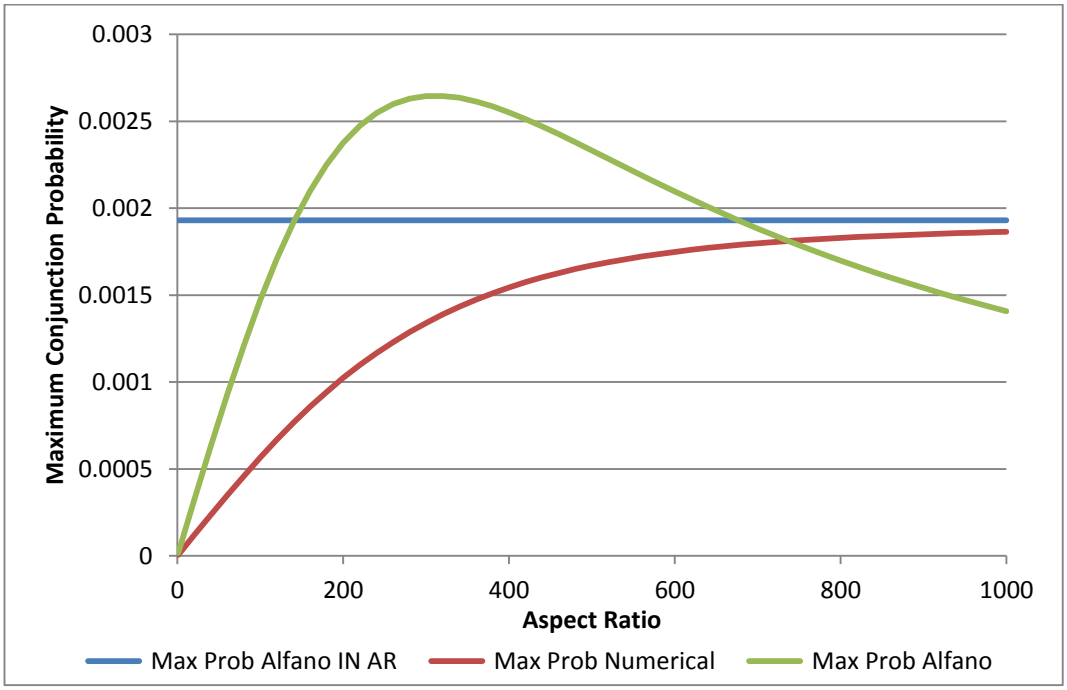

Figure 61: Numeric Maximum Conjunction Probability of the CASE 6 Conjunction VS Aspect Ratio. Max Prob. Alfano IN AR (Maximum probability with Infinite Aspect Ratio).

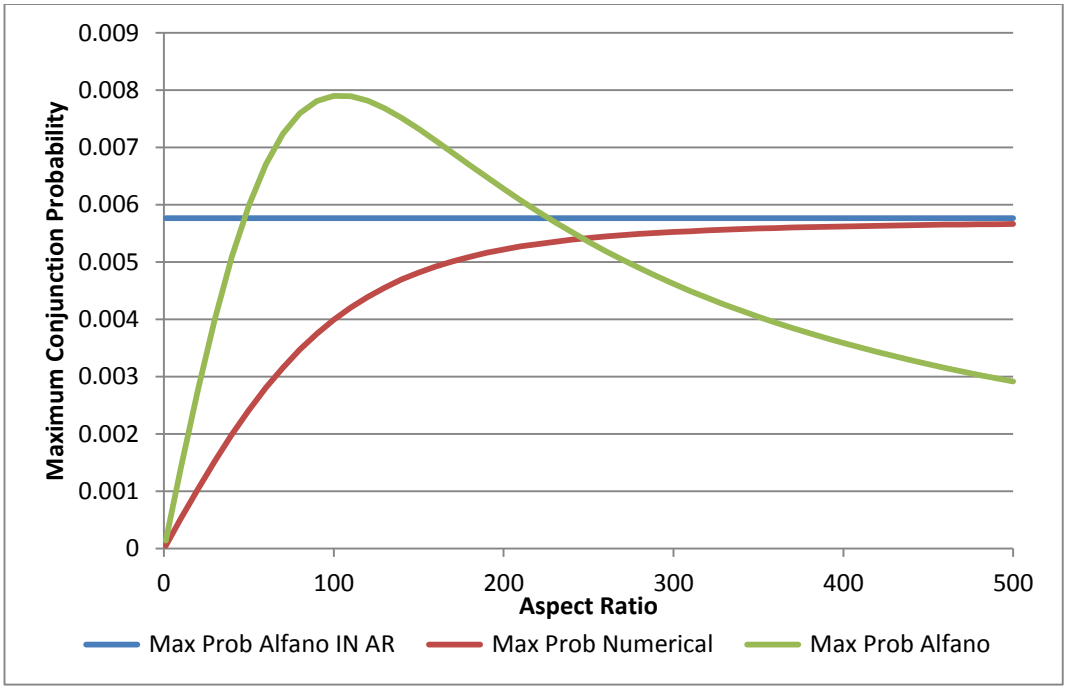

Figure 62: Numeric Maximum Conjunction Probability of the CASE 7 Conjunction VS Aspect Ratio. Max Prob. Alfano IN AR (Maximum probability with Infinite Aspect Ratio).

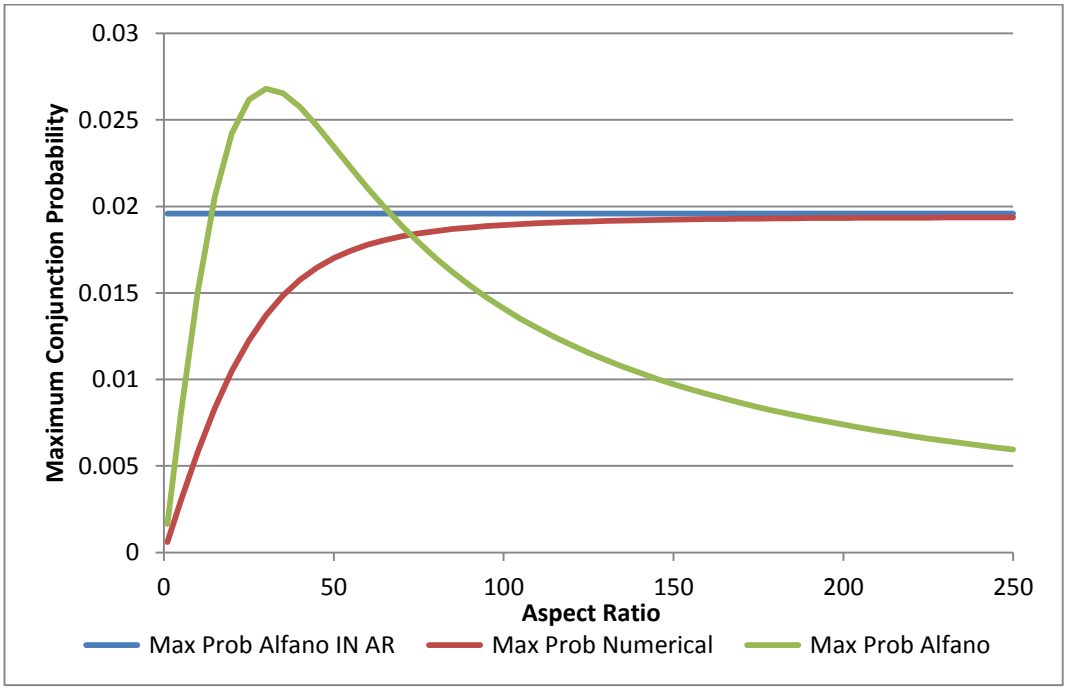

Figure 63: Numeric Maximum Conjunction Probability of the CASE 8 Conjunction VS Aspect Ratio. Max Prob. Alfano IN AR (Maximum probability with Infinite Aspect Ratio).

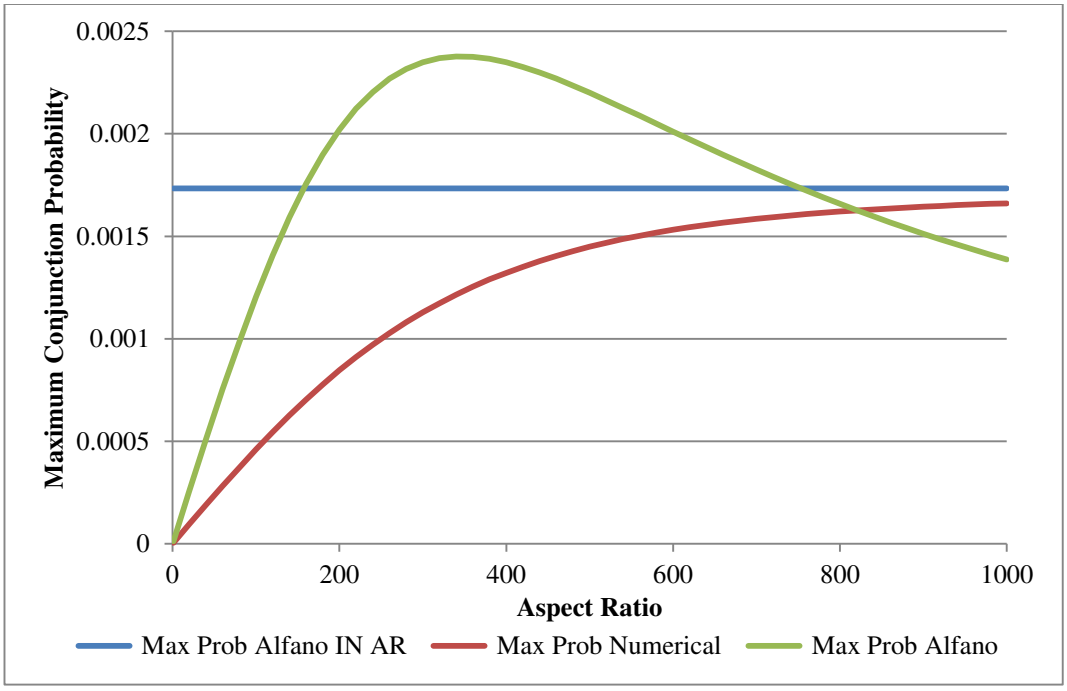

Figure 64: Numeric Maximum conjunction probability vs. aspect ratio of case 9. Max Prob. Alfano IN AR (Maximum probability with Infinite Aspect Ratio).